CALIBRATING A VHR SENSOR BASED ABOVEGROUND BIOMASS MODEL WITH UAV FOOTPRINTS IN A DUTCH TEMPERATE FOREST.

LUIS ALONSO FIGUEROA SÁNCHEZ
August, 2021

SUPERVISORS:
Ir. L.M. van Leeuwen (First Supervisor)
Drs. Ing. Margarita Huesca Martínez (Second Supervisor)

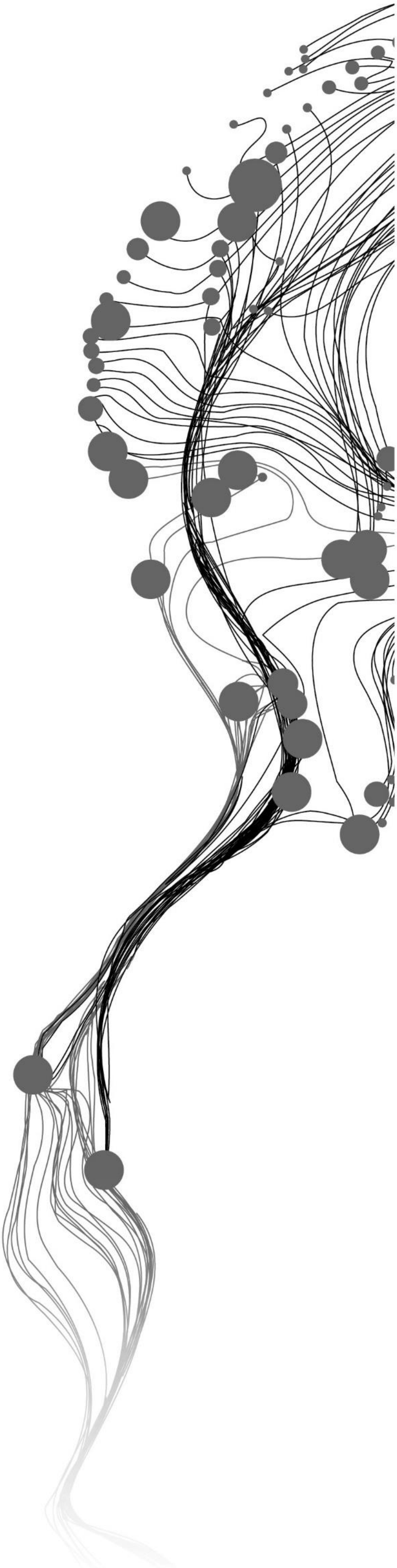

CALIBRATING A VHR SENSOR BASED ABOVEGROUND BIOMASS MODEL WITH UAV FOOTPRINTS IN A DUTCH TEMPERATE FOREST.

LUIS ALONSO FIGUEROA SÁNCHEZ
Enschede, The Netherlands, August, 2021

Thesis submitted to the Faculty of Geo-Information Science and Earth Observation of the University of Twente in partial fulfilment of the requirements for the degree of Master of Science in Geo-information Science and Earth Observation.
Specialization: Natural Resource Management

SUPERVISORS:
ir. L.M. van Leeuwen (First Supervisor)
drs. Ing. Margarita Huesca Martínez (Second Supervisor)

THESIS ASSESSMENT BOARD:
dr. R. Darvishzahed Varchehi
dr. Tuomo Kauranne (External Examiner, Lappeenrranta University of Technology, Finland)

ABSTRACT

Forests play a vital role in the sequestration of carbon dioxide from the atmosphere, this in turn mitigates climate change. The carbon stored in forests can be found in different pools. Aboveground biomass (AGB) is one of the main pools that is most commonly monitored. As anthropogenic pressure on these ecosystems increases in the form of deforestation and forest degradation, reliable methods for the quantification of AGB over extensive areas have to be developed. Allometric equations can be used to estimate AGB by using biometric tree data. In large areas, this is time consuming and non-practical. Therefore, the UNFCCC has promoted the use of remote sensing technology to achieve this task. Unmanned Aerial Vehicles (UAVs) and satellite constellations are earth observation technologies that have been used extensively in forestry applications. UAVs are known to be highly customizable and easily operatable whilst providing very high spatial resolution data over small areas. Satellite constellations are exploring the boundaries of big geodata by providing high spatial resolution data in shorter revisit times, but have the disadvantage of providing small spectral resolutions. Previous research has used these remote sensing technologies in combination to map AGB. Linear regressions have been widely used to relate AGB and an explanatory feature derived from the sensor in order to map AGB. But linear regressions have been established to relate both sensors resulting in high errors at very high spatial resolutions. The addition of UAV data and machine learning algorithms may solve previous shortcomings. This study aims at estimating AGB through the use of a combination of UAV data, high spatial resolution satellite imagery and machine learning algorithms in a mixed temperate forest, Haagse Bos, Netherlands.

A model calibration approach is proposed for this study in which the satellite AGB model is based on the output of a UAV AGB model. To achieve this, an object-based image analysis was implemented to segment coniferous and broadleaf tree species to obtain explanatory features from UAV data. The accuracy of the watershed segmentation was evaluated by using three performance metrics: over segmentation, under segmentation and total segmentation error. A total of 42 explanatory features were obtained based on multispectral layers, vegetation indices, canopy height model and gray-level co-occurrence matrices. Random Forest (RF) and Support Vector Machine (SVM) regression algorithms were used to predict AGB based on the explanatory features. Based on the UAV AGB estimations, explanatory features were extracted from the satellite image at a pixel level. The RF and SVM algorithms were again assessed by the performance metrics calculated from a 10-fold cross validation and a test set.

The study's analysis showed that the estimations of AGB performed better when generating two separate models for coniferous and broadleaf tree species in both the UAV and satellite stage. For the estimation of AGB with the UAV data, the information provided by the canopy height model gave the most predictive power to both models. Following this explanatory feature, the coniferous regression model preferred the texture layers while the broadleaf model gained more information with the red band layer and the crown projected area of each canopy. Both tree types recorded their best performance in the SVM regression algorithm. With only the 15 most important explanatory features, the coniferous model obtained the highest R^2 of 73.7%. The broadleaf model obtained its highest R^2 of 62.6% with the tops nine features. In the satellite data, the inclusion of elevation data was necessary to improve the results of the regression models. The canopy height model was the most important feature for both predictive models. In both cases, the Random Forest algorithm outperformed the performance metrics of the SVM algorithm. The highest R^2 recorded for the coniferous tree species was of 54.0% by using the top 13 explanatory features. The broadleaf model recorded a lower performance in comparison. Using the 20 most important features, an R^2 of 43.6% was obtained. The moderate performances of the VHR model can be attributed to the error propagation provided by the location of the measured trees, individual tree segmentation, and overestimation and underestimation of the UAV regression models.

Keywords: AGB, Machine Learning, UAV, Tree Segmentation, Feature Importance, Explanatory Features, Remote Sensing Synergy

ACKNOWLEDGEMENTS

I would like to thank my first supervisor, ir. L. M. van Leeuwen, for the valuable discussions and critical feedback done in my thesis work. I also appreciate the moments in which we would discuss topics that were outside of the academic field; it definitely helped during the most challenging moments of the pandemic. I would also like to thank my second supervisor, drs. ing. M. Huesca Martínez, who would offer her time to aid me in my learning process of machine learning algorithms. In several occasions, she went above and beyond to help my research.

I also extend my sincere thanks to dr. R. Darvish for her thorough and constructive feedback during the various assessments of my thesis work. I would also like to thank drs. R. G. Nijmeijer, NRM course director, for overseeing the development of this work in the proposal and mid-term stages. A special thanks to dr. M. Belgiu for her help in starting my journey into coding for what seemed something so complex at the beginning. Your availability and interest in my work is appreciated and has sparked my interest in machine learning and several coding languages.

A very special thanks to the fieldwork team: Srilakshmi Gnanasekaran, Hasan Ahmed, Lesa Chundu, Efia Addo and Euphrasia Chilongoshi. From cold, rainy weather to ticks in tall grass, it was always a pleasure to be out on the field with this team. I would also like to thank Ba. T.M.R. Roberts and MSc. C. Marcatelli for collecting UAV data through several days of work.

To the friends made along the way, I can't thank you enough for the needed laughs and bonding made in these two years, especially during the pandemic. I've learned so much from so many cultures: the food, the languages, the different ways of seeing the world. Thanks for making me feel that I was not alone and that we all shared similar struggles, not only academically. I appreciate that we kept our conflicts only during our boardgame sessions.

To MSc. Catarina Lourenço, which I know hates being included in acknowledgements, but you just made my work so much easier. Your insights and critical feedback of my work, your guidance through learning how to use Stack Overflow and keeping me motivated through the toughest of tough. I can't thank you enough.

Finally, I would like to thank my family which have supported me even though I keep going further and further away from home. You are my foundation, thank you for your unconditional love and support, and for always pushing me to be the best I can.

Thank you,
Luis Alonso Figueroa Sánchez
August 2021.

TABLE OF CONTENTS

LIST OF FIGURES

LIST OF TABLES

LIST OF ACRONYMS

ACR	American Carbon Registry
AHN	Actueel Hoogtebestand Nederland
LiDAR	Light Detection and Ranging
AGB	Aboveground Biomass
CCBA	Climate, Community, and Biodiversity Alliance
CHM	Canopy Height Model
CO_2	Carbon dioxide
CPA	Canopy Projection Area
DBH	Diameter at Breast Height
DGPS	Differential Global Positioning System
DSM	Digital Surface Model
DTM	Digital Terrain Model
ESA	European Space Agency
FAO	Food and Agriculture Organization of the United Nations
FRA	Forest Resources Assessment
GCP	Ground Control Point
IPCC	Intergovernmental Panel on Climate Change
MLA	Machine Learning Algorithms
OOB	Out-of-bag
REDD+	Reducing Emissions from Deforestation and Forest Degradation
RF	Random Forest
SfM	Structure from Motion
SVR	Support Vector Regression
UAV	Unmanned Aerial Vehicle
UNFCCC	United Nations Framework Convention on Climate Change
USAID	United States Agency for International Development
VCS	Verified Carbon Standard

1. INTRODUCTION

1.1. Background Information

According to the Global Forest Resources Assessment 2020 (FRA 2020), forests cover accounts for 30.8% of global land cover (FAO & UNEP, 2020). Forests play a vital and recognized role in the sequestration of carbon from the atmosphere. They are known to sequester and store more carbon than any other ecosystem on the planet and have the potential to sequester about one-tenth of global carbon emissions by 2050 (Gibbs, Brown, Niles, & Foley, 2007). Once a forest has been altered (i.e., degraded or deforested), the carbon stored in the trees is released, reducing the area of carbon sinks on the planet and adding more CO_2 to the atmosphere. From 2000 to 2009, deforestation accounted for 12% of global CO_2 emissions (IPCC, 2014). In Europe, about 42% of the land area is covered with forests which translates to the absorption of 417 million tons of CO_2 equivalent in 2017 (Eurostat, 2018).

Thus, it is of high relevance to not only increase the carbon sinks in our planet but also to maintain the ecosystems that we currently have. Furthermore, there is a need to continuously measure the amount of carbon that forests have in order to detect changes over time or determine the health of forests. These measurements enable both private and public stakeholders to implement appropriate strategies and policies for forest conservation. This led the United Nations Framework Convention on Climate Change (UNFCCC) to establish a program that mitigates climate change through forest management, also known as Reducing Emissions from Deforestation and Forest Degradation (REDD+). The REDD+ framework has its own method for measuring, reporting, and verifying (MRV) the carbon stocks in forests in developing countries (USAID & FCMC, 2013). This has led the way for organizations such as Verified Carbon Standard (VCS), Climate, Community, and Biodiversity Alliance (CCBA), Plan Vivo, and The American Carbon Registry (ACR) Standard to also develop their own methods for quantifying carbon stocks in forests.

Aboveground tree biomass refers to the weight of the portion of a tree found above the ground surface that had all of if water content removed to reach a constant weight (Sar & Further, 2020). The most direct way of estimating aboveground biomass in a forest is the destructive method, also known as the harvest method (Vashum & Jayakumar, 2012). This destructive sampling method is extremely tedious and not always practical; this process requires trees as samples, which in turn removes parts of the carbon sinks. Thus, the use of allometric equations is practical. Allometric equations describe the relationship between one, easily measurable parameter of a tree to another non-measurable one (i.e. the trunk diameter of a tree correlated to the trunk weight) (Sar & Further, 2020). Several biometric parameters can be used to determine the biomass of a tree, such as diameter at breast height (DBH), the height of the tree, and wood density (Basuki, van Laake, Skidmore, & Hussin, 2009). DBH is essential in assessing biomass because it is highly effective at explaining more than 95% of the variation of aboveground biomass (Brown, 2002). Carbon stocks are typically derived with the assumption that 50% of aboveground biomass is made out of carbon (Schlesinger & Bernhardt, 2013). The process of measuring biometric parameters as input in allometric equations over a large area is, again, unwieldy and impractical. Measurements on the field are difficult to obtain over large areas, time-consuming, and require effort from multiple trained personnel (Hickey, Callow, Phinn, Lovelock, & Duarte, 2018; Nordh & Verwijst, 2004).

To ease the process of biomass estimation inventories at a national and sub-national level, the UNFCCC has recommended the use of remote sensing methodologies as a non-destructive alternative (SBSTA, 2009). These techniques can provide large-scale and accurate biometric information for the estimation of biomass in forests. Several authors have proven a direct correlation between biometric data captured in the field and quantifiable parameters captured in remote sensing techniques (Anderson, Kupfer, Wilson, & Cooper, 2000; Hirata, Tsubota, & Sakai, 2009; Shimano, 1997).

Previous remote sensing methods of estimating biomass used multispectral broadband sensors to relate existing vegetation indices to vegetation biometric parameters (Clark et al., 2001). Examples of these are low spatial resolution satellites like MODIS (Nguyen, Jones, Soto-Berelov, Haywood, & Hislop, 2020; Xue, Ge, & Ren, 2017). Satellites with medium spatial resolution (10 to 30 meter/pixel) such as GeoEye and QuickBird (Jachowski et al., 2013; Kross, McNairn, Lapen, Sunohara, & Champagne, 2015) have been used to estimate AGB with remote sensing. Other studies have integrated the use of textural layers from satellite images and proved that the accuracy Improves when using spectral and texture layers in combination (Dang et al., 2019; Xie, Chen, Lu, Li, & Chen, 2019). Common drawbacks of using these types of multispectral broadband sensors include cloud coverage, low spatial resolution, and the non-suitability of revisit times of the sensors (Koh & Wich, 2012).

Satellite images with high to very high spatial resolution (30 centimetre to 5 meter/pixel) have the ability to identify singular objects; depending on the satellite, canopy structure can be identified. Studies using very high spatial resolution images with multispectral capabilities obtained good performance on model fitness for estimating aboveground biomass in coastal wetlands by using vegetation indices derived from the four spectral bands (Miller, Morris, & Wang, 2019).Drawbacks of this type of data is the high cost of some providers. Another disadvantage of high spatial resolution satellites is the low spectral resolution offered by these satellites, often only offering the visible range (red, green and blue) and possible the near infrared bands (red edge and NIR). This type of technology is becoming more available to national governments and institutions through several partnerships.

Hyperspectral remote sensing data is capable of capturing a great number of narrow bands which enables the generation of multiple spectral metrics and highly detailed spectral profiles. Studies have used hyperspectral data and laser scanning technology as tool to derive forest structure features or classes for biomass estimation (Kattenborn, Lopatin, Förster, Braun, & Fassnacht, 2019; Lu et al., 2020; McClelland, van Aardt, & Hale, 2019; Zou et al., 2019). Hyperspectral information could better differentiate species which would serve as an important feature to train regression models at a UAV level. The main limitations of this type of data is the availability and the cost, but new promising satellite missions are expected to surpass these limitations (Galidaki et al., 2017).

An alternative active sensor that can be used in biomass assessment is LiDAR (Light Detection and Ranging). LiDAR technology generates a set of points that model terrain and surface, also knows as a digital terrain model (DTM) and digital surface model (DSM) (i.e., the forest floor and the canopy of the trees). A canopy height model (CHM) can be calculated from the difference between these two models (Phua et al., 2016). Other metrics can be derived from each individual tree, such as the percentile of heights, the percentile of intensity, or the amount of returns (Roussel et al., 2020). The output describes the height of trees, which is another biometric parameter that is significantly correlated to AGB. When combined with other biometric data such as DBH, the allometric model becomes more accurate (Chave et al., 2014; Drake et al., 2003; Mtui, 2017). Laser scanning sensors can greatly aid in the segmentation of individual trees and would also produce more accurate canopy height models. However, the acquisition of this type of data is costly and, similarly to the multispectral broadband sensor, the reduced frequency of data acquisition renders accurate forest monitoring impossible (Beland et al., 2019).

Synthetic Aperture Radar (SAR) data has been widely used as another alternative for the estimation of biomass. This type of data can surpass most of the common problems found with optical sensors like cloud cover and penetration of forest canopy layers. SAR's C and L bands with HH and HV polarization have been found to be the best combination for the estimation of broadleaf and coniferous forests (Sinha, Jeganathan, Sharma, & Nathawat, 2015). Limitations in SAR data are also varied and complex. For now, the acquisition of radar data is costly when compared to freely available optical data and there is a limited amount of satellite constellations that acquire this data. Another main limitation for SAR data is its common saturation problems in dense vegetation shown in the C, L and P bands (Joshi et al., 2017; Nuthammachot, Askar, & Stratoulias, 2020).

Unmanned Aerial Vehicles (UAVs) are remotely piloted aircrafts that are easy to operate and can acquire high-resolution images at a low cost (Akturk & Altunel, 2019). UAVs can also acquire images with large overlap between them, which allows the calculation of a 3D point cloud from which surface and terrain models can be derived using Structure from Motion (SfM). The SfM process utilizes matching points identified in the overlapping images to generate a 3D reconstruction of the surface through a dense point cloud of spatially referenced points (Dempewolf, Nagol, Hein, Thiel, & Zimmermann, 2017). The generation of a CHM with the use of this technology can be done accurately and with high spatial resolution (centimetre-wide pixels). UAVs have enough spatial resolution to perform proper tree segmentation by identifying the Crown Projected Area (CPA) (Lin, Meng, Qiu, Zhang, & Wu, 2017; Modica, Messina, De Luca, Fiozzo, & Praticò, 2020). Previous studies have proven that the relationship between CPA and DBH can be used as input in allometric equations and hence to estimate AGB, thus being able to delineate and use the canopy area of each individual tree provides useful information to predictive models (Shimano, 1997).

Although UAVs have many advantages, the spatial coverage for most types of UAVs (e.g., small multi-rotor drone) is a limitation. The main limitation to these types of UAV's is the battery capacity which does not only dictate the flight time (approximately 20 minutes for the DJI Phantom 4), but also provides the necessary energy to operate any external sensor mounted to it (e.g., multispectral sensor). This has lead to the fact that UAVs are mostly used as a sampling tool or as a means for getting intermediate data in sampling patches of a large forest area (Wang et al., 2020). Since forest inventories are required at a national to sub-national level or for large areas, the use of UAVs might seem impractical. However, UAV and satellite constellations can complement each other to overcome their shortcomings. The relationship between UAV and satellite constellations was defined by Emilien (2021) as multiscale explanation and model calibration. Multiscale explanation studies the same object at different spatial scales: the data extracted at a finer scale from a small site is used to explain information from a larger extent with coarser resolution. Model calibration refers to the use of one data source to calibrate a model based on the other data source.

For the synergy between sensors to be successful in predicting aboveground biomass at different scales, there has to be a relationship between field data and UAV data, and subsequently, a correlation with the satellite imagery. Once biomass has been calculated from field observations, a biomass prediction model can be generated from the relationship between an explanatory feature (i.e., reflectance, vegetation index, height) derived from remote sensing data and the estimated biomass (i.e., target variable). Another approach of extrapolating forest biomass sample into a map is the use of nonparametric algorithms such as Random Forest (RF) and Support Vector Regression (SVR). Machine learning algorithms (MLA) have gained popularity in the field of ecology due to their ability to classify or predict a target variable based on multiple explanatory features (Mascaro et al., 2014).

The spectral response of optical data, height metrics derived from UAV point cloud data, and image textures can be used as explanatory features from which MLA acquire information to recognize patterns, and make predictions on to what those features represent (Sar & Further, 2020). The high spatial resolution provided by UAV data makes it possible to extract explanatory features from individual trees. Such features may include the mean, maximum, and minimum reflectance values for each tree as well as derived vegetation indices derived from the available spectral bands. The vertical data provided by the UAV makes tree height available that can also be included as an explanatory feature; although height in dense vegetation has been proven to have errors (Alonzo, Andersen, Morton, & Cook, 2018; Jayathunga, Owari, & Tsuyuki, 2018; A. Navarro et al., 2020). The high spatial resolution of satellite images like the ones provided by the PlanetScope constellation of satellites makes it possible to extract features at a pixel level which resembles individual trees. Satellite imagery also provides spectral values that can be used to find a relationship with the biomass predicted with the use of UAV data. Recent literature has also calculated and used texture metrics in the form of Gray-Level Co-Occurrence Matrices (GLCM) (Dang et al., 2019).

The RF algorithm learns to identify complex patterns through a set of explanatory variables that describe the desired the target variable (i.e., forest features teach the model to predict biomass). RF generates a conglomerate of decision trees (hence the name) to either solve classification or regression problems. Simple or complex regressions can be generated with minor parameter tunning. More trees do not always translate into a better model. It does increase the computational time for the algorithm to generate the defined number of trees. A process of iteration between these two parameters needs to be developed to ensure the best prediction accuracy (Breiman, 2001).

Another advantage of using RF is the capability of learning which features are more important at describing biomass. Pandit et al. (2018) found that the features extracted from individual bands were less important in describing biomass when compared to vegetation indices and forest structure features. Feature importance is relevant because it allows the algorithm to focus more on variables that are more pertinent, while omitting variables that are irrelevant or highly correlated to other variables. Less variables also means that the model is less prone to overfitting, a common problem found in MLA.

The SVR algorithm is based on the same principles of the support vector machine (SVM) which has been widely used for classification of highly non-linear data (Chih-Wei Hsu, Chang, & Lin, 2008). The objective of the algorithm is to generate a hyperplane that best resembles the input target variable by learning from the explanatory features. Both SVM and SVR utilize kernels that project the data to a higher dimensional feature space which makes the classification or prediction a linearly solvable problem.

As of April 2020, several authors have studied the feasibility of using UAV imagery to upscale biomass to broader areas using satellite images. Similar methods found through literature review reveal that attempts to upscale biomass for boreal forests have yet to be thoroughly explored. Mangroves, on the other hand, have been subject to several studies in which field plots, UAV derived biomass and satellite data are integrated for wall-to-wall estimation of biomass. Navarro (2019) utilized multispectral imagery captured with UAV in order to derive features to generate plot-based aboveground biomass estimations to later train a SVR algorithm using features derived from Sentinel-1 and Sentinel-2. A plantation of mangroves was used as a study area. The performance of the generated output ranged from an R^2 of 71% to 90% at the satellite scale. The range of biomass values found for this study were low compared to the expected values for a boreal forest. Wang (2020) collected biometric data for several species of mangrove and related them to biometric parameters derived from UAV-LiDAR data by using a RF algorithm. The resulting biomass predictions were later used as a base to predict biomass at a pixel level with the use of vegetation indices derived from Sentinel-2 images. The study found that using UAV-LiDAR data as an intermediate step to estimating aboveground biomass yielded a better result than a traditional ground-to-satellite approach (R^2 of 62% and 52% respectively and RMSE of 50.36 versus 56.63 ton/ha). Zhu (2020) utilized UAV multispectral data and optical and SAR satellite data (Gaofen-2 and Gaofen-3) to estimate aboveground biomass in an artificial plantation of mangroves by using a RF algorithm. Several models were generated by combining the features extracted from each data source. The coefficient of determination of the various models ranged from values as low as 12% to a maximum of 61%; this value was achieved by integrating height values, which was also proven to be the most important feature. Iizuka (2020) used SAR data, UAV imagery and TLS information to predict tree volume in a conifer plantation by using RF and SVR algorithms. At the satellite level, the RF and SVR models yielded an R^2 of 66.5% and 51.9% respectively, proving that the integration of field data and several remote sensing data can reasonably predict biomass.

1.2. Problem Statement

The high spatial resolution and multispectral data of UAV imagery allow derivation of forest structure features. (Kachamba, Ørka, Gobakken, Eid, & Mwase, 2016; Miller et al., 2019; Ota, Ogawa, Mizoue, Fukumoto, & Yoshida, 2017)**.** These have been used to map AGB by creating simple linear regressions with field data (e.g., the relationship between DBH measured on-field and canopy projected area derived from UAV imagery). Prior studies have shown that the implementation of MLA, in specific RF and SVR, provide better accuracies among other empirical models when trying to predict biomass (Lu et al., 2020; Nguyen et al., 2020).

One of the limitations of small to mini multi-rotor UAVs is the spatial coverage in which they can operate. Although UAVs can be deployed with ease over several areas, covering extensive forest landscapes is inefficient due to the limited flight times that this type of technology offer. Also, the very high resolution of UAV data requires large storage space and entails longer processing times if used for very large areas. To overcome this issue, high spatial resolution satellite images can use information derived from UAV data as samples to create a wall-to-wall image of a much larger area (Emilien et al., 2021; Li et al., 2019; Riihimäki, Luoto, & Heiskanen, 2019; Wang et al., 2020). A two-step model calibration can be accomplished by establishing a relationship between (1) AGB calculated from field observations and UAV derived features, and (2) between AGB estimated from UAV derived features and satellite imagery features. Both processes can be done through the use of MLA, as shown in previous works (da Conceição Bispo et al., 2020; Lu et al., 2020; Miller et al., 2019; Zhang, Ma, Liang, Li, & Li, 2020).

Thus, this study aims to generate a method that uses aboveground biomass derived from UAV imagery to estimate biomass using satellite data, ensuring high accuracy carbon estimation of a large-scale carbon stock map. Furthermore, we set out to assess the role of features derived in both UAV and satellite data.

1.3. Research Objectives

The main objective of this research is to develop a MLA based method to predict aboveground tree biomass by using UAV and satellite data in two stages. The output generated by the UAV-based model will serve to calibrate the model using the satellite data.

1.3.1. Specific Objectives

1. To define feature importance of explanatory variables derived from UAV to be used in MLA in order to predict AGB;
2. To identify feature importance of explanatory variables derived from satellite imagery to be used in MLA in order to predict AGB;
3. To evaluate the change in performance metrics of the MLA with feature reduction based on importance;
4. To assess the accuracy of the AGB predictions done with UAV data in the different surveyed areas of Haagse Bos;
5. To assess the accuracy of the AGB predictions done with a combination of UAV data and satellite imagery for the entirety of Haagse Bos;

1.3.2. Research Questions

1. Which set of features derived from UAV data and satellite imagery can be used to estimate AGB using MLA?
2. Which set of features derived from UAV data are more important at predicting AGB?
3. How are the performance metrics impacted by different MLA and feature reduction in the UAV model?

4. How accurate is the machine learning algorithm in classifying aboveground biomass content using features derived from UAV data?
5. Which set of features derived from satellite data are more important at predicting AGB?
6. How are the performance metrics impacted by different MLA and feature reduction in the satellite model?
7. How accurate is the machine learning algorithm in classifying aboveground biomass content using features derived from satellite imagery?

1.4. Conceptual Diagram

The conceptual diagram shown in Figure 1 shows the synergy between earth observation sensors and the structure of the study area. Haagse Bos contains coniferous and broadleaf trees scattered in the forested area. Some areas are mixed forest, while other areas are kept to only one tree species. The trees serve as a carbon pool, storing aboveground biomass which can be estimated with allometric equations and features derived from remote sensing technology.

The other essential systems in this study are the earth observation sensors and platforms like UAVs and satellite constellation. These sensors are used to collect multispectral data at different spatial resolutions and covering different spatial areas in order to estimate AGB from the trees inside Haagse Bos. UAVs can only cover multiple small patches of land. Thus, the estimated AGB from UAV data can serve as the target variable to generate a regression model using explanatory features derived from satellite imagery.

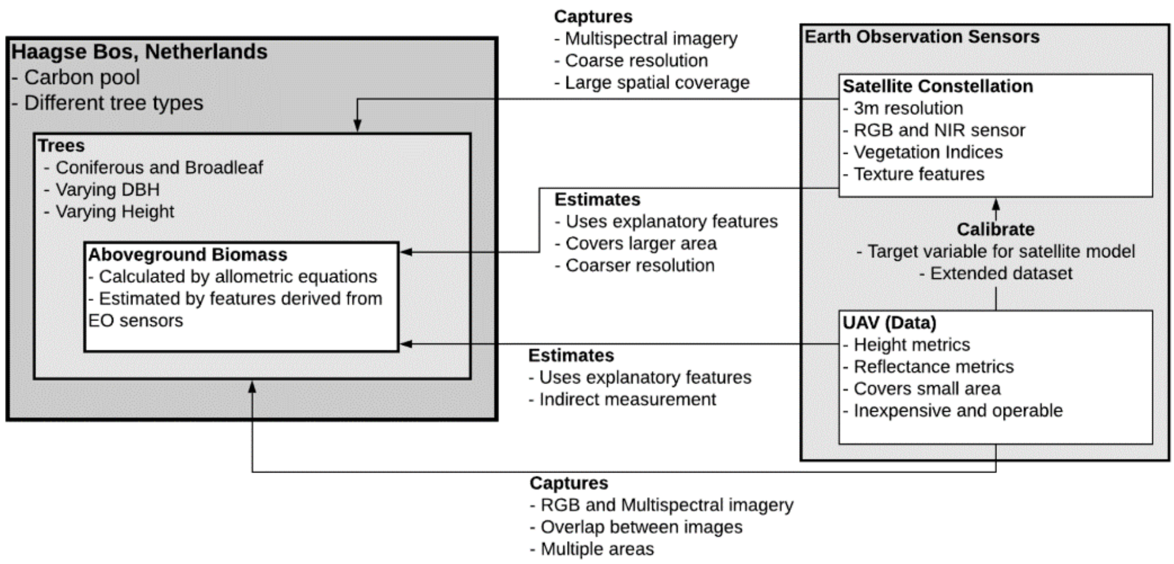

Figure 1. Conceptual Diagram

2. MATERIALS & METHOD

2.1. Study Area

The justification of the selection of the study area is partly due to the COVID-19 pandemic experienced throughout the year 2020 and 2021. The study area had to be a forest nearby the city of Enschede in order to facilitate transportation for the fieldwork team. The Haagse Bos lies near the city of Enschede. It is comprised of small patches of coniferous, broadleaf, and mixed forests. The Haagse Bos is a nature monument, which are considered a protected area with legal status under the Dutch Nature Conservation Act of 1998 (Mohren & Vodde, 2006). Previously, the Haagse Bos was used solely as a production forest, but has then been changed to conservation for its aesthetic values. Economic income for the protection of the forest is provided by some areas that are still used for wood production, but mostly it is the agricultural land that provides most of the revenue.

The forest had previously been used as a production forest, but in 1969, a part of it was bought by Natuurmonumenten and changed its status as a naturally managed forest (Damhof, 2020). Individual private owners assign Bureau Takkenkamp BV as a forest manager, thus this land is managed differently depending on the requests of the owners. Some land is used for the harvesting of timber to provide a steady income to the original holders of the land; other parts of the land do not allow the altering of the landscape as requested by the proprietors.

2.1.1. Geographical Location

Haagse Bos forest (Figure 2) is located between 6° 56' 25.728" E – 6° 58' 20.856" E and 52° 14' 57.192" N – 52° 16' 41.340" N. The study area is located in the province of Overijssel and lies between the boundary of the municipalities of Enschede and Losser. The area of Haagse Bos is around 300 hectares, this is including the patches of land scattered across the forest that are pasture.

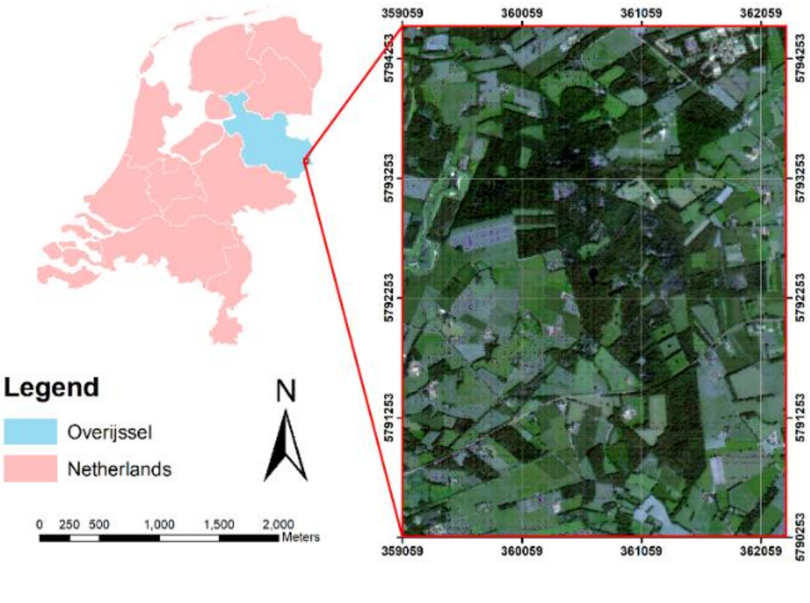

Figure 2. Study Area, Haagse Bos as seen by PlanetScope on 5th of August of 2020.

2.1.2. Climate & Topography

July is the hottest month of the year in the region with a recorded daily mean temperature of 22.8 °C. The coldest month is January with a daily mean temperature of 2.3 °C. Average precipitation over a year is around 785mm, with the months of July and August having 20% of the annual precipitation (KNMI, 2010).

2.1.3. Vegetation

The forest consists of young and mature broadleaf and coniferous species. A representative of Bureau Takkenkamp BV states that they have recorded twenty different species inside Haagse Bos. Since the study area used to be a production forest, the arrangement of the majority of the trees are in rows. From fieldwork done through the months of August through October of 2020, the most common trees encountered in the surveyed 90s are displayed in Table 1

Table 1. Common encountered species in Haagse Bos

Common name	Scientific name
Douglas Fir	*Pdseudotsuga menziesii*
Common Ash	*Fraxinus excelsior*
European Beech	*Fagus sylvatica*
European Larch	*Larix decidua*
European White Birch	*Betula pendula*
Norway Spruce	*Picea abies*
Pedunculate Oak	*Quercus rubra*
Scotch Pine	*Pinus sylvestris*

2.2. Materials

This section includes a brief description of the field equipment and software used to collect and process data for this study.

2.2.1. Field Equipment

The tools and equipment mentioned in Table 2 were used in the measurements of the trees during fieldwork data collection as well as capturing multispectral data of the forest.

Table 2. List of field equipment, brand and its uses.

Equipment/Tools	Brand	Use
UAV Drone	DJI Phantom 4	Image capture
Measuring tape (20m)	N/A	Delineation of boundary plots
Diametric tape (2m)	N/A	DBH measurement
Laser measurer	Leica DISTO D5	Height measurement
GPS	Garmin eTrex 20x	Navigation
Clinometer	Santo	Slope measurement
Form and pen	N/A	Data recording
DGPS	Leica GS14 DGPS	Recording of GCPs and plot location

2.2.2. Data Processing Software

The list of software used for processing and analysing the data from the study area are presented in Table 3.

Table 3. List of software and uses.

Equipment/Tools	Use

ArcMap 10.6.1	Geographic data processing and visualization
Pix4D Mapper	UAV data processing and visualization
ERDAS Imagine	Enhancement of UAV and satellite images
Microsoft Word	Thesis writing and preliminary reports
Microsoft Excel	Data analysis
R Studio	Statistical analysis
Agisoft Metashape	UAV data processing and correction
eCognition Developer	Individual tree crown extraction

2.2.3. Data

The UAV data used for this study was obtained through the use of a Parrot Sequoia camera mounted on a DJI Phantom 4. The satellite data was acquired by a PlanetScope satellite and additional height information from

Table 4. List of data used in this study

Data	Source	Acquisition Date
UAV Multispectral Images	Parrot Sequoia	September to October of 2020
Elevation data	DJI Phantom 4	September to October of 2020
Tree biometric data	Field work	September to December of 2020
LiDAR elevation data	Actueel Hoogtebestand Netherlands	Between the years 2014 to 2019
Satellite Image	Planet Labs Inc.	September 5th of 2020
Ground Control Points	Leica GS14 DGPS	September to October of 2020

2.3. Research Methods

The research method of this study was comprised of three general steps:

1. The first step involved the collection of field data through ground plots and the use of a small multi rotor UAV for the collection of UAV multispectral data. The acquisition of the satellite image was also accomplished in this step by requesting it to the corresponding company. Field data acquisition compiled individual tree parameter data (e.g., DBH, height, CPA, species), coordinates of the plot, plot characteristics, individual tree bearings, and GCPs coordinates. The data collection steps are surrounded by the red box in Figure 3.
2. The second step involved the processing of the collected information. Aboveground biomass was calculated from tree parameters measured on ground. These measurements were collected as ground truth data to be used as accuracy assessment and as a base for the upscaling of AGB estimation with UAV data and satellite imagery. With the use of Pix4Dmapper, UAV images were processed to generate orthophoto with reflectance values, 3D point clouds, DSM and DTM; the GCPs collected were used to georeference the UAV data. ERDAS Imagine was used to enhance the satellite image from September 2020 for feature extraction at a later stage. A set of explanatory features were extracted from the UAV orthophotos and the satellite image. A combination of reflectance values, height, and texture features were derived. The previous steps are delineated by the blue box in Figure 3.
3. The last step (data analysis) estimated AGB at both UAV and satellite scales. The RF algorithm and the SVR were used generate models trained with the derived explanatory features from both platforms. The RF algorithm also provides the importance of each feature in predicting AGB, which was used to remove redundant features. A 10-fold cross-validation, coefficient of determination, root-mean-square error, and relative root-mean-square error were calculated to assess the performance of the models generated and to quantify the impact of removing redundant features. The data analysis steps are marked in green in Figure 3.

Figure 3 shows the methodological steps of this research:

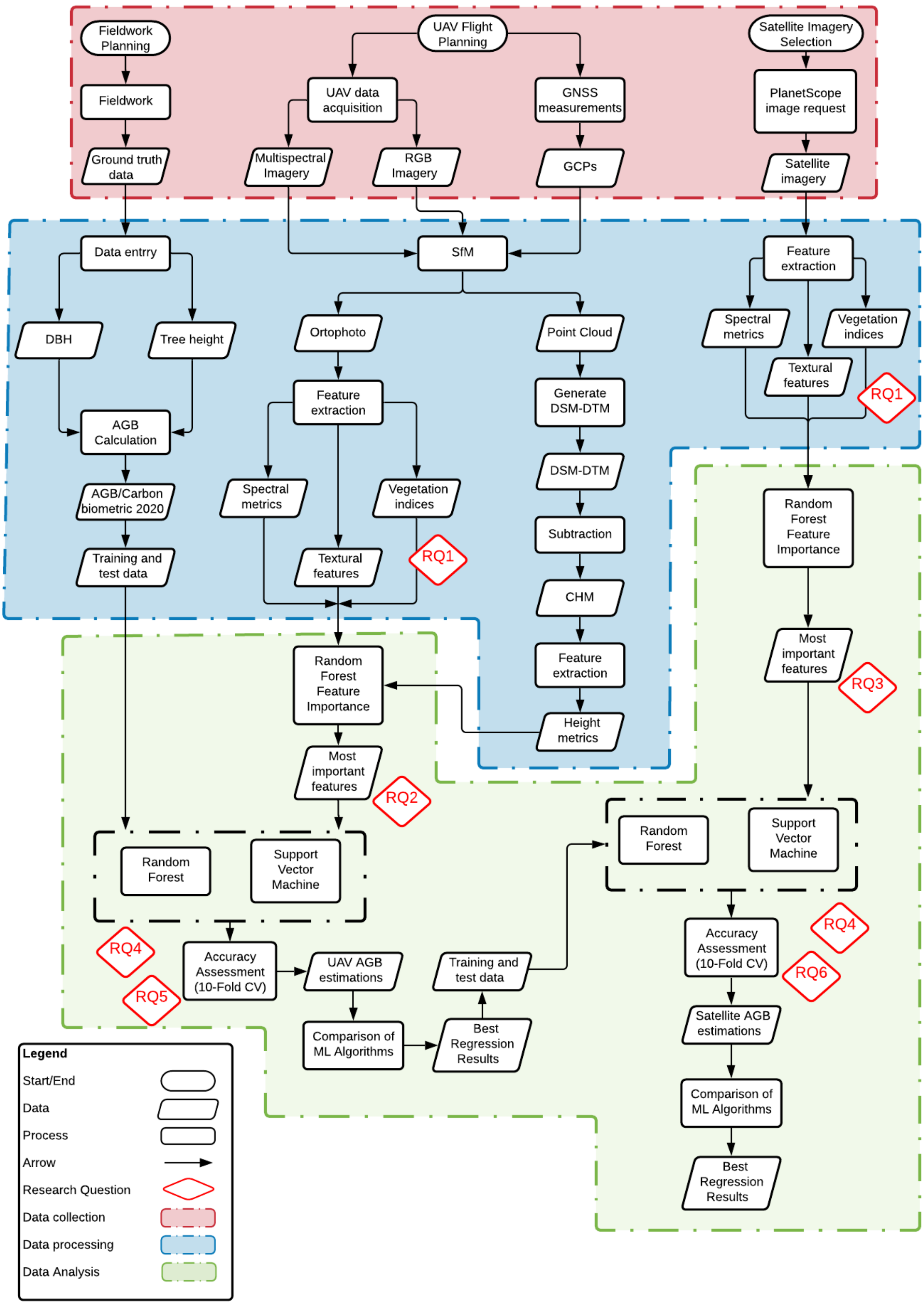

Figure 3. Flowchart of research method

2.4. Data Collection

2.4.1. Sample Plot Design

A plot design, plot shape, and plot size were established on an early stage of this research. A circular plot of 12.62m was chosen due to its simple correlation in representing $1/20^{th}$ of a hectare. It also minimizes the perimeter of the plot and makes the boundary easy to establish and be recognized by fieldworkers (Van Laar & Akça, 2005).

A stratified random sampling method for the ground plots was established based on canopy density. Vegetation distribution maps of the Haagse Bos were gathered to obtain a mixture of species in the sampling. Based on UAV flight areas, a fishnet was generated over the study areas according to plot size. A total of 1,823 potential plots (Figure 4) were generated, from which an equal number of plots were randomly selected and measured according to type of forest (i.e., coniferous and broadleaf forest). A total of 91 plots were measured during fieldwork. Due to cloud coverage on one of the acquired multispectral images, a total of 21 plots were omitted from further analysis. This resulted in 70 plots being used in the data analysis. Data was acquired between the months of August and October of 2020.

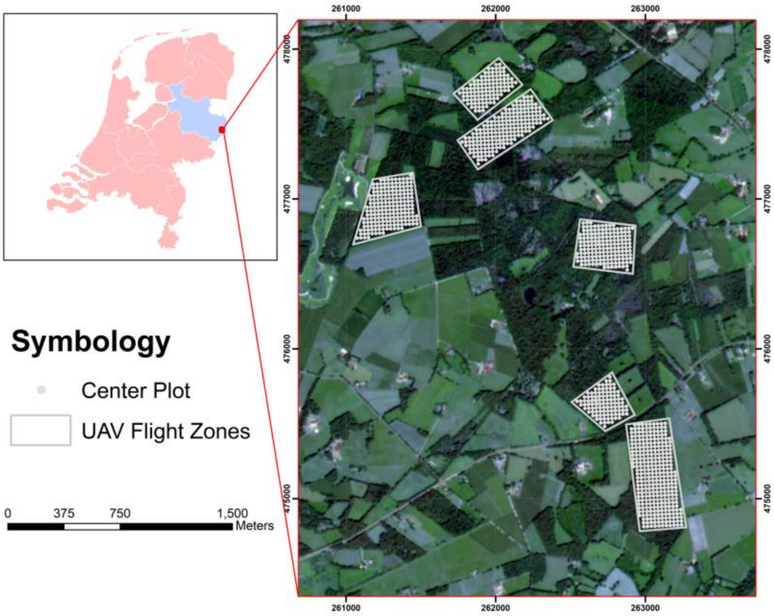

Figure 4. Potential Centre Plots inside Flight Zones

The list of materials presented in Table 2 was used during fieldwork. Upon arrival at a plot, the fieldwork team would identify the circular boundary, identify the trees inside the plot with tags. The height and DBH of the trees with a DBH higher than 10 centimetres were recorded. This method was generated to ensure that the capturing of field data was consistent throughout time and to guarantee the correct use of the spreadsheet to be filled in manually. The collection of data was accomplished by using a manual entry form (see Annex 1).

2.4.2. UAV Flight Planning

Trial surveys were done before the scheduled date for UAV data collection. The most noticeable error found was the absence of imagery in certain regions inside the flight area; this was due to the fact that during the day of the flight it was partially cloudy which made the Sun sensor to malfunction and cause and error as to how to register the metadata of the photographs.

The proposed solutions to evade this error from happening again were: (1) ensure that the day of UAV data collection is an entirely sunny or cloudy day to avoid Sun sensor confusion and homogeneity in the reflectance values, (2) run the UAV flight plan in parallel with the trajectory of the sun to reduce the variance in the reflectance values, and (3) if the past solutions still manifest absence of imagery, then utilize the Agisoft Metashape Software to correct the registration error manually.

2.4.3. UAV Data Acquisition

The designed flight plans were programmed in Pix4Dcapture in order to comply with the solutions proposed above (i.e., a parallel flight with the Sun's trajectory). Flight parameters were established before data collection, namely camera settings, ground sampling distance, overlap, flight height, area coverage and global navigation satellite system. A total of eight areas with an area between 13 to 16 hectares each were captured. The UAV drone carried cameras capable of capturing green, red, red-edge and near infrared (NIR) reflectance values. Table 5 summarizes the parameters used for the data acquisition.

Table 5. UAV flight plan parameters

Parameters	Information
Flight height	100m
Flight mission	Double grid
Flight speed	Moderate
Forward overlap	80%
Side overlap	60%
Image resolution	4000 x 4000 pixel
Captured area	~110 ha
Sensor	RGB & NIR

A total of 45 ground control points (GCPs) were collected by the fieldwork team using a GNSS. The number of GCP points determined the overall accuracy of the georeferencing of the image. A set of crosses printed on paper were placed in open spaces to obtain an image of the control point that were later used in the georeferencing process. Figure 5 exemplifies the distribution of GCPs during data acquisition.

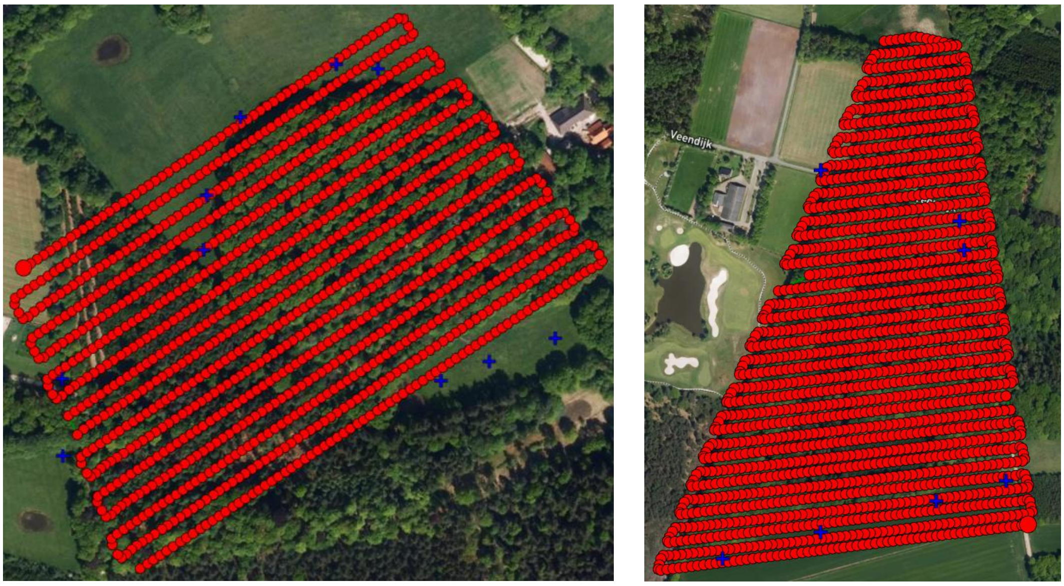

Figure 5. Distribution of GCP (blue cross) and acquired images (red dots) in Block 4 (left) and Block 123 (right)

2.4.4. Satellite Imagery Acquisition

A satellite image from PlanetScope was acquired through the Education and Research Program from Planet Labs, Inc. The image was obtained on August 19th of 2020, but the image was captured on August 8th of 2020. Table 6 summarizes the characteristics of the PlanetScope constellation of satellites and band specifications.

Table 6. Characteristics of Planet Scope satellite and sensor

Characteristics	PlanetScope
Owner/Distributor	Planet Labs Inc.
Ground Sample Distance (m)	3.7
Strip width	16
B1 - Blue (nm)	464 – 517
B2 - Green (nm)	547 – 585
B3 - Red (nm)	650 – 682
B4 - NIR (nm)	846 – 888

2.5. Data Processing

In order to generate regression models for AGB with MLA, we need to obtain explanatory features from both the UAV data and the satellite imagery. The first step is to calculate the AGB from field measurements to serve as a target variable. By using the UAV data, individual tree segmentation was achieved and feature extraction was done for individual trees to serve as explanatory variables to train the MLA. After obtaining AGB estimated from UAV data, feature extraction was done at a pixel level using the PlanetScope satellite imagery. The values from each individual pixel throughout the different layers served as the explanatory variables and the AGB estimated at the UAV stage was used as the target variable.

2.5.1. Biometric Data Processing

The field data for each plot was recorded in Excel. DBH and tree height measured in the field were used to calculate aboveground biomass and carbon stock for each tree using allometric equations and conversion factors as reviewed in the literature. Table 7 summarizes the sources used to obtain the allometric equations. The allometric equations were chosen according to their R^2 value and the operable ranges of DBH and height. All works used were based in Europe, but preference was given to equations that were developed inside the Netherlands or closest to in geographical position. The aboveground biomass was calculated for each tree, and an average is calculated per type of specie.

Table 7. Allometric equations of common tree species found in Haagse Bos.

Tree	Equation	R^2	Ranges of variables	Reference
Douglas Fir *Pseudotsuga menziesii* Netherlands	$\ln(\text{AGB[Kg]}) = -1.620 + 2.410\ \ln(\text{DBH})$	0.995	5 to 50 cm	(Bartelink, 1996)
Common Ash *Fraxinus excelsior* United Kingdom	$\text{AGB[Kg]} = -2.4718 + 2.5466\ \ln(\text{DBH})$	0.985	2.9 to 33 cm	(Zianis, Muukkonen, Mäkipää, & Mencuccini, 2005)
European Beech *Fagus sylvatica* Netherlands	$\text{AGB[Kg]} = 0.0798\ \text{DBH}^{2.601}$	0.988	10.7 to 61.8 cm	(Zianis et al., 2005)
European Larch	$\text{AGB[Kg]} = 0.1081\ \text{DBH}^{1.53}\ \text{H}^{0.9482}$	0.984	4 to 34 cm	(Zianis et al.,

Tree	Equation	R^2	Ranges of variables	Reference
Larix sibirica Iceland			4 to 16 m	2005)
European White Birch *Betula pendula* Sweden	$AGB[Kg] = 0.00087\ DBH^{2.28546}$	0.985	1.8 to 13.7 cm	(Zianis et al., 2005)
Norway Spruce *Picea abies* Germany	$AGB[Kg] = -43.13 + 2.25\ DBH + 0.425\ DBH^2$	0.995	10 to 39 cm	(Zianis et al., 2005)
Pedunculate Oak *Quercus robur* Germany	$AGB[Kg] = 0.0722\ DBH^{2.5135}$	0.970	4.5 to 46 cm	(Suchomel, 2012)
Scots Pine *Pinus sylvestris* Czech Republic	$AGB[Kg] = 0.1182\ DBH^{2.3281}$	0.980	2 to 16 cm	(Zianis et al., 2005)

2.5.2. UAV Image Processing

The images for each of the eight flight blocks were processed in Pix4DMapper in order to generate an orthophoto, DTM and a DSM. The 3D models were constructed from a series of overlapping 2D images captured by the UAV. By matching common points or objects in the image series (also known as key points), a reconstruction of a scene can be built. This is more commonly known as structure from motion (SfM) (Westoby, Brasington, Glasser, Hambrey, & Reynolds, 2012). By using this photogrammetric method, the Pix4D software creates a 3D reconstruction of the study area by matching key points observed in several images. This calculation of points from various camera position leads to the generation of a point cloud. Using GCPs, bundle block adjustment can be accomplished in order to georeference the 3D point cloud to coordinates from camera centres. For further processes, the distinction between ground points and vegetation points is made during this step. This classification is then used to create DTM and DSM layers. Since UAV imagery is not capable of penetrating the canopy structure, dense canopy areas tend to have a low point density. This leads to overgeneralized DTMs which affect the resulting CHM layers. After the generation of the initial outputs, the GCPs were loaded into the software for georeferencing. The GCPs served as a reference in various pictures to increase the precision of the georeferencing process. Once a dense 3D point cloud is generated, the generation of a DSM and a DTM can be done.

The height of trees is a basic property that indicates the structure of a forest. Known relationships have been proven to occur between DBH and height. This study calculated aboveground biomass with allometric equations which had DBH as an explanatory variable, thus obtaining the height variable from individual trees is highly relevant in providing information regarding biomass content. Although height was measured in the field, several authors suggest that field measured height tends to overestimate stature considerably (Jurjević, Liang, Gašparović, & Balenović, 2020; Y. Wang et al., 2019). UAV derived tree heights have been proven to serve as a good measure for tree heights, especially in open canopy areas (Krause, Sanders, Mund, & Greve, 2019). Thus, for this study, UAV derived heights were used as explanatory variables in the MLA, as opposed to field measured heights. To obtain this feature for later use in the regression models, a CHM was generated by subtracting the DTM from the DSM.

$$CHM = DSM - DTM \quad (1)$$

Equation 1. Canopy Height Model estimation

Previous studies have proven the strong correlation between aboveground biomass and vegetation indices derived from RGB and NIR reflectance values. They are highly relevant and have been widely used for the estimation of biomass content in agriculture and forestry applications (Poley & McDermid, 2020). The derived vegetation indices were in accordance to previous studies which used the Parrot Sequoia sensor (or similar sensor capturing red-edge and NIR data) in forestry applications. The generation of vegetation indices (see Annex 3) was executed in the Pix4D software. Individual bands were used to produce four vegetation indices (see Table 8) that were used in several studies to estimate aboveground biomass (Dang et al., 2019; Jin, Li, Feng, Ren, & Li, 2020; Wang et al., 2020; Zhang et al., 2020).
A total of four spectral bands and four vegetation indices, one DTM and one DSM were derived from each block that was covered by the UAV block. All of the layers corresponding to an individual flight block were compiled into a single tiff file. Previous works done in the Haagse Bos area had resampled the UAV images to 20 centimetres in order to reduce computational time of other tasks; it also reduced the amount of detail which was adding noise to the data. To resample the original spatial resolution to a standardized resolution of 0.2 meters between all flight blocks, a bilinear interpolation was used to obtain the average of the nearest cells and maintain the continuity of the data. Annex 2 summarizes the quality reports generated for each UAV flight block.

2.5.3. Satellite Image Processing

The obtained satellite image is a level 3A product from the PlanetScope constellation of satellites. This means that radiometric and sensor correction have been applied to the data, thus obtaining surface reflectance values. Plus, the image was orthorectified and projected to a UTM projection (Planet Labs Inc., 2016). The ERDAS Imagine software was used to reproject the satellite image in accordance to the UAV acquired data, which were projected to the RD New coordinate system (EPSG: 28992) in the Amersfoort datum. Since the satellite image covered an extensive area, an area of interest was generated creating subsets of the original images; this ensured that processing time was reduced.

2.5.4. Feature Extraction – UAV

During fieldwork, direction bearings from the plot centre to each individual tree were taken with a mobile application called Avenza Map. Orthophotos generated by the UAV images serve as a reference during fieldwork. Plot centre locations were later extracted to the ArcMap software to generate a point location layer. The extraction of features from UAV data was accomplished by the delineation of individual trees. At a satellite image level, feature extraction was accomplished at a pixel level.

Individual Tree Segmentation

The delineation of tree canopies was accomplished using eCognition Developer. Segmentation can either be done by a top-down or a bottom-up approach. Top-down means that larger objects in the image will be further segmented until a desired object is met; eCognition Developer offers chessboard segmentation, quadtree-based segmentation and multi-threshold segmentation algorithms. On the other hand, bottom-up segmentation merges smaller objects until a bigger and desired object is met by the user's criteria. The most commonly used segmentation algorithms are the multiresolution segmentation (MRS) and watershed segmentation (WS) (Benz, Hofmann, Willhauck, Lingenfelder, & Heynen, 2004). Dainelli (2021) reviewed 227 peer-reviewed scientific papers in recent literature involving the use of UAS in forestry applications and found that 46% of those studies used a form of WS to segment individual tree canopies. Said works were carried out with a variety of tree species including birch, spruce, scots pine, firs, larch, and mangroves. This segmentation algorithm requires a small amount of parameter tunning and, in this study, proved to be more efficient as segmenting canopies in comparison to MRS.

The WS creates objects by identifying the local maxima (or minima) based on brightness values or height values. The algorithm expands a regional object until it touches a neighbouring object. This algorithm is designed to work best with elevation data, thus the CHM generated by the UAV served as input for this algorithm.
A set of rules was established using the WS. Segmented objects were later refined by classifying objects that had a height lower or equal to 10 meters. These objects were removed because they were small trees which were difficult to segment properly and they do not contribute as much to the overall AGB content of the forest. Objects with an average reflectance value of 0.26 in the NIR band were classified as shadow and were also removed from the final output. Additionally, areas with an area equal or lower to 2.5 meters were omitted to further remove young trees, pasture fields and bare soil from being included to the segmented trees. All remaining objects were classified as trees and were subject to visual inspection and correction, as the WS is dependent of the quality of the CHM. Objects classified as tree with an area smaller than 10 pixels were joined with their closest and biggest neighbour, as they were deemed not feasible to be considered as individual trees through visual interpretation (see Annex 4). Young forests under the specified height threshold were removed due to the inability of the segmentation ruleset to perform a proper partition of young trees. The final objects were then exported with their respective features. Remaining isolated objects that were smaller than 5 m^2 were removed because they did not represent a meaningful canopy structure. Objects generated at the edge of all UAV orthophotos were also removed due to the visible distortions they presented. The ruleset can be referred in Annex 4.

Segmentation Accuracy Assessment

Image segmentation dictates the structure of the data to be used in any regression technique; thus, if low accuracy is present on the segmentation result, the error will propagate into the regression output (Hossain & Chen, 2019). According to Clinton et al., (2010), segmentation accuracy can be assessed through the over segmentation, under segmentation and total detection error of a specific object. A total of 175 clearly visible trees of different sizes were manually digitized for the accuracy assessment of the tree segmentation: 82 were coniferous trees and 94 were broadleaf trees. The area the segmented object and the digitized polygon were calculated through ArcGIS; the overlapping areas between the polygons as well as the remains of the polygons were calculated. Although the UAV images have normalized values, the total detection error was measured per block because of differences in lighting when the flight was accomplished. The ideal value for these assessments is 0, which means that the reference polygon and the segmented object are identical (or near identical).

$$Over\ Segmentation\ (X) = 1 - \left(\frac{ASW \cap AMD}{ASW}\right) \tag{2}$$

Equation 2. Over Segmentation Measure

$$Under\ Segmentation\ (Y) = 1 - \left(\frac{ASW \cap AMD}{AMD}\right) \tag{3}$$

Equation 3. Under Segmentation Measure

$$Total\ Detection\ Error\ = \sqrt{\frac{X^2 + Y^2}{2}} \tag{4}$$

Equation 4. Total Detection Error

Where ASW stands for area of the segmented object by WS algorithm, AMD stands for area of the reference polygon which is manually digitized in ArcGIS and the symbol “∩” represented the area of the segmented object that correctly lies inside the reference polygon.

Features from UAV Data

Four sets of features were derived from UAV data (see Table 8), using eCognition Developer. The first set of features was comprised of reflectance metrics, which correspond to the average and standard deviation of the pixel values found inside a segmented object. The second set of features include the derived vegetation indices from the spectral bands offered by the mounted UAV sensor. These vegetation indices were chosen after literature review which used the Parrot Sequoia sensor for forestry applications (Dainelli et al., 2021; Kopačková-Strnadová, Koucká, Jelének, Lhotáková, & Oulehle, 2021). Other vegetation indices were considered, but were omitted from the final dataset because they were meant for agricultural applications (e.g., wheat or rice biomass content) or used different spectral bands that are not available through the sensor used in this study (e.g., infrared wavelengths). The equations used for the generation of the vegetation indices can be found in Annex 3. The third set of features was comprised of height metrics given by the CHM layer. The set of height metrics included the average and standard deviation values found at individual tree object. The last set of metrics was comprised of Gray-Level Co-occurrence Matrices, which describe the texture of each individual layer. These set of features answers research question #1.

Table 8. Features derived from UAV data.

Metric	Explanatory Features	
Spectral	Brightness	Standard Deviation Green
	Mean Green	Standard Deviation Red
	Mean Red	Standard Deviation REG
	Mean REG	Standard Deviation NIR
	Mean NIR	
Vegetation Indices	Mean NDVI	Standard Deviation NDVI
	Mean WDVI	Standard Deviation WDVI
	Mean DVI	Standard Deviation DVI
	Mean NDRE	Standard Deviation NDRE
Biometric	Mean CHM	
	Standard Deviation CHM	
	Area	
GLCM	Correlation	0°
	Entropy	45°
	Homogeneity	90°
	Mean	135°
		All directions

The features from 14,480 segmented trees were extracted across all UAV flight blocks. The trees used for the training of the model were assigned their respective AGB values through spatial location. This process ensured a one-to-one relationship between AGB value and segmented tree. A total of 965 trees contained the biomass calculated from field data based on the trees measured during fieldwork and seen from the UAV orthophotos. The calculated AGB and the extracted features from each individual tree were used to train MLA in order to obtain a predictive model. The rest of the trees were assigned their AGB value by using the trained model based on the features extracted from each tree segmentation. Feature extraction resulted in a total of 40 explanatory variables

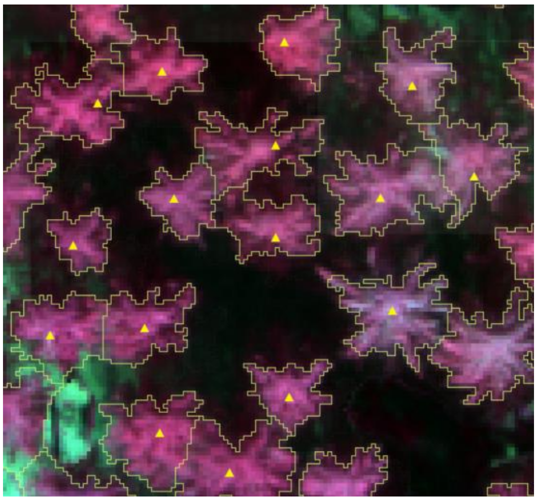

Figure 6. Segmented trees with spatial location of trees of plot 70 (yellow triangle)

2.5.5. Feature Extraction – Satellite

Generation of Additional Layers

The satellite imagery from PlanetScope provides four multispectral bands: blue, green, red and NIR. The red edge band is not available for the satellite image; thus, other vegetation indices were derived. The generated vegetation indices were chosen in accordance to previous published papers which used PlanetScope imagery to estimate biomass and displayed good correlations (R^2 > 60%). A total of six vegetation indices (NDVI, GNDVI, DVI, EVI, SAVI and SR) were generated for the whole study area of Haagse Bos (see Annex 3). A total of eight GLCM layers were generated through the *glcm* statistical package in RStudio by using the NIR band as a reference. The window (kernel) shift applied to the texture layers was specified to be a matrix of 3x3 in order to maintain the majority of the spatial extent. The statistics that were requested from the GLCM were correlation, entropy, homogeneity and mean. The contrast texture layer was eliminated from further tests due to the nature of the layer of having no values in large areas, thus reducing the amount of training and testing data. Since the layer depends on the intensity of contrast in a local window, homogeneous landscapes will generate an output of no values (i.e., NA).

A canopy height model was generated by using the DTM and DSM created from the LiDAR point cloud from Actueel Hoogtebestand Nederland (AHN). The original resolution of the AHN data is provided at 50 cm resolution, but this includes voids in the canopy. The spatial resolution of the generated CHM layer was resampled and aligned to match the resolution and grid placement of the PlanetScope image. The voids that were present in the canopy structures were filled by the bilinear interpolation resampling method.

Pure Pixels

In order to train a satellite model, values stored in individual pixels of the satellite image were used. For the extraction of pixel values in the satellite image, objects segmented in the UAV stage were used as a reference. In this stage, pixel values with varying intersection levels with a UAV-segmented object (0 – 100% of overlap) were extracted. This was done in order to investigate the role of "pixel purity" in the prediction of biomass values. In this context, "pixel purity" was defined as the percentage of overlap with the UAV-segmented object, meaning that a pixel with 100% overlap (i.e., fully covered by a UAV-segmented object) was considered a pure pixel. In turn, this concept was closely related to a measure of quality of the data and quality of the georeferencing between the images, since lower overlap corresponded to a mix of tree and non-tree parts of the pixel.

Small fractions of a tree segment can be part of a pixel; therefore, a fishnet was generated on top of the study area to be able to quantify the amount of area that is present in a pixel covered by a tree object. The bigger the area covering a pixel, the higher the "pixel purity" is at representing the object. Once the tree objects were intersected by the fishnet, the area was calculated and the biomass represented by that pixel was added to the new polygons (see Figure 7). A point was generated for each new polygon generated by the intersection of the fishnet and the segmented tree objects; said point lied inside the polygon and was not allocated at the centroid of the polygon. The X and Y coordinates were extracted for each point, as well as the biomass, the type of specie the object represents and the unique identification of the polygon it is a part of.

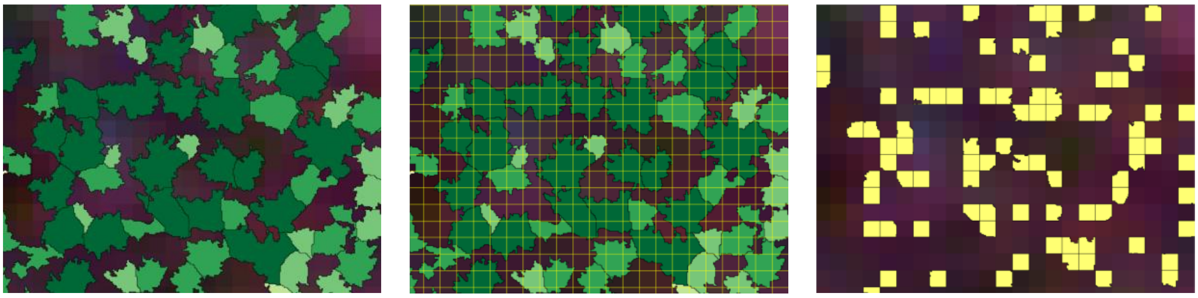

a) b) c)

Figure 7. Generation of pure pixels

Coniferous trees are, in average, smaller in canopy area than a broadleaf, thus an entire pixel of 9m² covering a young conifer would be highly improbable. Likewise, small objects that were inside a pixel without covering it in its majority was highly present after intersecting the fishnet with the tree segments. To go around these issues, the area intersected by the fishnet and the UAV segmented object was taken into account in the creation of the dataset.

Various models were generated to test the performance of the MLA with the admittance of pixels with a varying degree of purity. All models were generated by using all pixels in a 10-fold cross-validation SVR to assess the overall performance of the model and reporting the result given by the test set. All models were built by using a dataset containing both types of trees (broadleaf and coniferous). First, only pixels which were fully covered were taken into account (e.g., polygons with an area of 9m² in the case of the PlanetScope satellite image). Afterwards, the threshold was lowered by 5% each iteration.

Influence of Pixel Purity of MLAs Performance Metrics

The biomass values predicted in the UAV stage for each tree were transferred to the corresponding pixels. The biomass was then calculated to be represented as ton per hectare. The *raster* package in RStudio was used for the extraction of pixel values using the coordinates for each point and the multiple raster layers generated beforehand. Once the extraction process was accomplished, points with no values in any of the features were eliminated from the dataset. These objects fall out of bounds of the satellite image and account for <1% of the total amount of pixels.

Using pixels which have a "pixel purity" of a 100% recorded a R^2 of 37.5% with an RMSE and MAE of 58.5 and 45.4 tons per hectare respectively. By including pixels which are covered up to 60%, the accuracy of the model recorded a coefficient of determination of 46.7% and an RMSE and MAE of 66.9 and 51.2 tons per hectare. The total amount of objects used for the dataset at this threshold was of 11,270 objects Figure 8 shows the variations between the performance metrics with the fluctuating pixel coverage.

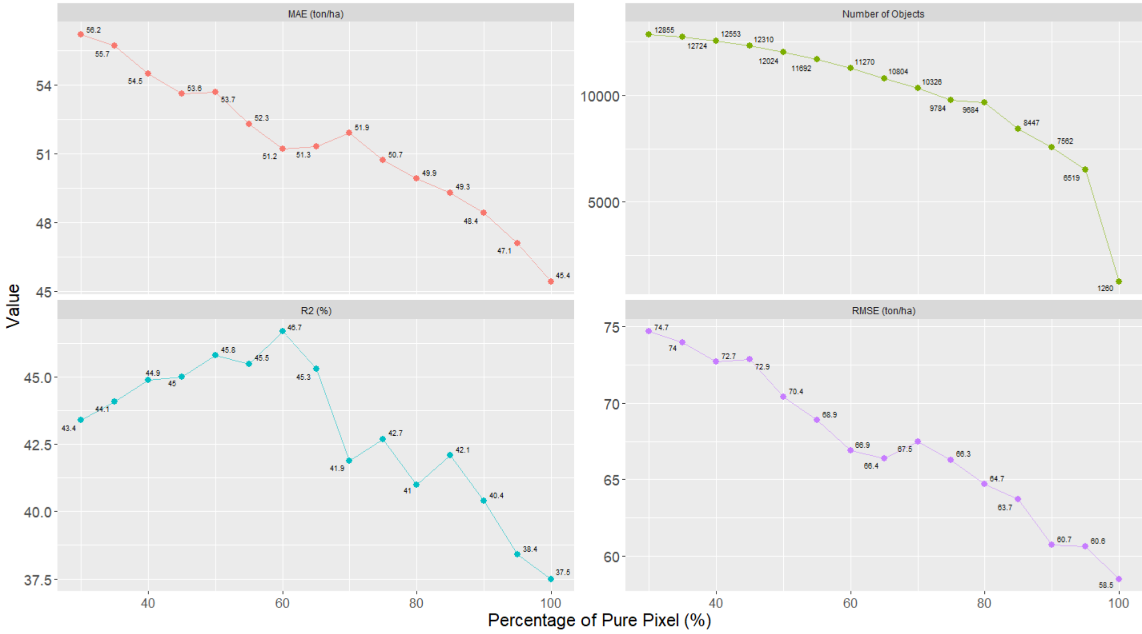

Figure 8. Change in Performance Metrics with Varying Pixel Coverage

Features from Satellite Imagery

For satellite imagery, a set of metrics comprised of spectral band values, vegetation indices and GLCM layers was generated. Table 9 answers the research question #1. The vegetation indices were calculated from the individual spectral bands, creating an individual raster file for each new vegetation index. The equations used for the vegetation indices can be found in

Annex 3. For the creation of GLCM layers, the *glcm* statistical package was used in RStudio. The NIR band served as input for the function to create GLCM layers in all directions, thus creating eight layers as an output.

Table 9. Features derived from satellite imagery.

Metric	Explanatory Feature	
Spectral	Green	Red
	Blue	NIR
Vegetation Indices	NDVI	EVI
	GNDVI	DVI
	SR	SAVI
GLCM	Mean	Dissimilarity
	Variance	Entropy
	Homogeneity	Second Moment
	Contrast	Correlation
Biometric	Canopy Height	

The values for mean and standard deviation of all explanatory features were calculated per polygon (i.e., segmented trees) which were composed of different pixels. These values were used to assess the variability of each explanatory feature per individual tree. The mean and standard deviation were obtained to for each layer in order to generate a total of 38 features for each segmented tree object. The trees found in the six areas captured by UAV have been segmented and their AGB estimated. These values are now used as the target variable while new features are generated from the satellite image. Feature extraction was done at a pixel level by using the segmented objects from the UAV images as a reference and a fishnet matching the spatial resolution of the image. The intersection between the fishnet and the previously segmented objects allowed an area threshold to be established.

2.6. Data Analysis

2.6.1. Aboveground Biomass Estimation

Estimation of forest AGB was done with MLA`, using features (i.e., explanatory variables) derived from UAV data and satellite images (da Conceição Bispo et al., 2020; J. Lin, Wang, Ma, & Lin, 2018; Navarro et al., 2019; Zhang et al., 2020; Zhu et al., 2020). In this study, two different MLA were applied: Random Forest and Support Vector Regression. These were chosen due to their ease of use and to their effectiveness at predicting AGB (Ali, Greifeneder, Stamenkovic, Neumann, & Notarnicola, 2015; Dang et al., 2019; Zhang et al., 2020).

For the correct implementation of machine learning regressors, the data was split into a training and a test set. The first provided information that allows the model to adjust its parameters, effectively learning to perform the task at hand (in this case, AGB estimation). The latter was used to evaluate the performance of the trained model. For this study, a 70/30 split was used for training and testing the data.

Random Forest

Random Forest, by default, generates decision trees using a random selection of two thirds of the individual trees as training data with bootstrapping (resampling of the data with replacement). The rest of the data is called OOB data (out-of-bag), which is not used to train the model, but instead to estimate the error and determine variable importance (Breiman, 2001).

The most important parameters in RF are *mtry*, which represents the number of explanatory features available for splitting at each node of the decision tree and *ntree,* which is the number of trees necessary to achieve an AGB prediction. For this study, a ntree of 500 was used throughout all of the models. The performance of the models was assessed with several iterations of ntree (100, 250, 500, 1,000 and 1,500), but no further improvements were noticed past 500 trees and the computational time was increased considerably past this threshold. The parameter mtry was left in its default value, that being the number of total explanatory features divided by three (Breiman, 2001). These parameters can be tuned during the training process, aiming to improve the fit of the model to the training data. This algorithm is able to provide information regarding the importance of each of the features used in training. With this knowledge, it is possible to exclude less relevant or redundant features, decreasing computational time without compromising performance (Belgiu & Dra, 2016). Furthermore, this information contributes to model interpretability and eases debugging.

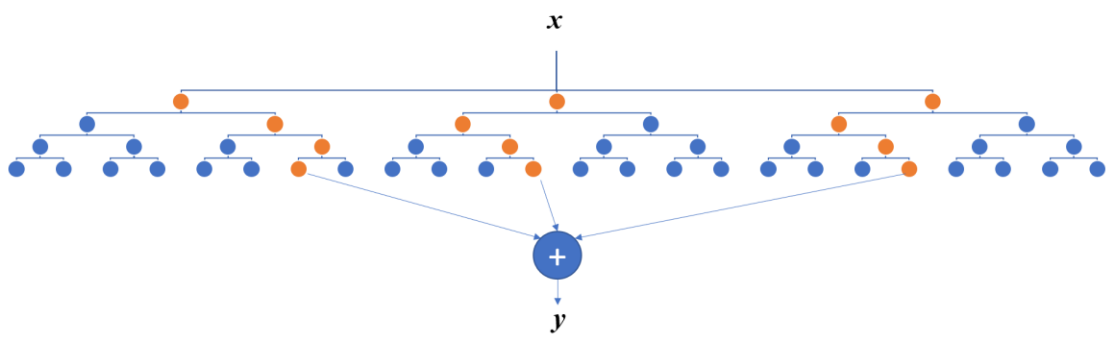

Figure 9. Basic structure of Random Forest for Regression

Figure 9 depicts the basic structure of a random forest in which each tree makes a prediction on AGB based on the features from the training data. Each decision made in a single tree (orange circles) are taken considering the option with the lowest error. After each tree has made a prediction, the results are then averaged to output a final prediction.

Support Vector Regression

Support Vector Machine is a machine learning algorithm commonly used for classification challenges. However, it can easily be adapted for regression. This algorithm finds a hyperplane in an n-dimensional space (*n* being the number of explanatory features) that best fits the target data. To do this, it uses support vectors, which are data points that lie closest to the line that is required to fit the data, also called the hyperplane boundary. The most relevant parameter in the case of an SVR is the kernel type, which are a set of mathematical functions which take the explanatory features as input and transforms them into a higher dimensional space in which the hyperplane is built. The most used kernel types are linear, sigmoidal, polynomial and radial. The radial basis function is typically used because it is relatively easy to tune and is better at generalizing big datasets like the ones used in this study.

When using the radial basis function, two more parameters should be taken into account. These are the cost of constraint (C) and gamma (g). The cost parameter adds a penalty for each data point that does not fall inside the decision boundary. From a regression perspective, these points are harder to predict, thus increasing the error and are penalized more. A low C value usually leads to a poorly fitted model, while a high C value may lead to overfitting. The gamma parameter controls the distance of influence of a training point, thus low values of gamma mean a more generalized hyperplane, whilst high gamma values lead to a detailed hyperplane (Bruzzone & Persello, 2010). Figure 10 shows the structure of a one-dimensional support vector regression, meaning that the regression is built on one explanatory feature (x) which explains the target variable (y). The black line represents the regression output (hyperplane), while the red dotted line represents the boundary line and the support vector are represented as a white circle with a cross.

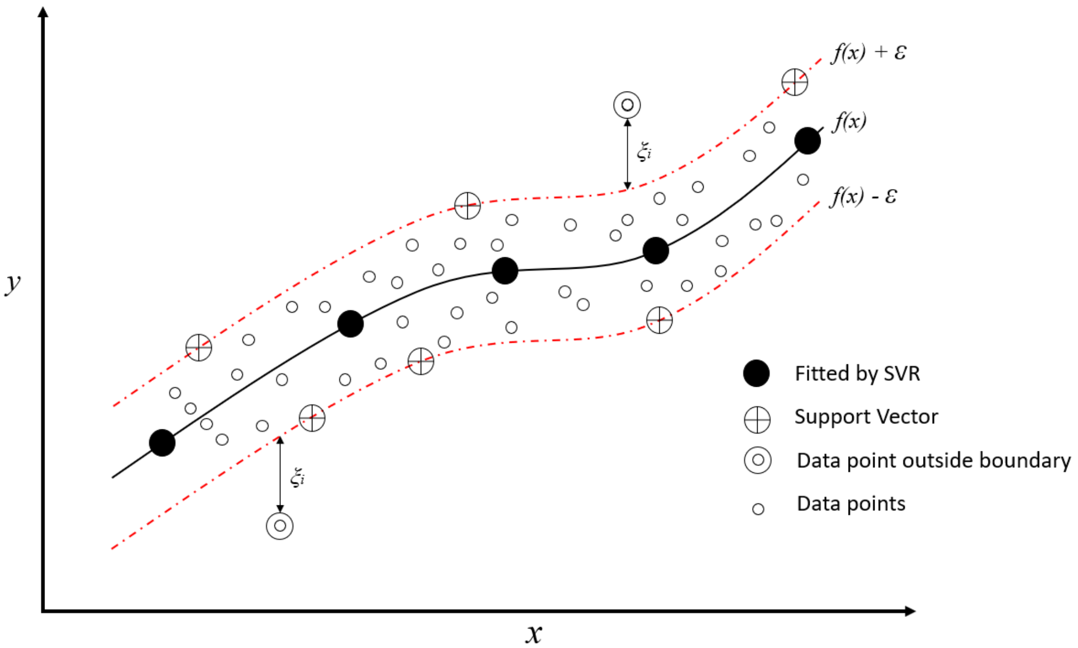

Figure 10. Basic Structure of Support Vector Regression

Several models were generated to test the output and compare the performance. Three general models were tested, all of the trees combined (coniferous and broadleaf), and then two models in which the trees were segmented between tree types. The same process was followed using the explanatory features derived from the satellite data.

Feature Reduction

A feature reduction process was implemented once the optimal machine learning algorithm was identified. Similar features were intended to be used as input (e.g., NDVI and GNDVI), thus feature reduction allows the model to perform more efficiently whilst not compromising performance by taking the most relevant features in the regression model. Although RF is commonly used as a classifier and as a regression algorithm, it has also been known to be used as a feature selection algorithm (Reif, Motsinger, McKinney, Crowe, & Moore, 2006). In regression problems, RF measures node impurity with the residual sum of squares before and after the split on each individual explanatory variable averaged over all of the decision trees (James, Witten, Hastie, & Tibshirani, 2014). The higher the node purity given by that variable, the more important it is at providing information to the model in estimating the target variable.

Since RF builds decision trees in a randomized fashion, an iteration process for splitting the dataset was developed to gather node impurity information during each iteration. The original dataset is first split into training and testing set, but the testing set is ignored for this process. The training set was split into ten equal size folds. A fold would then be further split into ten equal subsamples in order to use nine subsamples to build a model and then testing the model with the remaining subsample. This process was repeated ten times, to complete one iteration. Once an iteration was complete, the original dataset would then be split again into training and testing to then repeat the process two more times.

The node impurity would be accumulated, ensuring that the importance of the feature was representative by gaining the information over thirty models. Once the features were ranked per order of importance, the least important features were removed one by one until the performance of the model generated reached its highest with the least number of variables.

2.6.2. Accuracy Assessment

Both MLA were validated through 10-fold cross validation. In k-fold cross validation, the training set is subdivided into *k* equal size subsamples called folds; *k-1* folds are used to train a model while the remaining fold is used to validate said model. K-fold cross-validation is used to ensure that randomness is implicit throughout different splits of the data, increasing robustness and preventing overfitting. If this is achieved, performance across validation folds should be similar (i.e., low standard deviation). Figure 11 is a general scheme of how a 10-fold cross validation is performed as explained previously.

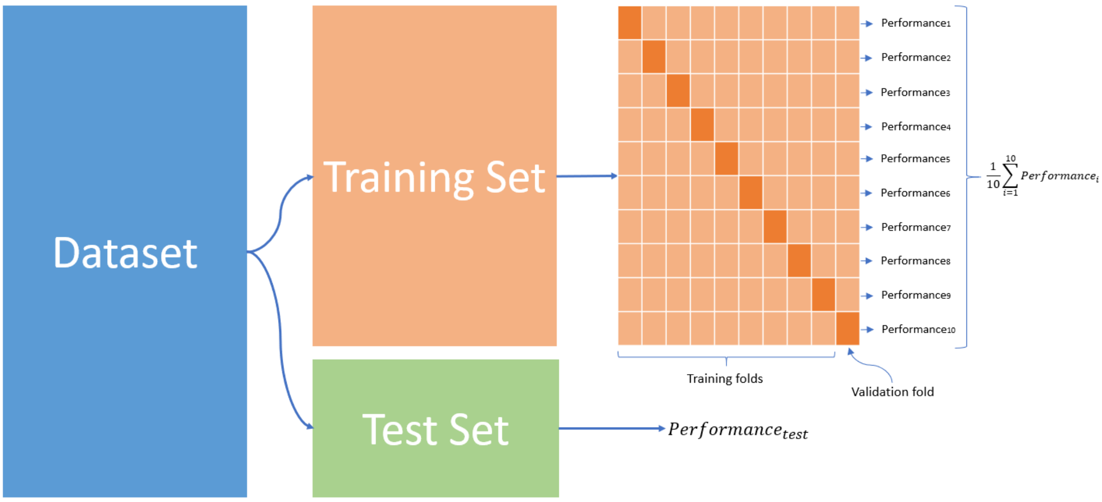

Figure 11. Schematic of a 10-Fold Cross-Validation.

Several performance metrics were calculated for each validation fold, as well as for the test set: coefficient of determination (R^2), root-mean-square error (RMSE) and mean absolute error (MAE) between predicted AGB and observed AGB. The formulas for these metrics are presented below.

$$R^2 = 1 - \frac{\sum_i (y_i - \hat{y_i})^2}{\sum_i (y_i - \bar{y_i})^2} \tag{4}$$

Equation 5. Coefficient of determination

Where y_i is the actual observed AGB, $\hat{y_i}$ is the predicted value of AGB, and $\bar{y_i}$ is the mean AGB value from field measurements, and:

$$RMSE = \sqrt{\sum_{i=0}^{n} \frac{(\hat{y_i} - y_i)^2}{n}} \tag{5}$$

Equation 6. Root-Mean-Square Error

where i represents each of the predictor features used in the model, and:

$$MAE = \frac{1}{n} \sum_{i=1}^{n} |y_i - \hat{y}| \tag{6}$$

Equation 7. Relative Root-Mean-Square Error

3. RESULTS

3.1. Field Data Collection

3.1.1. Descriptive Analysis of Field Measurements

A total of 1,238 trees were measured across 70 plots. After removing trees that were covered by higher canopy trees (i.e., unseen trees by the UAV orthophoto), a total of 965 trees remained. The conifer type trees account for 67.8% of the total trees while the broadleaf accounted for the remaining 32.2% of the trees. The most common tree on the field was Douglas Fir, corresponding to 27.7% of the total count of trees; the least common tree was the Common Ash, accounting for 2.24% of the total number of trees. Figure 12 summarizes the distribution of trees per species in the final dataset used to train the MLA.

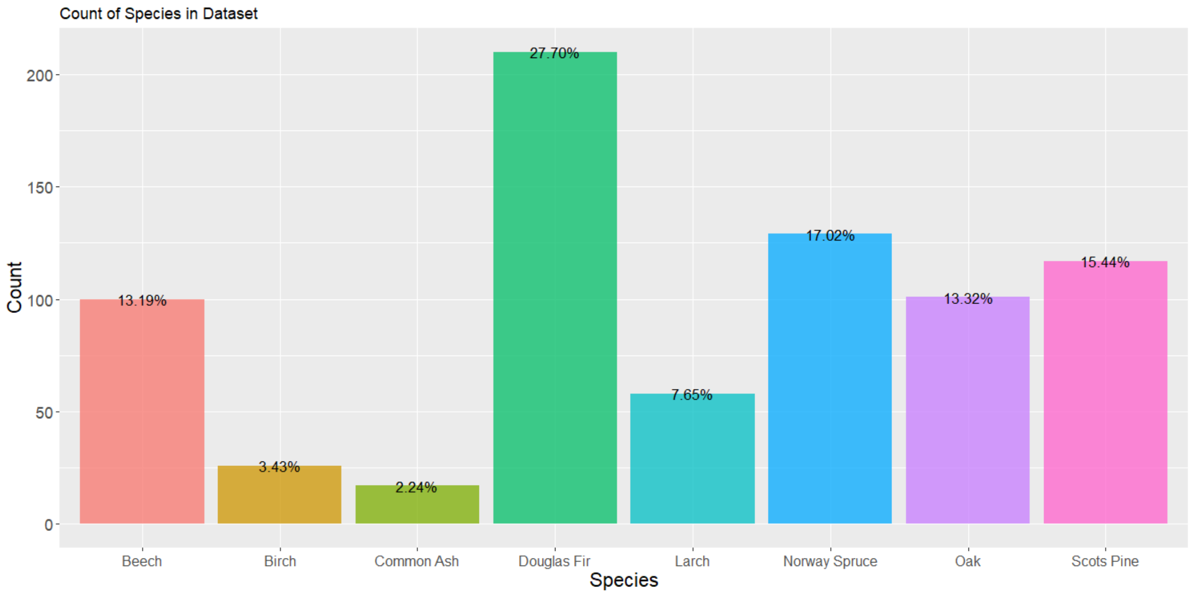

Figure 12. Count of Species in Dataset.

The average DBH for broadleaf trees was of 35.5 centimetres with a standard deviation of 11.6 centimetres. For coniferous trees species the average DBH was of 34.2 centimetres with a standard deviation of 9.4 centimetres. Having the greatest number of observations, Douglas Fir had an average DBH of 36.3 centimetres and a standard deviation of 9.7 centimetres. The least encountered tree, Common Ash, had an average DBH of 28.5 centimetres and a standard deviation of 19.2 centimetres. Figure 13 shows the average and quartiles for each tree species.

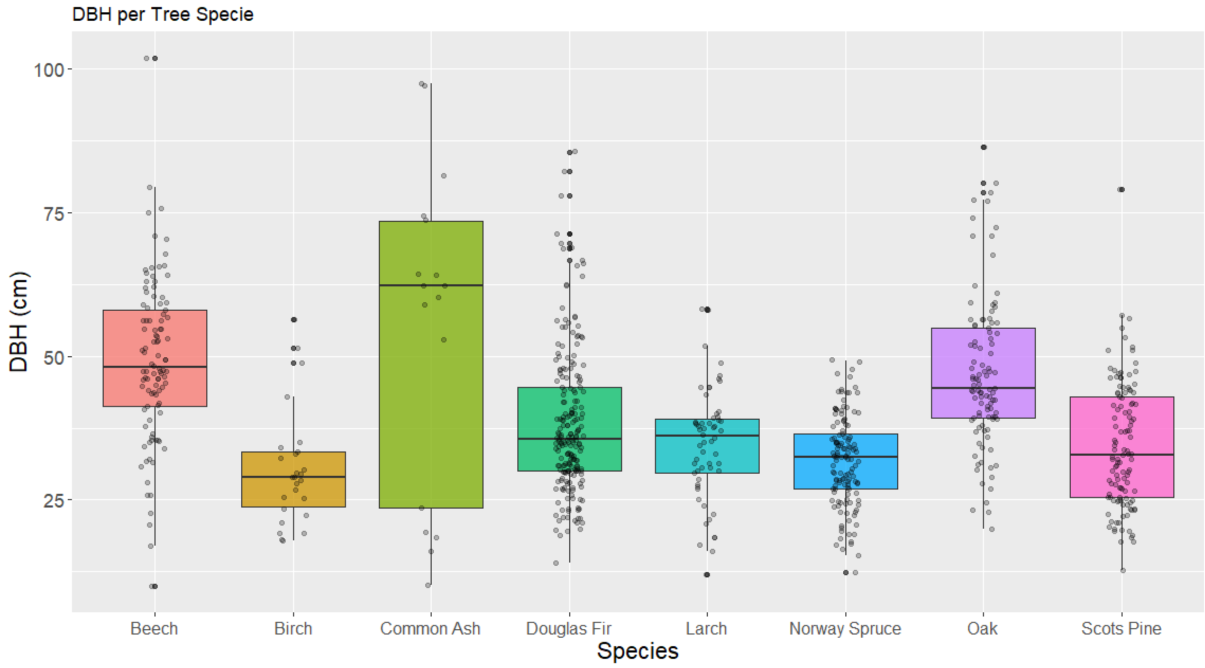

Figure 13. DBH distribution per Tree Species

The average height measured on field for broadleaf trees was of 20.2 meters with a standard deviation of 4.0 meters. Coniferous trees were recorded to have an average height of 21.5 meters and a standard deviation of 3.2 meters. Figure 14 shows the distribution of averages and percentiles per tree species.

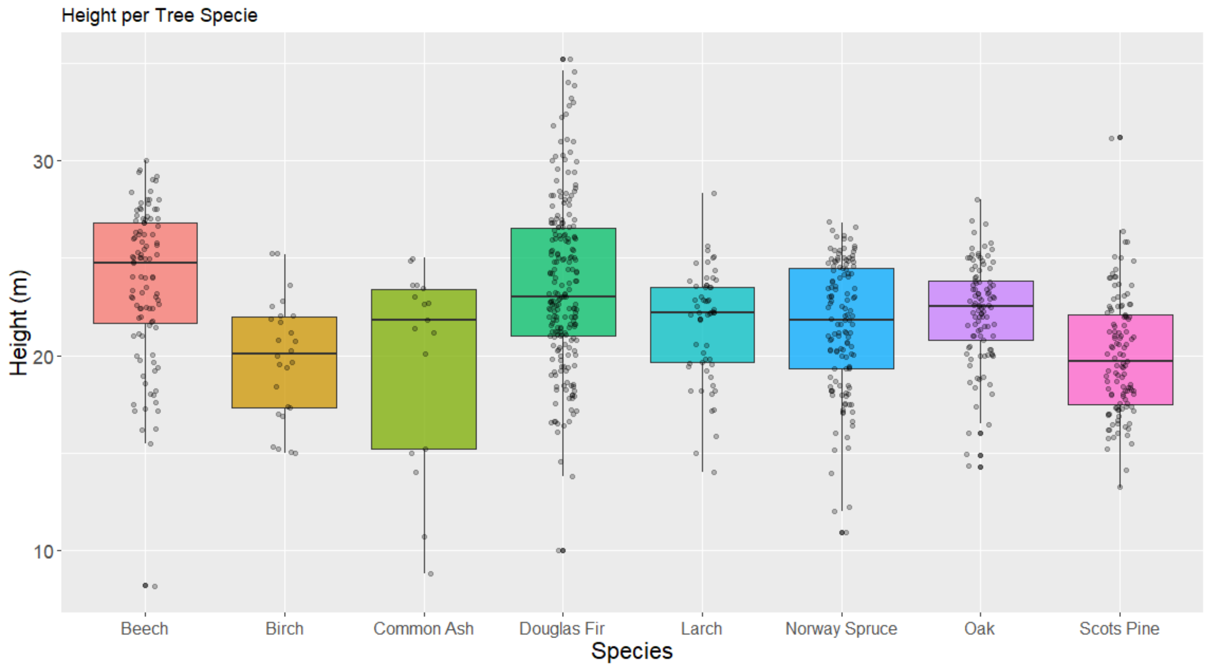

Figure 14. Height distribution per Tree Species

The exponential relationship described by R^2 between DBH and UAV CHM height is highest in Norway Spruce and Douglas Fir species. The same can be said for Common Ash, but then again, the number of encountered trees of this species was the lowest on the field, favouring a better relationship between the variables. Oak shows a low exponential relationship at a mere 4.9%. Figure 15 shows the exponential relationship between the two variables; coniferous trees species have, on average, a better correlation between DBH and height.

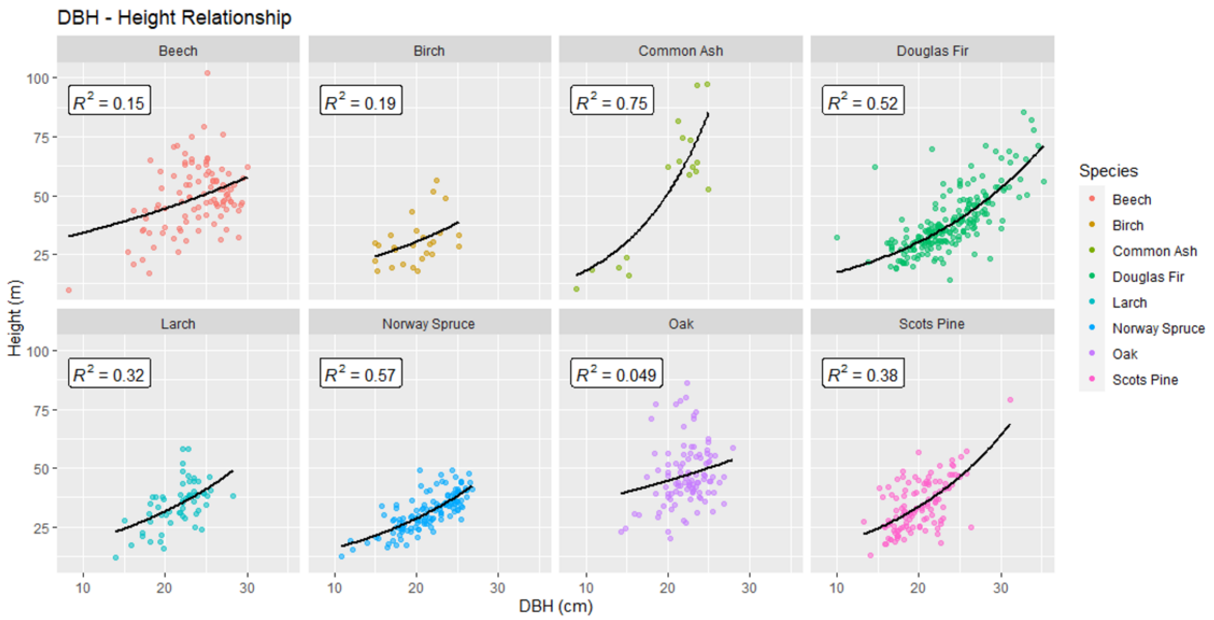

Figure 15. DBH – Height Relationship per Tree Species.

CPA is widely used as a proxy for the estimation of AGB. From the segmentation process of individual trees, the relationship between CPA and DBH is poor across all species. Oak obtained the lowest correlation between these two variables at a mere 0.5%. Figure 16 shows the exponential relationship between the two variables. In this case, broadleaves have a better correlation between DBH and CPA except for Oak. The relationships between CPA and height with DBH is important to note as it will play a role in the feature importance in the MLA.

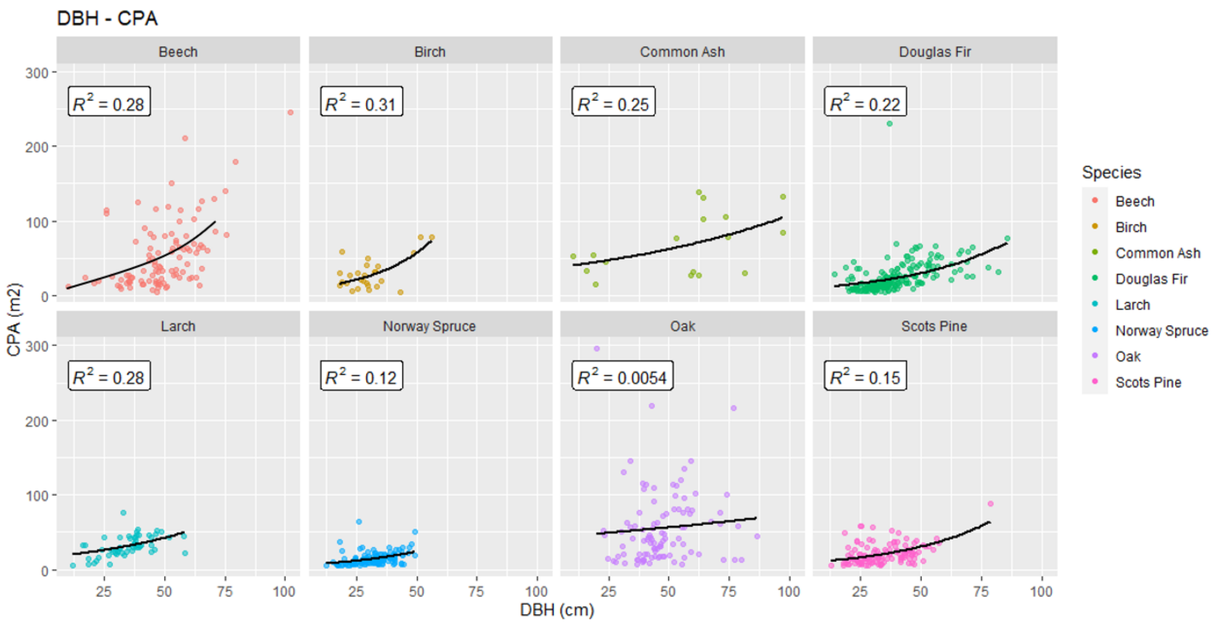

Figure 16. DBH – CPA Relationship per Tree Species.

After calculating the biomass with the allometric equations (see Table 7), the average biomass of broadleaf trees was of 895.6 kilograms per tree with a standard deviation of 614.6 kilograms. On the other hand, the average biomass of coniferous tree species was of 536.6 kilograms per tree with a standard deviation of 324.4 kilograms. The average aboveground biomass for all trees was 716 kilograms per tree with a standard deviation of 470 kilograms. Table 10 summarizes the statistics for aboveground biomass per tree species.

Table 10. Descriptive statistics for Aboveground Biomass

Species	Mean Biomass (kg)	St. Dev. Biomass (kg)	Max Biomass (kg)	Min Biomass (kg)	Trees (unit)
Beech	1,263.6	586.4	2,175.2	23.5	127
Birch	645.3	465.6	1,974.0	185.7	33
Common Ash	632.9	892.8	2,177.5	27.6	22
Douglas Fir	684.6	443.0	2,238.9	62.0	267
Larch	485.3	295.6	1,444.1	38.8	74
Norway Spruce	483.1	231.9	1,100.7	48.8	164
Oak	1,040.5	513.5	2,218.0	132.8	129
Scots Pine	493.5	327.0	1,458.8	44.7	149

Higher variation can be seen for broadleaf trees, while coniferous trees have lower standard deviation in AGB values. Figure 17 illustrates the mean aboveground biomass value and percentiles per tree species.

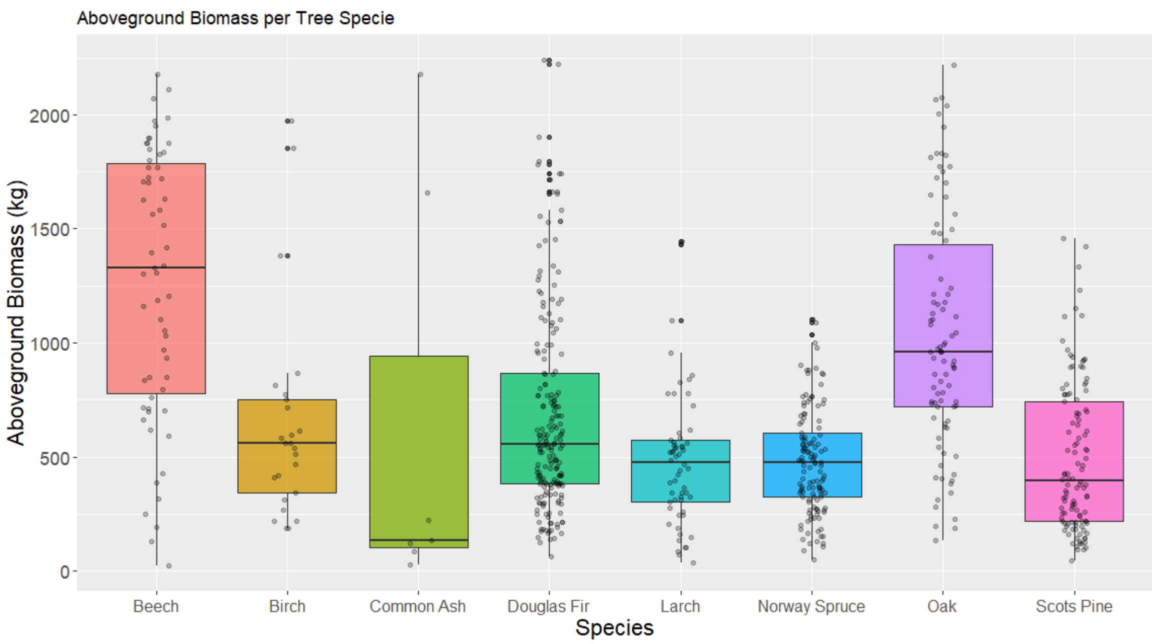

Figure 17. Aboveground Biomass distribution per Tree Specie

3.2. Remote Sensing Data Processing

3.2.1. Individual Tree Segmentation – UAV

The individual tree segmentation resulted in 14,480 trees across all UAV blocks. A fraction of the segmentation output is exemplified in Figure 18.

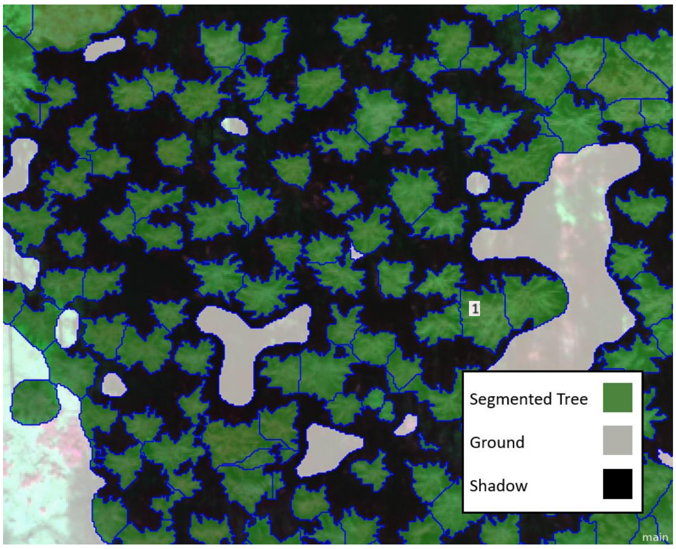

Figure 18. Objects generated to achieve tree segmentation in dense broadleaf canopy.

Objects with a low height are marked in white while shadow is marked in black. The resulting segmented tree objects are left in colour green. Figure 19 better displays the quality of the segmentation of coniferous and broadleaf tree species.

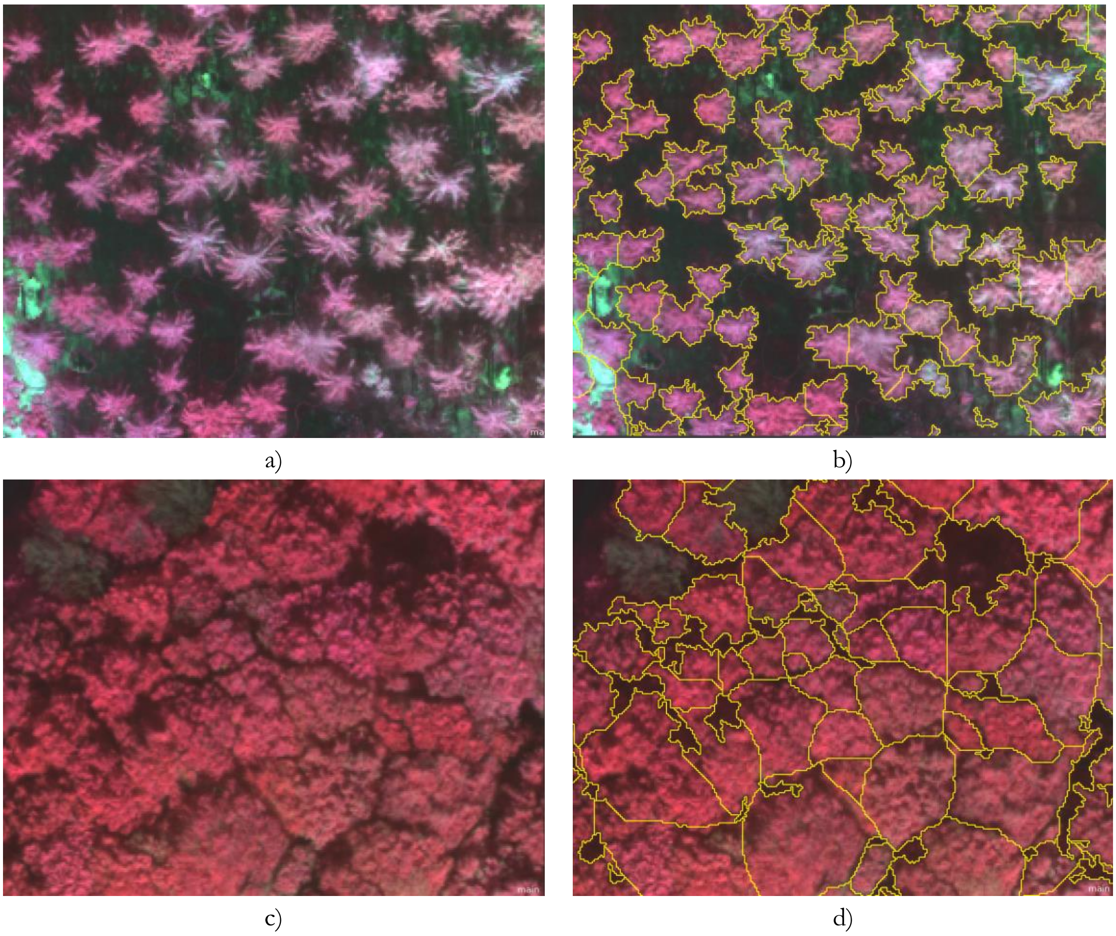

Figure 19. Segmentation of coniferous trees (a & b), and broadleaf trees (c & d).

The total detection error in the tree segmentation between UAV blocks varies from a minimum of 7.7% to a maximum of 12.8% for coniferous species, and from a minimum of 8.4% to a maximum of 13.6% for broadleaf species. The average total detection error per type of tree for each block is described in Table 11:

Table 11. Total Detection Error of Species per UAV Block

Tree Type	UAV Block					
	Block 4	*Block 5*	*Block 8*	*Block 9*	*Block 10*	*Block 123*
Broadleaf	8.9%	10.9%	13.6%	8.3%	8.4%	8.4%
Conifer	11.8%	10.0%	12.8%	10.0%	8.8%	7.7%

3.3. Data Analysis

3.3.1. Biomass Estimation with UAV Data

Table 12 shows the different models and performance metrics obtained in the validation set, across the ten folds of cross-validation, as well as on the external test set. The SVR returned a coefficient of determination of 71.1% and 60.6% for coniferous and broadleaf respectively. On the other hand, the RF regression model reported a coefficient of determination of 60.0% and 53.7% for coniferous and broadleaf respectively.

Table 12. Combination of models and performance metrics for biomass estimation.

Machine Learning Algorithm	Combination	Validation Set			Testing Set		
		RMSE (kg/tree)	*MAE (kg/tree)*	*R2 (%)*	*RMSE (kg/tree)*	*MAE (kg/tree)*	*R2 (%)*
Support Vector Regression	**Combined**	669.1	572.6	63.0	521.0	293.9	53.0
	Conifer	***298.5***	***159.9***	***72.2***	***250.8***	***178.5***	***71.1***
	Broadleaf	***485.6***	***373.6***	***63.9***	***439.7***	***364.1***	***60.6***
Random Forest	**Combined**	405.7	263.7	60.4	523.0	309.5	51.1
	Conifer	264.5	190.2	65.8	338.3	203.3	60.0
	Broadleaf	488.4	401.2	66.9	639.8	499.3	53.7

.

For the coniferous tree species, the most important explanatory feature was the average height captured by the CHM, followed by the standard deviation of the CHM inside the object. The textural features provided by Entropy in all directions, 45-degree shift and 90-degree shift also contributed to the prediction, but it is overshadowed by the contribution of the height (see Figure 20). By using all of the features in the coniferous tree species, the coefficient of determination was 69.4%. Through several iterations in which least important features were removed first, the highest accuracy metrics on the test set were reached by using 15 explanatory features (R^2 of 73.7%). By using 14 or 16 features, the model's performance maintained its accuracy in the same range. The model's performance was also higher by using the top 8 features at 72%, but results with 9 or 7 features differed from this value (see Annex 5).

For the broadleaf tree species, the canopy height was once again the most important feature, but the spectral values in the red band played an important role in the model. Area of the segmented trees was another biometric parameter with accumulated importance. Out of the top 5 most important features, the coniferous model obtained information from three textural features. In comparison, the broadleaf model only includes two textural features in the top 10 most important features, thus accentuating the importance of reflectance values from spectral bands and vegetation indices. This answers the research question #2.

To answer research question #3, feature reduction was accomplished through an iterative process of taking out the least important features and measuring the accuracy metrics in the test data set. By using 40 explanatory variables, the model's accuracy was of 59%. The best performance was obtained by using the top 9 features, which improved the output of the model to 62.6% (see Annex 6).

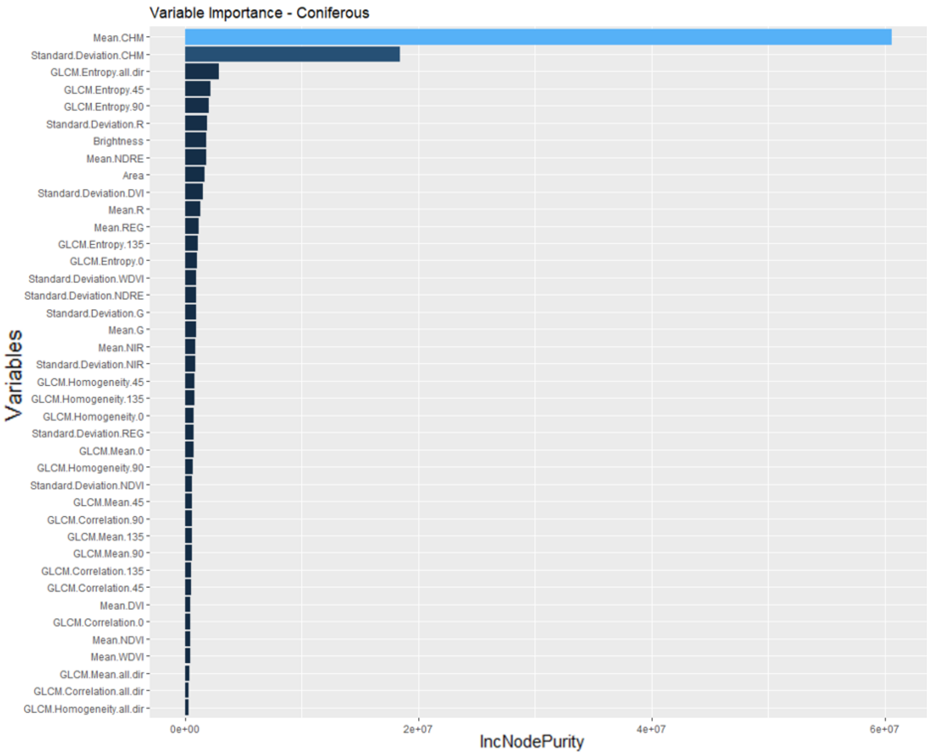

Figure 20. Feature Importance for Coniferous trees at the UAV level.

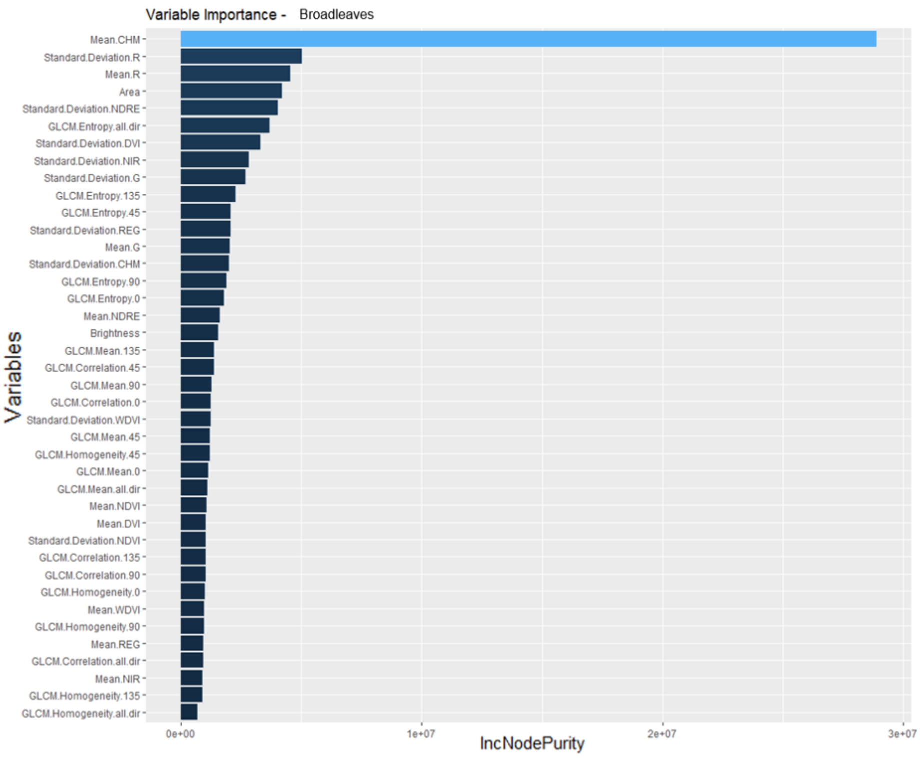

Figure 21. Feature Importance for Deciduous trees at the UAV level.

Once the features were selected, the training set of data was submitted to a 10-fold cross-validation to assess the performance of the model with reduced features. The C and g hyperparameters were tuned during each fold by using a grid search; the best values for cost and gamma are selected from the model with the lowest mean squared error. A cost of 1 and gamma 0.11 were used for the model because they obtained the lowest recorded error. For the coniferous tree species model, an average coefficient of determination of 71.4% was achieved on the validation set with a standard deviation of 4.7%. The lowest score on the cross validation was of 63.0% whilst the highest score was of 80.4%. Similarly, the test set performed within the range of the cross-validation results with an R^2 of 73.7%.

Table 13. Results of 10-Fold Cross Validation and Test Set for UAV-based Model for Coniferous (left) and Broadleaf (right) Tree Species

Coniferous

Fold	R^2 (%)	RMSE (kg/tree)	MAE (kg/tree)
1	74.3	263.6	187.5
2	63.0	268.2	194.8
3	68.8	458.3	241.8
4	72.5	447.2	236.7
5	69.6	313.8	213.8
6	80.4	211.9	155.2
7	70.0	324.7	206.5
8	68.3	441.4	238.1
9	77.4	203.2	146.3
10	69.3	231.5	161.3
Average	***71.4***	***316.4***	***198.2***
St. Dev.	***4.72***	***94.3***	***33.64***
Minimum	***63.0***	***458.3***	***241.8***
Maximum	***80.4***	***203.2***	***146.3***

Broadleaf

Fold	R^2 (%)	RMSE (kg/tree)	MAE (kg/tree)
1	55.9	587.6	477.4
2	50.7	723.9	568.6
3	53.7	534.7	463.3
4	62.7	500.9	409.2
5	56.3	590.8	468.4
6	51.7	611.6	492.5
7	54.0	474.7	370.5
8	68.3	488.1	403.6
9	65.3	651.9	498.6
10	57.3	556.6	441.3
Average	***57.6***	***572.1***	***459.4***
St. Dev.	***5.61***	***74.0***	***53.7***
Minimum	***50.7***	***474.7***	***370.5***
Maximum	***68.3***	***723.9***	***568.6***

TEST SET		
R^2 (%)	**RMSE (kg/tree)**	**MAE (kg/tree)**
73.7	215.0	156.6

TEST SET		
R^2 (%)	**RMSE (kg/tree)**	**MAE (kg/tree)**
62.6	439.7	364.1

For broadleaf tree species, an average R^2 of 57.6% was achieved in the cross-validation, and a standard deviation of 5.6% was calculated from the 10 outputs. The test set reported an R^2 of 62.6%, well within the range of values seen in the cross-validation. The values for RMSE and MAE for the broadleaf tree species are, on average, 572.1 and 459.4 kilograms respectively. This is due to the aboveground biomass distribution present in broadleaf and conifers. For this model, the optimal C and g were of 1 and 0.08 respectively. Table 13 summarizes the results found at every fold and on the test test; this answers research question #4. In both models, trees with higher biomass were being underestimated and trees with low biomass were being overestimated. Trees closer to the average AGB values were better predicted in both models (i.e., closer to the 1:1-line, higher coefficient of determination) (see Annex 7 and Annex 8) The average predicted values of AGB for coniferous and broadleaf was of 579.5 and 1,103.7 kg/tree respectively. The standard deviation of broadleaf is 502.0 kg per tree, while the coniferous trees have a slightly lower standard deviation at 324.6 kg per tree.

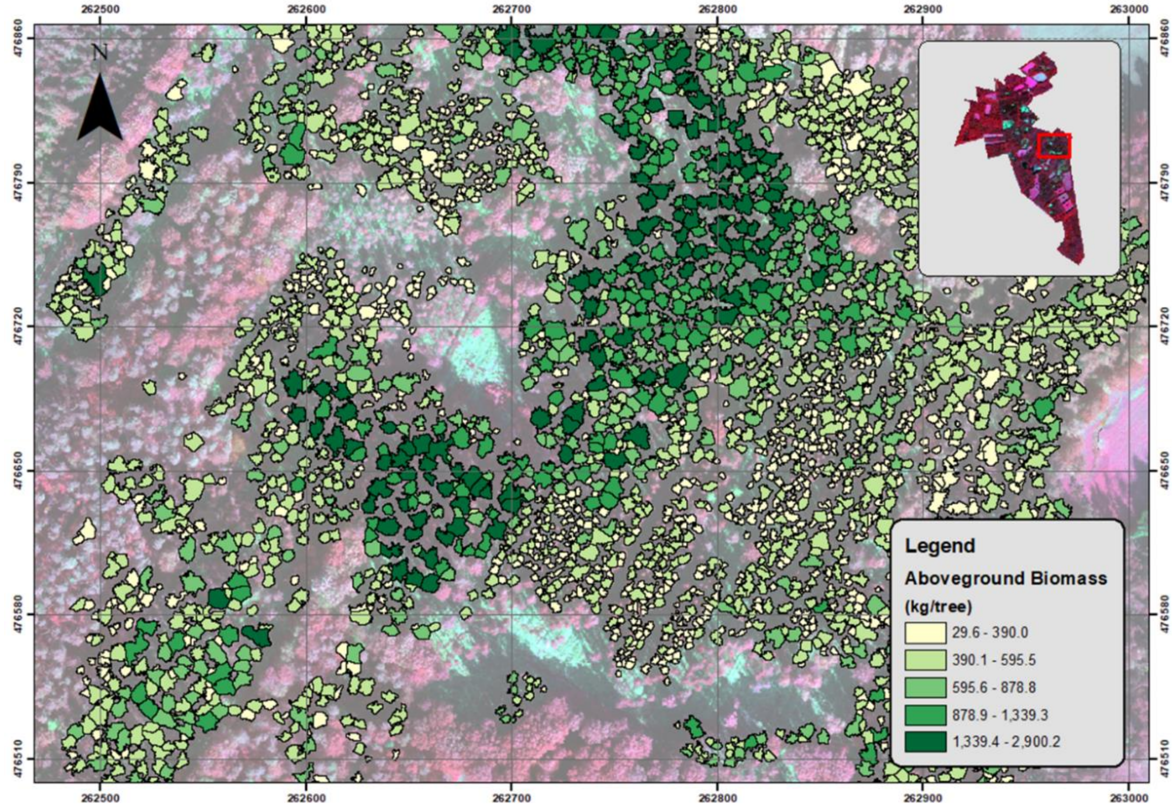

Figure 22. Output of coniferous model in UAV flight over Block 8.

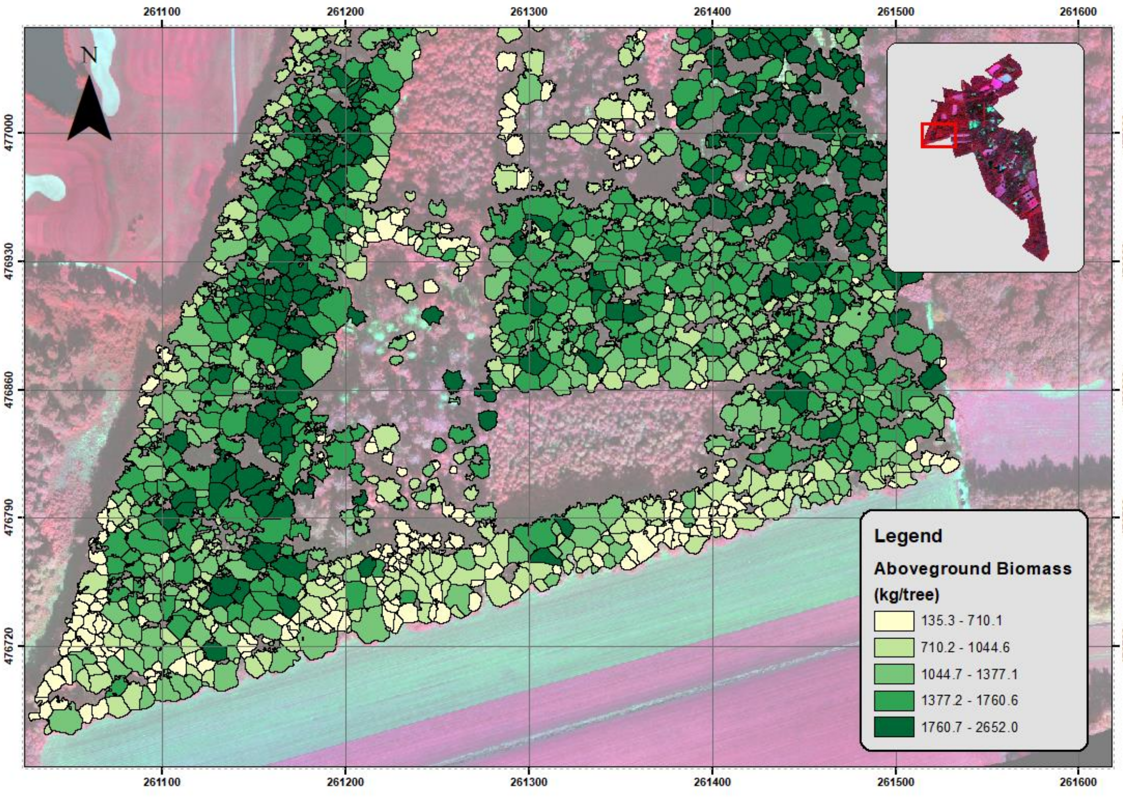

Figure 23. Output of deciduous model in UAV flight over Block 123.

Table 14 summarizes the regression results for both trees. These values are in accordance with the values estimated from the field (see Table 10). Two exemplifications of the generated output can be seen in **Error! Reference source not found.** and **Error! Reference source not found.**

Table 14. Distribution of AGB values (kg/tree) across tree types - UAV

Type	Count	Minimum (kg/tree)	Maximum (kg/tree)	Mean (kg/tree)	Standard Deviation (kg/tree)	Sample Size (Training)	Sample Size (Test)
Conifer	654	168.5	2,075.3	579.5	324.6	458	196
Broadleaf	311	205.4	3,856.5	1,103.7	502.0	218	93

3.3.2. Biomass Estimation with Satellite Data

RF and SVR were once again used to generate different models using different set of explanatory variables. The dataset was used combining both tree types, and were later divided to generate an individual model for coniferous and broadleaf trees. All models were subject to a 10-fold cross-validation as well as reporting the performance on an unseen dataset. Table 15 summarizes the results found for the initial models which did not consider CHM as an explanatory feature and were built on individual bands, vegetation indices and texture metrics.

Table 15. Summary of generated models without CHM layer.

Without CHM		Validation Set RMSE (ton/ha)	Validation Set MAE (ton/ha)	Validation Set R2	Test Set RMSE (ton/ha)	Test Set MAE (ton/ha)	Test Set R2
Support Vector Regression	**Combined**	74.5	57.0	34.1	74.5	57.3	34.4
	Broadleaf	90.5	70.0	32.3	88.7	68.5	32.8
	Conifer	***61.0***	***48.0***	***39.1***	***60.9***	***47.0***	***39.7***
Random Forest	**Combined**	69.9	51.6	41.9	73.7	58.3	36.0
	Broadleaf	***81.9***	***60.5***	***44.4***	***86.4***	***68.2***	***35.1***
	Conifer	56.5	41.5	47.6	61.0	47.9	39.2

Coniferous aboveground biomass recorded an R^2 at 39.7% and a RMSE and MAE of 60.9 and 47.0 kilograms in the test set. For the broadleaf's aboveground biomass predictions recorded a coefficient of determination of 35.1%; in this case, RF outperformed the SVR model. The difference between the training set and the test set is more pronounced in the RF models than in the SVR models. The difference in R^2 values does not go beyond 10%, thus neither of the MLA are overfitting the output.

The highest performance obtained by only using spectral data, vegetation indices and textural features was poor in the context of aboveground biomass estimations (39.7% and 35.1% for coniferous and broadleaf respectively). Since aboveground biomass estimations were initially calculated from allometric equations using DBH, height information is highly important to the generation of regression models, as exponential relations exist between these two variables (see Figure 15). To add height data into the regression models, the AHN was used to generate a CHM. This layer was used as supplementary data to generate models with RF and SVR. Table 16 summarizes the results obtained with the different models which included CHM related features.

Table 16. Summary of generated models with CHM layer.

With CHM	Validation Set RMSE (ton/ha)	Validation Set MAE (ton/ha)	Validation Set R2	Test Set RMSE (ton/ha)	Test Set MAE (ton/ha)	Test Set R2

With CHM		Validation Set			Test Set		
		RMSE (ton/ha)	MAE (ton/ha)	R2	RMSE (ton/ha)	MAE (ton/ha)	R2
Support Vector Regression	**Combined**	68.5	52.0	45.1	68.9	52.9	46.8
	Broadleaf	83.7	64.1	42.6	86.3	66.9	39.3
	Conifer	52.2	40.8	55.2	53.8	41.8	52.4
Random Forest	**Combined**	63.0	46.0	54.3	67.2	52.8	45.9
	Broadleaf	**56.7**	**77.1**	**51.7**	**82.6**	**65.4**	**42.5**
	Conifer	**47.9**	**35.2**	**62.6**	**53.0**	**41.7**	**52.5**

The RF models for coniferous and broadleaf tree species obtained an R^2 in the test set of 54.0% and 43.9% respectively. The SVR recorded a coefficient of determination in the test set of 52.4% and 39.3% for the coniferous and broadleaf tree species.

The most important feature for the coniferous model was the average CHM feature. The importance of this feature is more than double of that of the second and third most important features, standard deviation of DVI and standard deviation of GNDVI. Texture layers such as mean and variance also contributed in the model's performance; other textural layers such as homogeneity, dissimilarity and entropy did not give significant information about the biomass predicted at the pixel level (see Figure 24).

The average and standard deviation of the CHM were the most important features for the broadleaf model, but did not play a role as big as in the coniferous model. Textural features from contrast and homogeneity followed in importance. The average value of vegetation indices like SAVI, NDVI and SR did not provide useful information to the model and displayed low importance. Figures 24 and 25 show the ranked importance of features utilized in the satellite model, thus answering the research question #5.

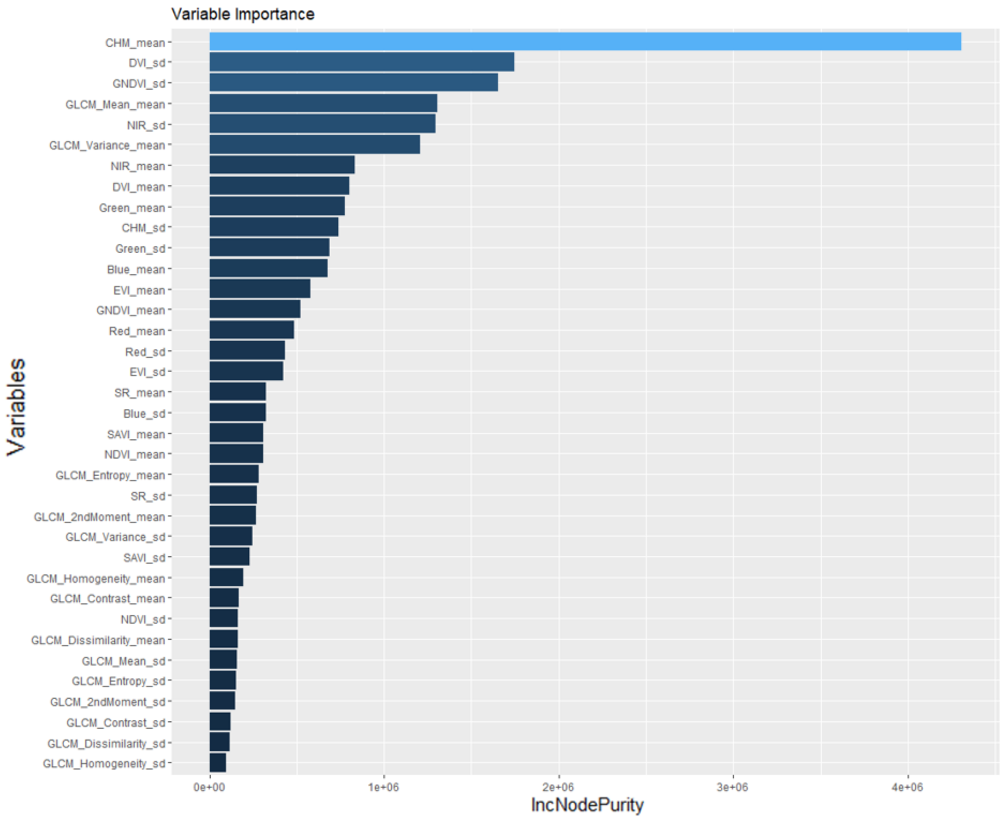

Figure 24. Feature Importance for Coniferous trees at the satellite level

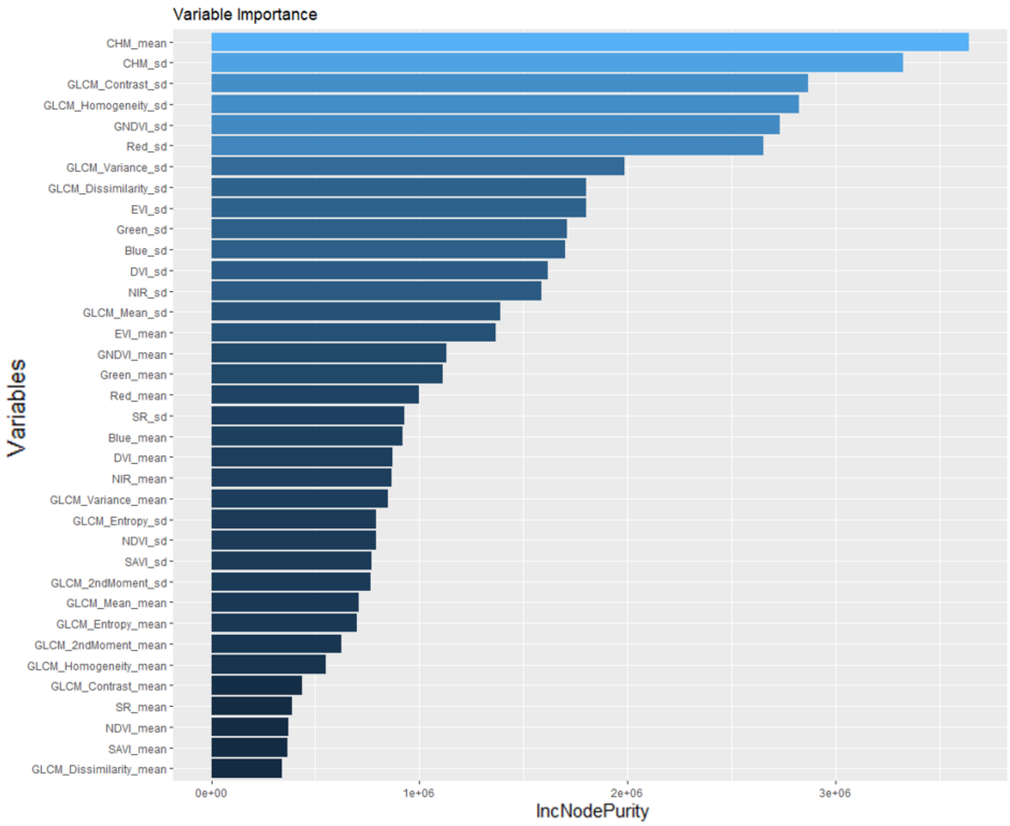

Figure 25. Feature Importance for Broadleaf Trees at the Satellite Level

To answer the research question #6, several models were trained for both the coniferous and broadleaf species in order to assess the impact of feature reduction. When the coniferous tree species model was trained using all of the 40 features extracted, it recorded a coefficient of determination of 53.2%. When the model was tested with 13 features the R^2 went up to 54.5% (see Annex 10). When testing a broadleaf model's performance metrics using 40 features the coefficient of determination was recorded at 42.6%. By using the 25 most important features, this performance metric was recorded at being 43.5% (see Annex 11).

Once the most important features were identified, more robust models were generated by only using the most important features identified through the feature selection process. The CHM layer was included in the assessment of performance metrics. All models were subjected to a 10-fold cross-validation and the model's performance metrics were also evaluated through the use of the test set.

For coniferous tree species, the average coefficient of determination found across all folds was of 62.2% with an RMSE of 47.9 kilograms and a MAE of 35.2 kilograms. The standard deviation across all folds for the R^2 was of 2.9% and 1.9 and 1.2 kilograms for RMSE and MAE correspondingly. The test set performance recorded an R^2 54.0% and 53.0 and 41.7 kilograms for the RMSE and MAE respectively. The parameters used for the model was a cost of 1 and a gamma of 0.027. Table 17 summarizes the findings of the validation set and the test set.

The model generated for the deciduous tree species recorded an average coefficient of determination of 51.7% across all folds. The average RMSE value was 77.1 kilograms per tree and the MAE was of 56.7 kilograms per tree. The test set recorded an R^2 of 43.6% with an RMSE of 82.6 kilograms per tree and a MAE of 65.4 kilograms per tree. The cost and gamma used for the elaboration of this model was of 1 and

0.045 respectively. The answer to research question #7, a summary of the results found in the validation set and the test set can be best reviewed in Table 17.

Table 17. Results of 10-Fold Cross Validation and Test Set for
Coniferous (left) and Broadleaf (right) Tree Species Satellite-based Model

Coniferous

Fold	R^2 (%)	RMSE (ton/ha)	MAE (ton/ha)
1	57.2	50.4	37.0
2	62.1	48.9	35.6
3	66.3	46.3	34.0
4	60.7	49.8	36.9
5	58.6	50.6	36.5
6	65.3	47.5	34.9
7	65.9	44.5	33.3
8	64.1	47.0	34.6
9	62.3	48.6	34.1
10	63.0	46.0	34.4
Average	62.6	47.9	35.2
St. Dev.	***2.9***	***1.9***	***1.2***
Minimum	57.2	46.0	33.3
Maximum	66.3	50.6	37.0

TEST SET		
R^2	**RMSE (ton/ha)**	**MAE (ton/ha)**
54.0	53.0	41.7

Broadleaf

Fold	R^2 (%)	RMSE (ton/ha)	MAE (ton/ha)
1	51.2	76.3	56.8
2	54.3	74.2	53.6
3	52.2	76.3	55.8
4	52.7	76.7	56.6
5	53.9	76.1	55.7
6	48.0	76.4	57.3
7	49.9	79.8	57.7
8	54.9	76.7	57.3
9	50.0	80.6	59.5
10	50.4	78.0	57.3
Average	51.7	77.1	56.7
St. Dev.	***2.1***	***1.8***	***1.5***
Minimum	48.0	74.2	53.6
Maximum	54.3	80.6	59.5

TEST SET		
R^2	**RMSE (ton/ha)**	**MAE (ton/ha)**
43.6	82.6	65.4

In both models, the fitted line between observed and predicted values does not follow the 1:1 line (i.e., $R^2 = 1$), this means that at lower biomass predictions were being overestimated and at high biomass predictions were being underestimated. Since the coniferous model recorded a lower RMSE and MAE, the slope of the fitted line is not as low as in the case of broadleaf. Larger differences between observed and predicted values for the broadleaf model were perceived. This difference was more pronounced at higher biomass values (AGB > 300 ton/ha). Annex 12 and Annex 13 visualizes the relationship between observed and predicted values for the AGB estimations for both the coniferous and broadleaf model. The fitted line showcases the over and under estimation of biomass across the range of possible values.

Table 18. Distribution of AGB values (ton/ha) across tree types - Satellite

Type	Count	Minimum (ton/ha)	Maximum (ton/ha)	Mean (ton/ha)	Standard Deviation (ton/ha)	Sample Size (Training)	Sample Size (Test)
Conifer	5,493	23.8	483.6	245.8	86.4	3,845	1,648
Broadleaf	5,881	25.4	565.3	237.1	122.2	4,116	1,765

The average AGB value predicted for the broadleaf is 237.1 ton/ha, while the average for conifers is 245.8 ton/ha. The standard deviation for the predicted values of AGB in the broadleaf trees is of 122.2 ton/ha, and 86.4 ton/ha for the coniferous trees. Both trees were equally distributed in the resulting dataset. The resulting values for AGB across tree types is summarized in Table 18. Figure 26 displays the output from both the coniferous and broadleaf regression models at a satellite level with an overall accuracy of 54.0% and 43.6% respectively.

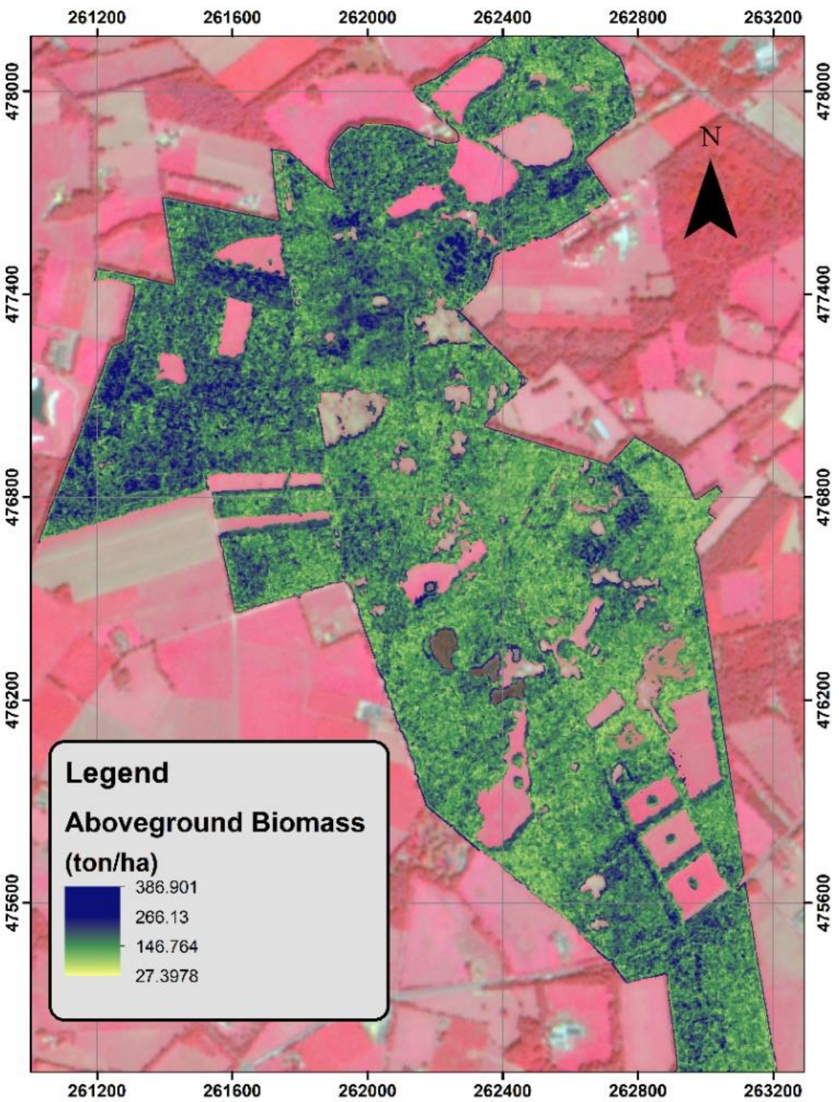

Figure 26. Output from both the Coniferous and Broadleaf Satellite-Based Models.

4. DISCUSSION

4.1. Data Collection

In this section, discussion regarding the measurements taken during the field collection process, the acquirement of UAV images and the limitations presented during this phase of the study are discussed.

4.1.1. Field Data Acquisition

Both the DBH for the coniferous and broadleaf tree species were right-skewed, meaning that the mean tends to be on the lower values (see Figure 13). This is attributed to a restraint in data collection in which only trees with an equal or higher DBH of 10 centimetres were captured in the resulting database as they do not contribute any significant AGB (Brown, 1997). A normal distribution in the majority of the tree species (exception of the Common Ash and Norway Spruce) were attributed to this restraint. For height data acquisition, a handheld laser scanner was used which would use trigonometric equations to calculate the height of trees. The most common limitation encountered was the overlap of trees which occluded the top of trees from line of sight. When compared to the heights obtained with UAV SfM, the recorded R^2 reaches 38%, which denotes a large difference between both values. When compared to height values extracted from the AHN dataset, the R^2 reaches 31%, which provides even further evidence that height values captured during fieldwork are unreliable. Wang (2019) compared aerial and terrestrial laser scanners to field measured heights and found that field measurements tend to overestimate the height of all trees. When comparing heights obtained from the UAV SfM and the AHN CHM, the relationship is far better with an R^2 of 73%. Figure 27 shows the relationship between both heights derived from the UAV and AHN layers, but a clear bias is visible. On average, UAV SfM derived heights tend to be 3.5 meters (bias of 18.9%) higher than that of AHN CHM heights. This explains how the line of equality and the trendline are parallel to each other. This may be attributed to the low point density areas produced by the UAV SfM which produce generalized DSMs that do not capture the complexity of canopy structure, but instead creating a smoother surface. Jayathunga (2019) tested the effects of image downscaling on a CHM derived from LiDAR data in a mixed conifer-broadleaf forest in Japan. The study found that the process would smooth the canopy structure creating less defined tree crowns and overestimating height values.

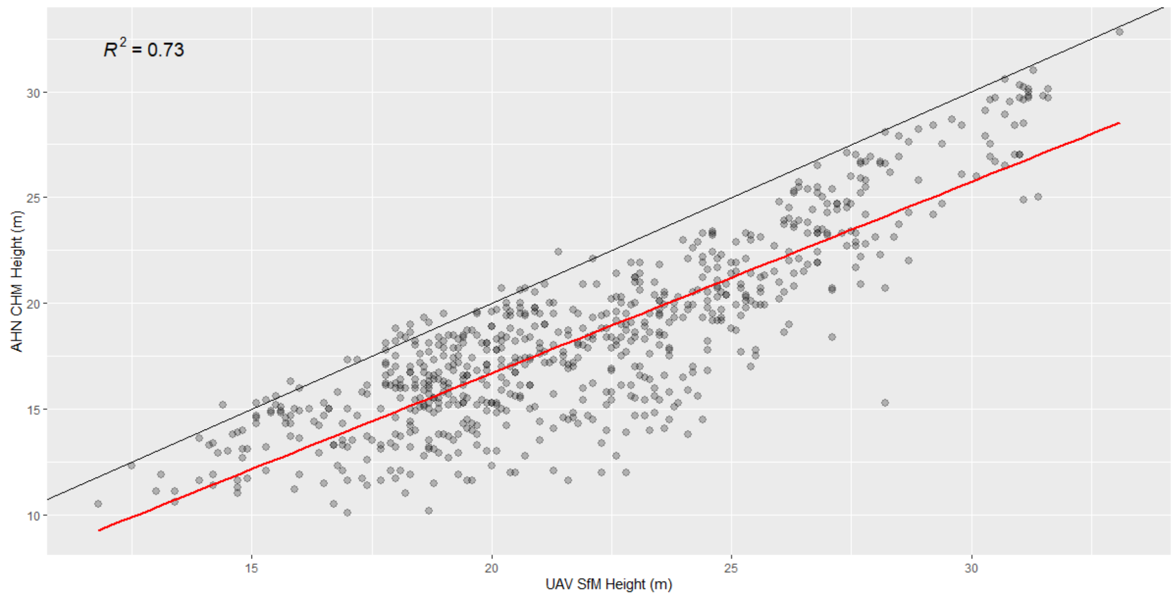

Figure 27. Relationship between UAV SfM Heights and AHN CHM Heights for Segmented Trees. Trendline is marked in red and 1 to 1 line is marked in black.

When calculating the location of trees in GIS software through bearings and distances, some trees appeared to be misplaced. This is attributed to the unavailability of a DGPS in order to precisely obtain the coordinates of the centre plots. The answer to this was the use of Avenza Map mobile application which allows the user to use georeferenced orthomosaics as a reference on the field. The main drawback of this is that the user is subject to any spatial location errors that the images might have. Another consequence was the loss of mobile GPS signal inside the forest, therefore the team had to rely on the canopy structure seen from the orthophoto in order to obtain a location. Often times, trees that were clearly identifiably in the orthophoto were selected as plot centres, but this did not guarantee an exact location due to trees growing at an angle or similar trees standing close to each other. By using plot photos, identification and correction of tree locations was possible in order to counter the loss of GPS signal during the field.

4.1.2. UAV Data Acquisition

For this study, two regression models were established by using field data, UAV imagery and satellite images. For this to be possible, all three datasets were acquired in a parallel time frame to ensure similar explanatory features across all data. One of the main advantages of the use of UAVs for this study was the minimal time and labour that was required to cover extensive areas inside the study area. Areas which had noticeable errors (e.g., missing images or blurry output) due to gusts of wind during acquisition were corrected in Pix4D or eliminated in order to avoid the introduction of error. The UAV was equipped with a Parrot Sequoia which was able to capture red edge and near infrared reflectance with its multispectral sensor. By having only four bands available, only a limited amount of vegetation indices were generated.

4.1.3. DBH and Features Derived from UAV Data

The relationship between DBH and height is widely used to characterise forest stands and is often used to predict biomass (Mugasha, Bollandsås, & Eid, 2013). Since the aboveground biomass was calculated from field measured DBH, the variability on these recordings reflected on the output. Higher standard deviation was recorded in the values of AGB for broadleaf species, while coniferous species were more consistent and obtained AGB values closer to the mean in comparison. Figure 15 shows that the average exponential relationship between UAV CHM height and DBH in conifers is higher in coniferous species than in broadleaf trees. The poor relationships described between these two variables is mainly due to the poor quality of the CHM produced by both the DSM and DTM. A great limitation to elevation information derived from UAV SfM is the inability to acquire ground observations in highly dense areas, as well as only being able to detect the emergent layer of the forest vertical structure (Anderson & Gaston, 2013; Dainelli et al., 2021). Previous research has proven that heights derived from UAV SfM tends to be underestimated mainly due to the low point density required to properly detect tree tops (Dempewolf et al., 2017; Krause et al., 2019). Poorer R^2 values are present when relating DBH with field measured heights. This is mainly due to the limitation previously discussed in which tree tops were blocked by overlapping trees which led to false readings. An alternative to this would have been to use the AHN layer which has a vertical accuracy of 20 cm and a standard deviation of 5 cm. The temporal difference between data captures posed a limitation in the use of this dataset (see Figure 29).

While the average height recorded from the UAV SfM and the AHN elevation data differ from the height recorded on field, the relationship between height and DBH are still better in the conifers than in the broadleaf trees. This difference persisted when using heights derived from the CHM generated from UAV-SfM and from the AHN height information. When evaluating the standard deviation of the regression output (AGB values) for either the UAV or satellite-based models, the broadleaf recorded higher deviation, while the coniferous tree species displayed more consistent results.

Another biometric feature derived from UAV imagery was the CPA obtained through the segmentation of individual trees. As other studies have shown, a relationship between CPA and DBH can be established in order to use CPA as a proxy for the estimation of AGB (Hussin et al., 2014; Qazi et al., 2017). The CPAs obtained in this study displayed poor relationship with the DBH measured on field. The quality of the CPA relies heavily on the individual tree segmentation. The poor quality of the DSM generated a CHM layer which was then used to delineate trees with a WS segmentation algorithm. Still, relationships between these two variables are, on average, higher in broadleaf trees when compared to coniferous.
Both height and CPA are highly relevant explanatory features for the estimation of AGB as it was proven during the evaluation of feature importance in both the coniferous and broadleaf models. Although both tree types preferred the information provided by the CHM layer, the broadleaf regression model obtained more predictive power from the CPA explanatory feature. Meanwhile the coniferous model barely considered this same feature in the final model.

4.2. Data Processing

In this section, the method for individual tree crown segmentation in the UAV phase is discussed. The "pixel purity" approach for building the dataset to estimate biomass is discussed as being a contributor in the performance of the regression models.

4.2.1. Tree Crown Delineation from UAV Images

A poor CHM layer can lead to a poor segmentation process, which in turn can affect the accuracy of biomass estimation. After attempting to segment various UAV images, the most consistent results throughout the various orthomosaic were product of the use of the WS algorithm by using the CHM generated by the SfM. Since the WS utilizes the local maxima and minima to delineate objects, the needle type structure of coniferous tree species was favourable in comparison to the overlapping branches found commonly in broadleaf forests. In dense canopy areas, the WS had trouble distinguishing between one tree and the other. In some cases, two broadleaf trees would be delineated as a single tree due to the overlapping nature found in these forests. Navarro (2020) found a similar trend in mangroves, which tend to absorb the canopies of other trees which cannot be detected as individual trees due to the overlap of the branches. Another reason for the poor segmentation in dense broadleaf forest areas is attributed to the poor quality of the CHM due to low point densities. A low point density cloud would generalize the surface of canopies often merging, what would be clearly, two separate trees. Also, trees that were partially or totally covered by taller trees were ignored in the segmentation process due to the absence of height data provided by the UAV imagery. The structure of the top canopy layer of Haagse Bos in broadleaf forests is formed by trees with the same height. This affects the creation of a detailed DTM since ground points are scarce. These findings are consistent with previous studies in which coniferous and broadleaf trees are segmented (Hussin et al., 2014; Tiede, 2006; Yang, He, Caspersen, & Jones, 2017).

Effect of Canopy Density on Individual Tree Segmentation

Dense areas of conifer tree species obtained better segmentation results as displayed in Block five, nine and ten. Similar results were found by Fujimoto (2019), in which individual coniferous tree species in Japan were successfully identified with an accuracy between 86.0% and 92.3%. This segmentation performance was mainly attributed to the tree distribution between conifer trees which do not overlap. These areas showed a high contrast in reflectance values between shadow and top parts of the trees. In areas where there was a low presence of trees, the WS performed poorly. The resulting objects from this area tend to be slightly larger compared to the more precise manually digitized objects (see Figure 28). This might be attributed to the high reflectance values below the tree corresponding to bare soil. Block 8 of the UAV flight had large areas of bare soil due to recent felling activities taken place in late 2019 due to a harsh infestation of bark beetle; the WS for this block showed the weakest performance in comparison to the rest with an error of 13.6% for broadleaf and 12.8% for coniferous trees Block 8 was also the latest of the areas to be captured by the programmed UAV flights, thus a difference in spectral reflectance in the foliage was expected. Another factor to take into account is the quality of the CHM generated by the DTM and DSM derived from the UAV. The DSM generated in Pix4D does not clearly delineate canopy trees in medium to dense canopies, instead it smoothens edges due to the lack of points generated in the initial point cloud. A common example of this smoothing effect in the CHM is its inability to properly identify branches which stand out. Also, the DTM had a much larger ground sampling distance in comparison to the DSM across all blocks. This is due to the lack of ground returns found in most blocks, meaning that large areas had and averaged value of height that does not accurately represent reality.

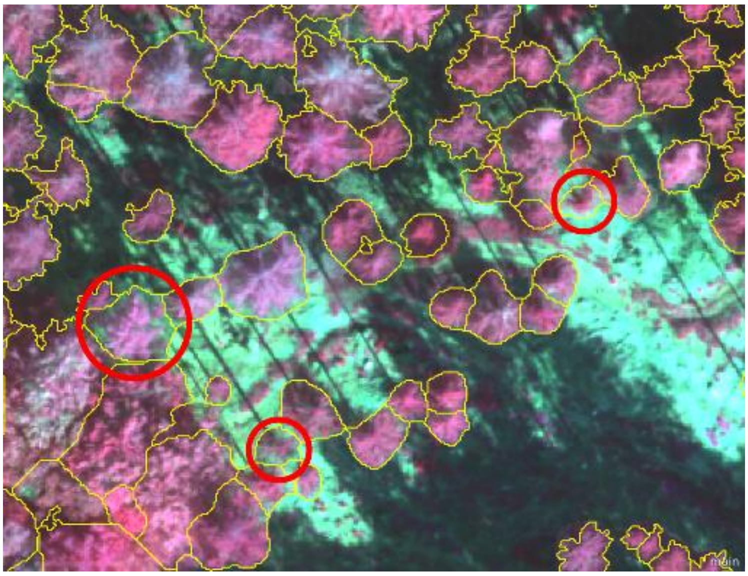

Figure 28. Common errors found in tree segmentation with bright background

Effect of Segmentation Algorithm

To measure the influence of the segmentation algorithm over the performance of the machine learning output, a new segmentation process was used. Flight block 8 was used as a subset area due to the high number of conifers present. A MRS was first applied to the RGB orthophoto which created large segmented objects based on the change on reflectance values. To further segment these objects into meaningful canopies, a WS was applied by using the CHM generated by the SfM. The trees segmented by MRS recorded a total detection error of 18.6%. The regression obtained with this segmentation algorithm recorded an RMSE and a MAE of 416.6 and 293.8 kg per tree respectively; the model with the lowest error recorded was using the SVR algorithm, similar to what was shown previously in the results section. The original trees segmented by the WS recorded a total detection error of 12.8%. The regression model results using these segmented trees displayed lower values of RMSE and MAE of 286.6 and 208.5 kg per tree respectively. The results found through the generation of these models prove that the segmentation process plays a crucial role in the formation of a dataset. Similar findings were demonstrated by Hussin (2014) who compared the influence of different segmentation algorithms on AGB predictions; less accurate tree crown delineation resulted in higher variation of AGB predictions.

Segmentation Performance Across Blocks

The errors recorded in the training set made by the SVR algorithm were evaluated per UAV flight block to assess any relationship with the segmentation process or any difference in the reflectance values between orthophotos. The coniferous model displayed a consistent performance throughout the UAV flight blocks; the R^2 throughout flight blocks was, on average, 73.7% and recorded a standard deviation of 4.3%. RMSE and MAE values for the different flight blocks were similar, this revealed that coniferous tree species across the forest had similar values of AGB. Higher variation in AGB values among flight blocks was present for broadleaf trees. An average R^2 of 53.2% and a standard deviation of 27% were recorded across flight blocks. The higher standard deviation when compared to the coniferous trees was due to Block 9 having a low R^2 of 3.5%. This was caused by the low number of trees (9 trees in total) for which the AGB predictions were poor. Despite the low performance in this block, the overall average of the model for the broadleaf trees was not significantly affected since the trees present only represent 4.1% of the training data.

The AHN layer was initially an option for the generation of a more precise CHM layer from which to segment trees. The main limitation that halted this option the temporal inconsistencies found between the UAV orthomosaics and the AHN layer. As of writing this thesis, the latest available AHN layers were generated with laser scan data captured between the years 2014 and 2019. This time difference between data captures clearly shows up in areas of the forest which suffered felling activity due to bark beetle infestation between the years 2019 and 2020. Thus, the segmentation relied solely on the CHM produced by the SfM of the UAV imagery.

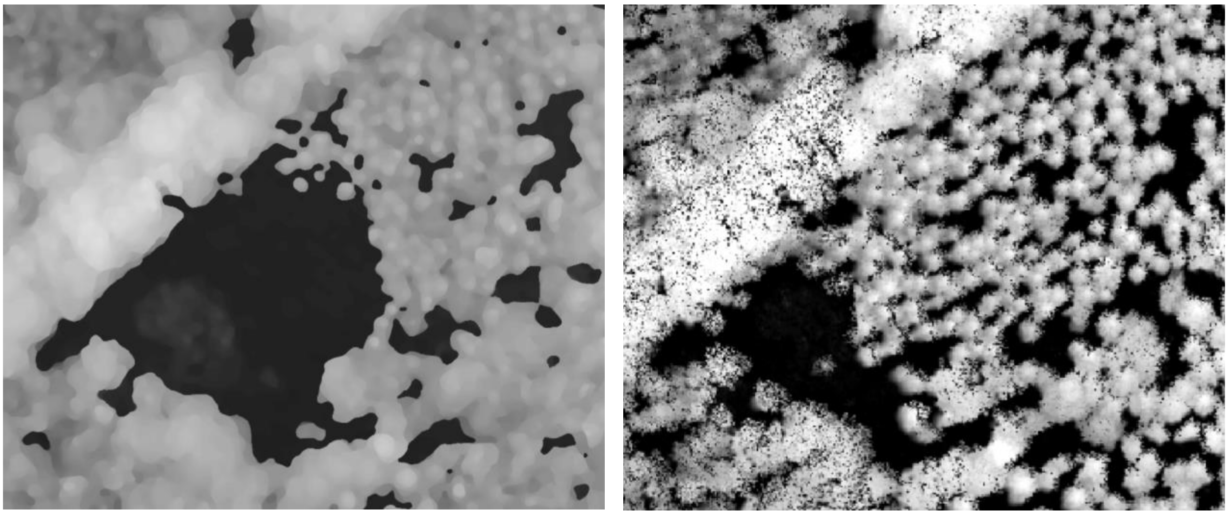

UAV CHM AHN CHM

Figure 29. Comparison of CHM layers in Block 9.
Felling of trees with bark beetle infection are clearly identified.

4.2.2. Pure Pixels

The "pixel purity" was evaluated through an iterative process of modifying the threshold of the objects that were included in the dataset. The number of objects included in the dataset, the coefficient of determination, RMSE and MAE were measured during each iteration to assess the changes in performance of each model. Whilst the coefficient of determination increases up to a maximum of 46.7% when the threshold is lowered to 60% of coverage, it does so at a cost of including more variability in the biomass values. Including more variability into the biomass values in turn increases the RMSE and MAE. What was opted for in this study was to obtain the highest performance with the lowest amount of error. The increase in objects used for training does not always mean that the quality of the dataset will improve, a trade-off between quantity and quality of data is shown in the multiple graphs in Figure 8. The more data that was fed to the model, the more noise that was introduced which in turn increased the error and lowered the coefficient of determination. The overall R^2 value reaches a maximum at 60% of the coverage of pure pixels and begins to degrade when we continue to reduce the threshold; the other performance metrics increase as the threshold reduces. In other words, the RMSE and MAE constantly increase due to the increasing error provided from the variation allowed in the target variable. All further models generated considered pixels which were covered by a segmented object by 60% up until pixels that were completely covered.

4.3. Data Analysis

In this section, the predictive models of aboveground biomass from the UAV and satellite data are discussed. Limitations caused by the structure of the data and the capabilities of the MLA are compared to the results found in recent available literature.

4.3.1. Aboveground Biomass Estimation – UAV

The first approach into training the model was to combine both types of trees (coniferous and broadleaf). The benefits of doing this was to avoid classifying the trees, which in itself is another issue prone to error. Another benefit of combining both tree types was the size of the dataset, resulting in more training samples which tend to improve machine learning regression output. By combining both tree types, the coefficient of determination for the test set results was poor at around 53.0% by using the SVR and 51.1% in the RF. This models also showed larger performance difference (i.e., overfitting) in comparison to the models that took into account the species type. For this model the MAE tells us that the predictions were off by an average of nearly 300 kilograms per tree. Feature reduction was troublesome for this model because the accumulated feature importance between runs would be different. Only the mean CHM value maintained itself as the most important feature, but this was also giving away information on how the regression was interpreting the explanatory features. Upon further review, the splitting of the data played a role in the selection of feature importance. Training trees with a dataset containing a higher number of coniferous trees preferred textural features, while a training set with more broadleaf trees favoured spectral features. Consequently, a stratified random sampling with tree species in order to obtain consistent results throughout different models. With this consideration taken into account, no major improvements were noticed in the performance metrics, but the feature importance did not vary between models.

When separating the dataset into coniferous and broadleaf tree types, considerable improvements were noticed across the validations and test set. This can be attributed to the difference in average reflectance values as well as average height values. When combining both tree species into a single dataset, the model was not able to discriminate between tree types, let alone tree species. By splitting the data, the explanatory features became more consistent and more predictable. Further splitting of the dataset was attempted to generate regression models based on tree species, but due to insufficient training data for some species (e.g., Common Ash) and low accuracies, the opted approach was to maintain the dataset per tree type. Similar feature importance was found when generating tree type specific models. Coniferous trees gained better predictive power with textural features. Alonzo (2018) reported greater errors when modelling AGB for individual tree species, but gained better performance when grouping trees by type in a boreal forest located in Alaska.

The best performance perceived for the deciduous model was produced by using the SVR algorithm, the coefficient of determination recorded on the test set was of 60.3% with an RMSE of 439.7 kilograms per tree and a MAE of 364.1 kilograms per tree. As for the coniferous regression model, the best performance recorded was also produced by the SVR algorithm with an R^2 of 70.7%, well above the broadleaf and combined model. The RMSE and the MAE for the coniferous predicted output was of 215.0 and 156.6 kilograms per tree respectively. When both datasets only contained the most important features, further improvements to the output were recorded. For the broadleaf model, a 2% gain in performance was noted, whereas coniferous tree species a gained a 3% increase in performance. This is expected as we are avoiding the introduction of noise in the dataset by omitting those features which do not explain the variance in the target variable. Both the coniferous and the broadleaf model overestimated low AGB values and underestimated high AGB values. This can be attributed to the distribution of the training data which revolved more around the average value of AGB (see Annex 7 and Annex 8). Wang's (2020) work with mangroves in China suffered a similar effect in which low values of AGB were overestimated, while high values of AGB were being underestimated. Values which were similar to the average AGB value were closer to the line of equality.

These findings are similar to those found by Luo (2021), in which the dataset which had been divided by tree type (coniferous and broadleaf) yielded better results in comparison to a model which combined all trees. The study also found that elevation data and texture features have a high correlation with the AGB predictions, similar to what was found for coniferous species in this study. The difference with this study is that the model for broadleaf tree species had a similar performance to that of the coniferous species ($R^2 > 70\%$). Other studies that estimated AGB for mangroves also found that the features which provided the most amount of information was the height derived from the CHM (Lu et al., 2020; Wang et al., 2019).

Importance of Height and CPA as Explanatory Features

A systematic review of features influencing aboveground biomass estimation found that the inclusion of textural features in combination with multispectral data and structural variables gave better predictions. The added value of including textural metrics to regression models is that it includes information relevant to the surrounding environment due to the kernel used for calculating such metrics. Regression models which opted for individual sets of explanatory features (e.g., structural variables, reflectance values, vegetation indices) displayed poorer performance overall (Poley & McDermid, 2020). In this study, proxies for DBH such as height and/or CPA displayed poor relationships. Instead, training regression models with a variety of explanatory features displayed better results.

The difference in performance can be attributed to the relationship between DBH and the average height of the CHM layer for each tree species. The most important feature for both models is the average CHM value, which we've acknowledge to have accuracy problems. The difference between the models is that the coniferous model gains almost double the information from the same feature as compared to the deciduous model. On average, there is a better relationship between DBH and height for the coniferous trees (see Figure 15). Consequently, aboveground biomass estimations were heavily impacted by the strength of the relationship between DBH and height. Since DBH values were used in allometric equations to calculate AGB values, trees with better DBH-height relationship presented less difference between observed and predicted values in the regression output. Another explanation of the difference in performance of the models is that the variability in DBH measurements recorded on the field was much higher in the broadleaf trees. Then again, broadleaf tree species found more predictive power by using CPA as an explanatory feature, which coincides with better relationships between DBH – CPA found in Figure 16. These findings coincide with the work of Fang (2016), in which weaker logarithmic relationships between DBH and LiDAR measured height of trees lowered the R^2 and increased the RMSE of AGB estimations. The variability in DBH values was transferred into the aboveground biomass calculations, which were later used to train the MLA. Thus, the predictions were susceptible to contain higher variability. Finally, the number of trees used to train both models differed. This was primarily due to the forest structure of coniferous areas in Haagse Bos which had a higher tree density when compared to broadleaf areas. Around two thirds of the trees recorded were coniferous species, giving more training data for the model to obtain more predictive power for this tree type.

Comparing these findings to the work of Alonzo (2018), AGB estimations for boreal forest were done by obtaining features from WS obtained an accuracy of 85% on the validation set. The data used to segment the trees and the feature which was most important in the prediction of biomass was the CHM layer generated from LiDAR data. Other forest structure variables were derived from the LiDAR data such as percentile heights of the canopy crown and the crown base height. Li (2019) estimated aboveground biomass for mangroves by extracting the features of segmented trees with multi-resolution segmentation; the author used RF, SVR and artificial neural networks (ANN) as prediction algorithms. By using spectral metrics, vegetation indices, height metrics and textural features derived from UAV imagery, the author obtained an R^2 of 81% with RF, 80% with SVR and 75% with ANN. It is important to note that the author did not state the performance metrics of the test set, thus validation results tend to be over-optimistic.

4.3.2. Aboveground Biomass Estimation – Satellite

RF and SVR models did not differ in performance when only using spectral data, vegetation indices and textural features using the UAV derived biomass as the target variable. When omitting elevation data, the maximum coefficient of determination was obtained by the SVR model for coniferous tree species (39.7%). Broadleaf trees were slightly better predicted in the RF algorithm by recording an R^2 of 35.1%. By not discriminating the type of tree, the regression model's performance was found to be an average of the tree specific models. The better performance of one model over the other is attributed to the structure of the data; coniferous tree species had lower standard deviation in AGB values (86.4 ton/ha), while broadleaf species had higher standard deviation (122.2 ton/ha). Higher variation, especially in the higher end of the AGB range, contributes to higher error in the models. This higher variation stems from the past errors encountered in the UAV regression model, in which, yet again the broadleaf species obtained a higher RMSE. The propagation of error was to be expected because the base of the satellite regression model was the output generated by the UAV regression model.

As with the UAV regression model, the satellite-based model also suffered from overestimation of low AGB values and underestimation of high AGB values (see Annex 12 and Annex 13). For medium AGB values which were inside the main range of expected AGB values (150 to 330 ton/ha for conifers and 115 to 350 ton/ha for broadleaf), the MLA were able to gain more predictive power by having more training pixels. Values in the mid-range were better predicted, thus displaying less errors. Su (2020) used satellite radar imagery and machine learning algorithms in order to predict AGB in Chinese tropical forests. The RF algorithm was also subject to overestimation and underestimation in low and high values of AGB. It was mainly attributed to a saturation of the radar imagery, a common problem found when attempting to estimate biomass with this sensor. Zhang (2020) reported a similar range of AGB values being that were being better predicted (from 120 to 210 ton/ha); outside of these ranges forest AGB was again being overestimated and underestimated. This study used eight machine learning algorithms, from which the RF and SVR produced serious overestimations and underestimations of AGB.

Feature importance varied between the coniferous and the broadleaf regression models. When omitting height data, coniferous tree species gained more information through the mean values of vegetation indices, while the broadleaf model gained information through textural features. When adding tree elevation data, the models predictive power improved considerably (ΔR^2 = 12.8% for coniferous and ΔR^2 = 7.4% for broadleaf). These results are within the values found in literature review which used features derived from satellites and UAV based biomass (Iizuka et al., 2020; Navarro et al., 2019; Zhu et al., 2020). In both cases, the most important feature was the average value from the CHM layer. The standard deviation of the CHM layer provided more information to the deciduous model. The coniferous model relied its predictive power more on vegetation indices, on the other hand, the textural features provided more information to the prediction of broadleaf biomass.

By removing the least important features from the training of the models, the performance of the models improved. The best performance for the coniferous model was reached by using the top 13 features (R^2 = 54.5%); similar performance was recorded by using the top 12 features. For the broadleaf model, the performance also improved and was able to gain better predictive power. The top 25 features recorded the best performance with a coefficient of determination of 43.6%. It is important to note that the RMSE and MAE for both models decreased in accordance to the coefficient of determination. These findings are in line with other research papers which have trimmed the number of features used in the models for regression problems (Luo et al., 2021; Zhang et al., 2020). The reduction of features makes the model more interpretable by avoiding the introduction of noise of other variables and focusing on those explanatory features which explain the most variance in the target variable.

Spatial location features, such as the geographic location of the pixel and the standard deviation of the location of the pixels inside the segmented objects, were removed from the initial features. Several models were generated including these explanatory features and the performance metrics were overoptimistic (R^2 > 75%). Since the AGB in the UAV stage had been calculated per tree, the AGB had to be represented per a unit of area (ton/ha). By providing the spatial location of each individual pixel, the MLA could obtain the spatial extent of the individual trees in the form of standard deviation of spatial location. After examination of the relationship between each individual explanatory feature and the estimated AGB, it was found that there was a linear trend between standard deviation of spatial location and AGB values. This made these features the most important, even more important than the CHM layers. The predictions displayed clear delineations of biomass which did not match with the UAV predictions or with mature forest stands. These features were then omitted and the results were more in line to those found in the literature (Meyer, Reudenbach, Wöllauer, & Nauss, 2019).

4.3.3. Sources of Error and its Propagation

The moderate performance of the regression models can be attributed to several factors. The first induced error comes at the early stage of finding a tree with no precise GPS measurement. Although this was verified with on-ground photographs and centre plot locations, there is still uncertainty on the location of the trees. The second source of error would be due to the individual tree segmentation, most prominently in the broadleaf tree species. As stated before, dense canopy areas did not register ground points in order to generate a detailed DTM, and the overlapping structure of the trees did not allow for a proper delineation of individual trees. The errors for segmentation of individual trees range from a minimum of 7.7% toa maximum of 13.6%. The third source of error would be provided by the overlap between the segmented tree objects and the pixels from the satellite image. Going from an object-based to a pixel-based regression model induced errors by the uncertainty of the georeferencing between both layers and by the formation of the dataset based on pixel purity. The highest recorded R^2 was reached by allowing objects that covered up to 60% of the pixel; this was at the expense of higher RMSE and MAE in the AGB predictions. The fourth source of error comes from the overestimations and underestimation of tree AGB calculated from the UAV regression models. The UAV estimated AGB were used as the target variable for the satellite-based regression models (R^2 of 73.7% for coniferous trees and 62.6% for broadleaf trees). The aforementioned errors contribute to the overall performance of the final output provided by the satellite-based AGB model.

For both the UAV and the satellite regression models, performances varied between MLA. For classification and regression problems, there is no direct go-to solution as MLAs performance are highly dependent on the structure of the dataset. Authors which compared AGB predictions by using different

MLAs often obtained mixed results between them (Iizuka et al., 2020; Li et al., 2019; Zhang et al., 2020). While some MLA performed better in mangrove ecosystems, other algorithms performed best in temperate forests. The selection of explanatory features also varied as well as the spatial resolution that each study used. Even studies on the same type of ecosystem have presented different results using comparable MLA (Jachowski et al., 2013; Wang et al., 2019).

5. CONCLUSIONS & RECOMMENDATIONS

5.1. Conclusion

In this study, we used the results from a predictive AGB model built on UAV data to calibrate another AGB regression model using satellite imagery in Haagse Bos, The Netherlands. Random Forest and Support Vector Regressor were used as MLA in order to predict AGB values in both the UAV and satellite stages. For this purpose, several UAV flights captured small footprints of a much larger forest. Individual tree segmentation was done on each UAV flight block through WS in order retrieve explanatory features. AGB estimations on the segmented trees were calculated based on ground truth measurements. The segmented trees obtained from the UAV images were later used to extract pixel values from the satellite image in order to obtain AGB estimation at a pixel level. The coefficient of determination (R^2), the root-mean-square error (RMSE) and mean absolute error (MAE) were calculated for each model using a 10-fold cross validation and a test set. This study also focused on the importance of explanatory features derived from multispectral UAV and satellite imagery; the availability of vertical forest structure information was crucial in getting meaningful output in both regression models. Finally, the resulting dataset from the satellite image was also assessed through the pureness of pixels.

The original intention of this research was to solely use Random Forest, but SVR obtained better predictive power through the original dataset due to having more parameters to tune. At coarser resolutions, Random Forest has been shown to work better due to aggregation of values providing a better separability between a range of values (Sheykhmousa et al., 2020). Future research projects which aim to estimating AGB with MLAs should be encouraged to explore multiple algorithms in order to obtain better flexibility in hyperparameter tunning as well as better fits between prediction and observation. The following conclusions can be made from each research question:

1. Which set of features derived from UAV data and satellite imagery can be used to estimate AGB using MLA?

The features that were most commonly used in the prediction of AGB with UAV and satellite imagery were consulted in the literature review. Reflectance values, vegetation indices, biometric information and grey-level co-occurrence matrices were found to be used along several published scientific papers. For satellite images, reflectance values and grey-level co-occurrence matrices were extracted from individual pixels. Vegetation indices differed from the ones obtained through the UAV imagery due to the absence of a red-edge band in the PlanetScope sensor. Since the satellite image lacked vertical information, the AHN data was added to overcome this limitation. The average and standard deviation of each feature were also used.

2. Which set of features derived from UAV data are more important at predicting AGB?

For both tree type models generated with UAV data, there was a significant relationship between ground measured AGB and height values provided by the CHM layer. The coniferous regression model gained better predictive power by using the texture layers. The two features with highest importance were related to the CHM layer, followed by three features belonging to GLCM Entropy in various directions. The broadleaf regression model also displayed a strong relationship to the values obtained through CHM layer, but it gained less predictive power as compared to the coniferous model. The following features with higher importance were related to the red band and the area of the canopy.

3. How are the performance metrics impacted by different MLA and feature reduction in the UAV model?

Both tree types recorded their best performance in the SVR algorithm. By using all 40 explanatory features, the coefficient of determination for the coniferous and broadleaf models were of 71.1% and 60.6% respectively. When removing the least important features, the coniferous model increased its performance to an R^2 of 73.7%, which in turn reduced the RMSE and MAE. This peak in performance was obtained by using the top 15 explanatory features. The broadleaf model also increased its performance up to an R^2 of 62.6%; this performance was reached by using the top 9 features.

4. How accurate is the machine learning algorithm in classifying aboveground biomass content using features derived from UAV data?

After selecting the best performing machine learning algorithm and removing the least important features from the dataset, a 10-fold cross-validation and a test set were used to assess the performance of the models. The coniferous model recorded an R^2 of 73.7%, with an RMSE and a MAE of 215.0 and 156.6 kilograms per tree respectively. The average predicted AGB value for a coniferous tree was 579.5 kilograms with a standard deviation of 324.6 kilograms. The broadleaf model recorded a slightly poorer R^2 of 62.6%. Because of this, the RMSE and MAE for this model were of 439.7 and 364.1 kilogram per tree respectively. The average predicted AGB value for a broadleaf tree was higher when compared to the coniferous trees at around 1,103.7 kilograms per tree and a standard deviation of 502.0 kilograms. Both models overestimated low AGB values and underestimated high AGB values. The average and standard deviation of AGB values used to train the SVR algorithm were higher for the broadleaf trees than that of the coniferous trees, thus

5. Which set of features derived from satellite data are more important at predicting AGB?

The inclusion of vertical information by the addition of the AHN elevation layer improved both models' performance overall. In a similar fashion to what was experienced in the UAV stage, the coniferous and broadleaf regression models perceived the CHM layer as the most important explanatory feature; both models obtained most of their predictive power through the use of the CHM layer. By adding the CHM layer, the coefficient of determination increased from 39.7% to 52.5% for the coniferous model and from 35.1% to 42.5% for the broadleaf model. The reflectance values in the NIR band and vegetation indices gave the coniferous model more information about AGB, while texture and spectral information were preferred by the broadleaf model.

6. How are the performance metrics impacted by different MLA and feature reduction in the satellite model?

The dataset for both tree types performed slightly better by using the RF algorithm and when using the added elevation layer. The highest R^2 recorded on the test set for the coniferous regression model was of 52.5%; when reducing the models explanatory features to the top 13, the models performance increased to 54.0%. The broadleaf model recorded a lower performance in comparison. The coefficient of determination when using all of the explanatory was of 42.5%. By using the top 20 features, the model's performance improved to an R^2 of 43.6%.

7. How accurate is the machine learning algorithm in classifying aboveground biomass content using features derived from satellite imagery?

Once the best machine learning algorithm was identified and the least important features were removed, the best results for the coniferous model obtained an R^2 of 54%, which had an RMSE and a MAE of 53 and 41.7 tons per hectare respectively. The average predicted AGB value for coniferous species is 245.8 tons per hectare with a standard deviation of 86.4 tons per hectare. The best performance recorded for the broadleaf trees was an R^2 of 43.6% and a RMSE and a MAE of 82.6 and 65.4 tons per hectare respectively. For the broadleaf species, the average predicted AGB value was of 237.1 tons per hectare with a recorder standard deviation of 122.2 tons per hectare. Once again, the AGB values for the broadleaf trees used to train the MLA were, on average, higher than those AGB values for the coniferous tree species. Thus, higher values of RMSE and MAE were expected when compared to those found in the coniferous model. As in the UAV models, low AGB values were overestimated while the high AGB values were being underestimated, thus values closer to the average were less prone to higher errors.

5.2. Recommendations

- This study used UAV images to locate trees inside a plot, making the measurements prone to error due to the lack of GPS signal inside the forest. Even by recording the bearings and distance to the center of the plot, some trees were difficult or not possible to pinpoint in the UAV image. The use of a Differential Global Positioning System (DGPS) is recommended during fieldwork as it would provide precise measurement of location of trees.

- The method for data collection during fieldwork had to accommodate several other studies in the area. This, in turn, influenced how the feature selection was done in order to calibrate the satellite AGB regression. It is recommended to design the data collection taking into account the spatial resolution of the satellite image, making the plots align with the cell size of the satellite image (plot of 6X6 pixels which is around 500 m^2). This would make the generation of wall-to-wall satellite AGB estimations much simpler and avoid the complexities attached to pixel purity.

- The output elevation data generated per UAV block were poor in comparison to available LiDAR data. The DTM and DSM that were generated from the point cloud were not dense enough in some areas to generate meaningful output, thus certain UAV flight blocks had to be excluded (e.g., east side of block 123). Allowing the Pix4D software to calculate a greater number of matching points would increase the quality of the point cloud and thus, the generated elevation data. This, of course, entails greater computational expenses such as time and higher processing power. A higher quality CHM would lead to better tree segmentation in the UAV stage. If possible, the use of LiDAR is preferred by literature and it is becoming more available.

- The use of different satellite products would be encouraged, especially if the satellite images contain a higher variety of multispectral bands to generate additional vegetation indices. The availability of a higher number of spectral bands commonly comes at the cost of coarser spatial resolution (e.g., Sentinel-2 vs. PlanetScope). This is also encouraged because the effect of spatial resolution was briefly tested during this study.

- Although this research project utilized two of the most recognized MLAs used in remote sensing applications, it is highly encouraged to explore more and/or optimized MLA. Examples of other algorithms are gradient-boosted regression tree (GBRT), artificial neural networks (ANNs), multivariate adaptive regression splines (MARS), and k-nearest neighbors (kNN). Some of these MLAs would require the fieldwork to have been implemented in a different fashion as they work best by obtaining features from pixels rather than objects (i.e., individual tree segments). Embedded to the aforementioned algorithms is a higher grade of difficulty due to the number of parameters that need to be tuned. Nevertheless, these can provide a better fit for the regression model.

6. ANNEX

Annex 1. Manual Data Entry Format

Data sheet for forest tree parameters in Haagse bos							
Observer name:						Date:	Plot #:
Central point		Logitude (X):				Latitude (Y):	
Plot radius:		Plot dominant species:					
Forest density:		High			Medium		Low
General comment:							
Tree #	Species	DBH (m)	Height (m)	CPA (sq.m)	Tree position		Comment
					Distance from centre point (m)	Compass bearing (degrees)	

Annex 2. Summary of Quality Reports for each UAV flight block.

Block	Ground Sampling Distance (cm)	Total Area (ha)	Calibrated Images	Georeferencing RMSE (m)	GCPS	Average Density (per m³)
123	11.0	58.8	6,336 (99%)	0.059	5	3.45
4	11.2	32.1	4,400 (100%)	0.085	10	3.45
5	11.4	35.5	3,468 (99%)	0.070	6	2.33
8	11.5	33.4	4,500 (100%)	0.046	9	3.45
9	11.7	38.9	4,750 (100%)	0.012	6	3.45
10	10.8	54.2	7,092 (98%)	0.090	5	1.45

Annex 3. Vegetation Indices calculated from UAV and Satellite bands

Metric	Equation	Usage: UAV	Usage: Satellite	Reference
NDVI	$NDVI = \frac{NIR - Red}{NIR + Red}$	X	X	(Bannari, Morin, Bonn, & Huete, 1995)

Metric	Equation	Usage UAV	Usage Satellite	Reference
GNDVI	$GNDVI = \frac{NIR - Green}{NIR + Green}$		X	(Buschmann & Nagel, 1993)
DVI	$DVI = NIR - Red$	X	X	(Bannari et al., 1995)
NDRE	$NDRE = \frac{NIR - Red\ Edge}{NIR + Red\ Edge}$	X		(Clarke, Moran, Barnes, Pinter, & Qi, 2001)
WDRVI[1]	$WDRVI = \frac{(\propto NIR - Red)}{(\propto NIR + Red)}$	X		(Gitelson, 2004)
EVI	$EVI = \frac{2.5(NIR - Red\ Edge)}{(NIR + 6 * Red\ Edge - 7.5 * Blue + 1)}$		X	(Huete et al., 2002)
SR	$SR = \frac{NIR}{Red}$		X	(Major, Baret, & Guyot, 1990)
SAVI[2]	$SAVI = \frac{NIR - Red\ Edge}{NIR + Red + L}(1 + L)$		X	(Bannari et al., 1995)

Annex 4. eCognition Ruleset for Tree Segmentation

Classes:

Remove1 (Shadow/Dark objects in NIR Band (Layer 4))
Remove2 (Low height objects in CHM Layer (Layer 6))
Trees

Process: Main:

Watershed Segmentation
watershed segmentation: watershed segmentation on -Layer 6 creating New Level
Refinement
pixel-based object resizing: loop: at New Level: shrink using Remove2 where Layer 4<=0.26
pixel-based object resizing: loop: at New Level: shrink using Remove1 where Layer 6<=2.5
remove objects: with Area <= 10 Pxl at New Level: remove objects (merge by shape)
Extract assign class: unclassified at New Level: Trees export vector layer: Trees at New Level: export object shapes to D:\...

[1] The value of ∝ was set to 0.1
[2] The value of L was set to 0.5

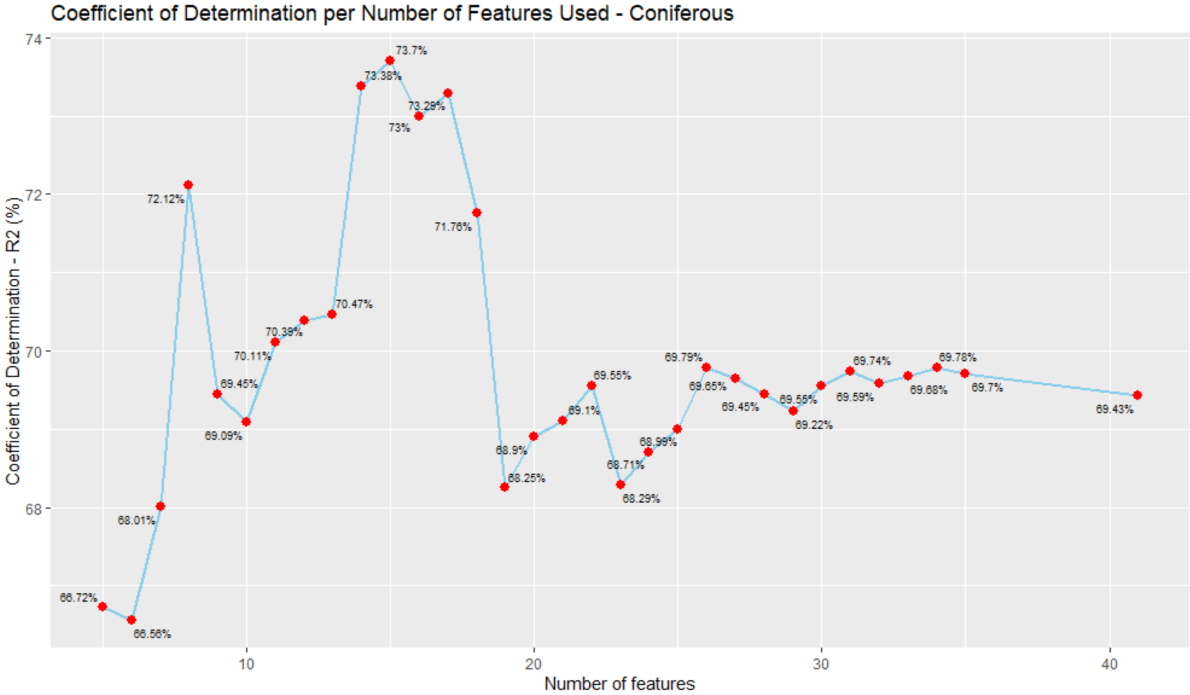

Annex 5. Feature reduction vs performance metrics of Coniferous UAV model

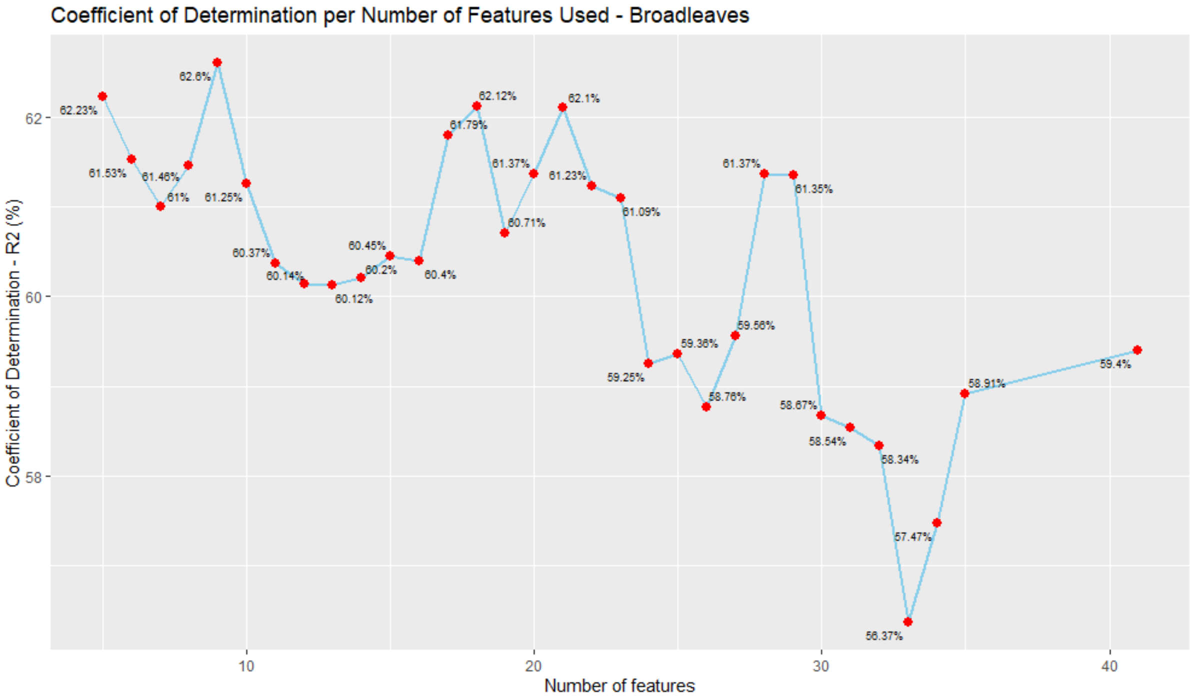

Annex 6. Feature reduction vs performance metrics of Broadleaf UAV model

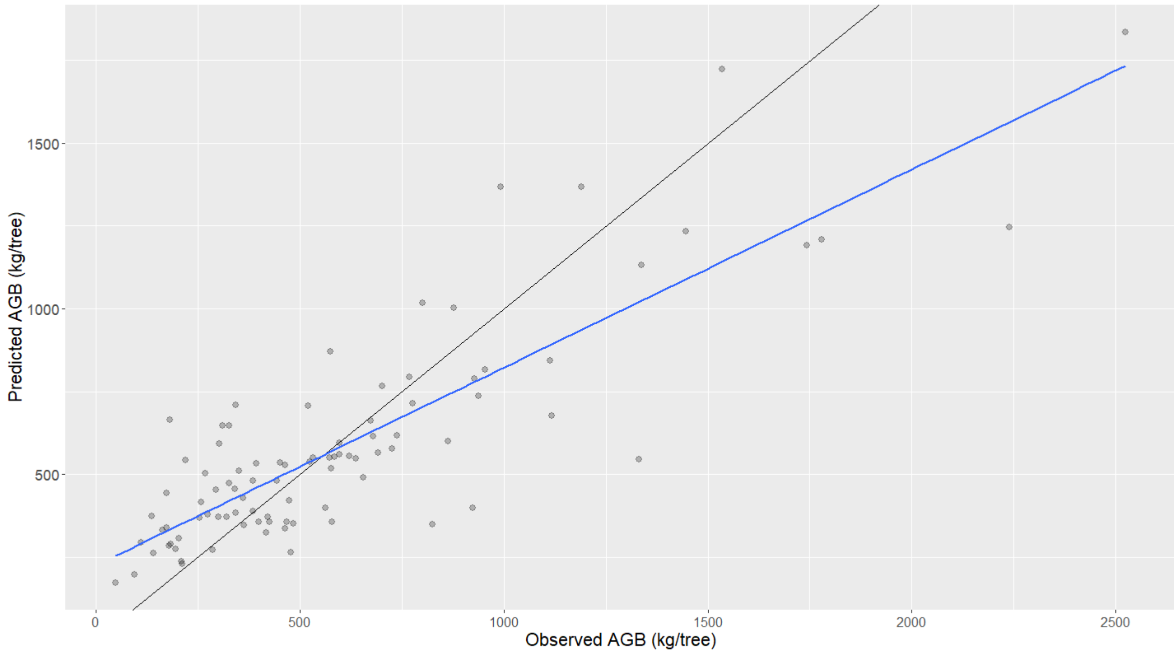

Annex 7. Scatter plot diagram for coniferous regression model – UAV

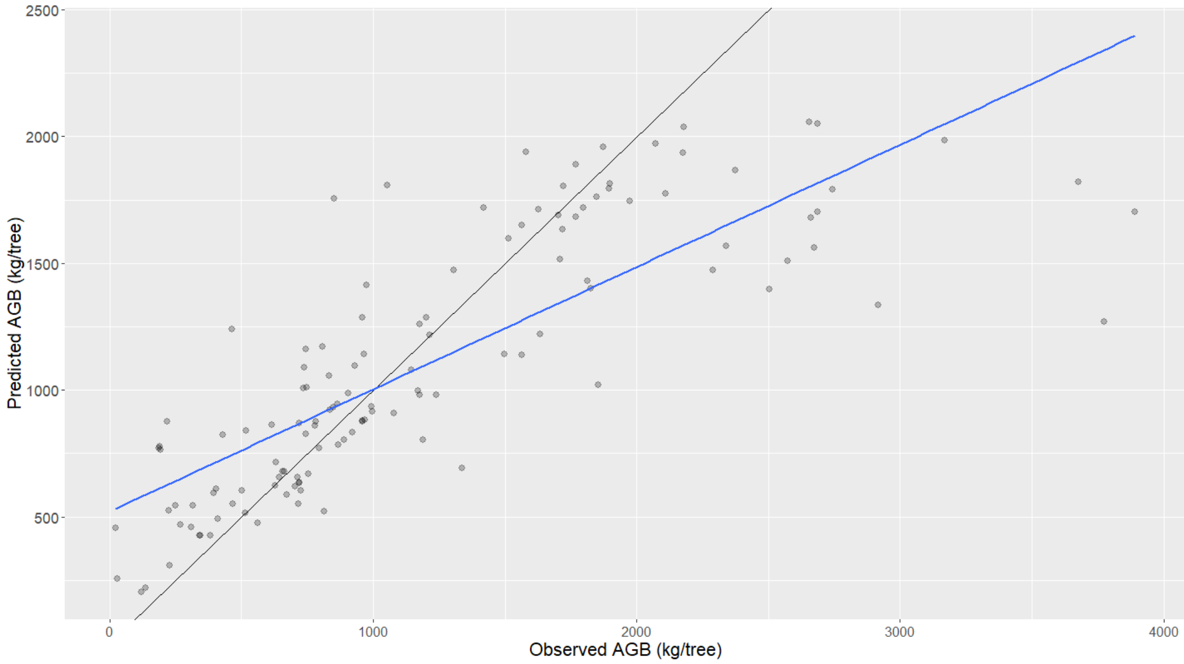

Annex 8. Scatter plot diagram for broadleaf regression model – UAV

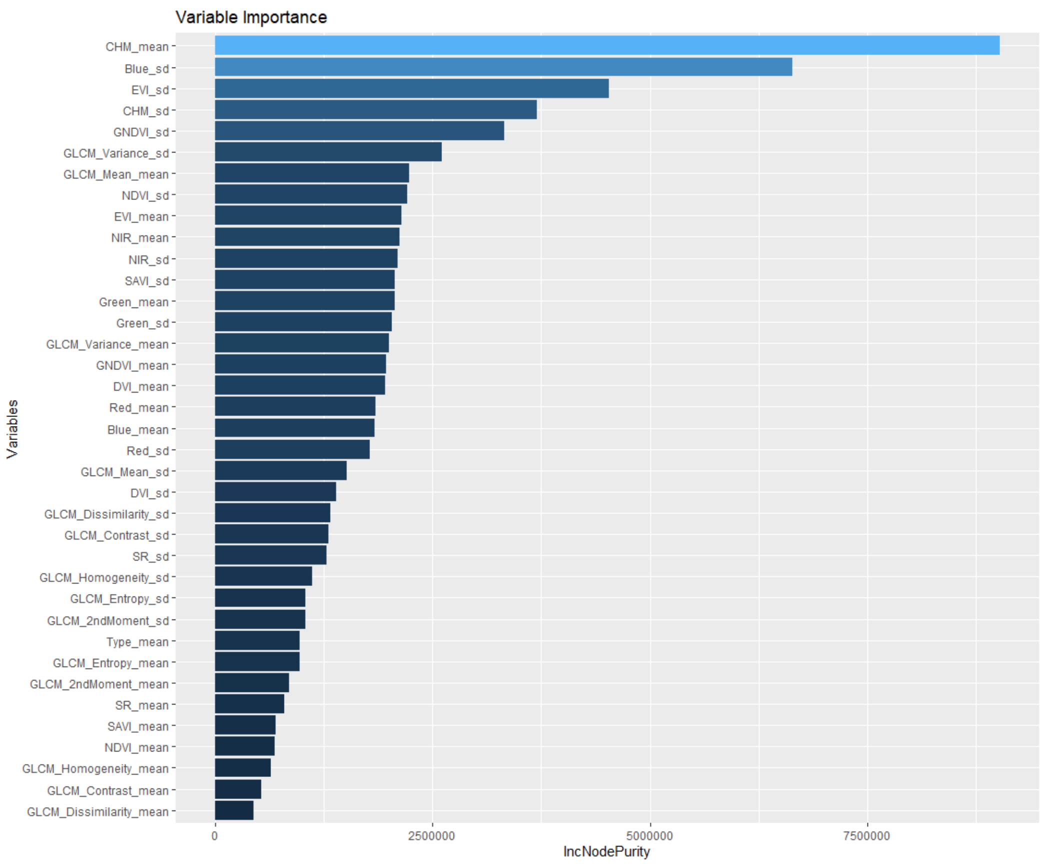

Annex 9. Feature Importance for Combined tree type at the satellite level.

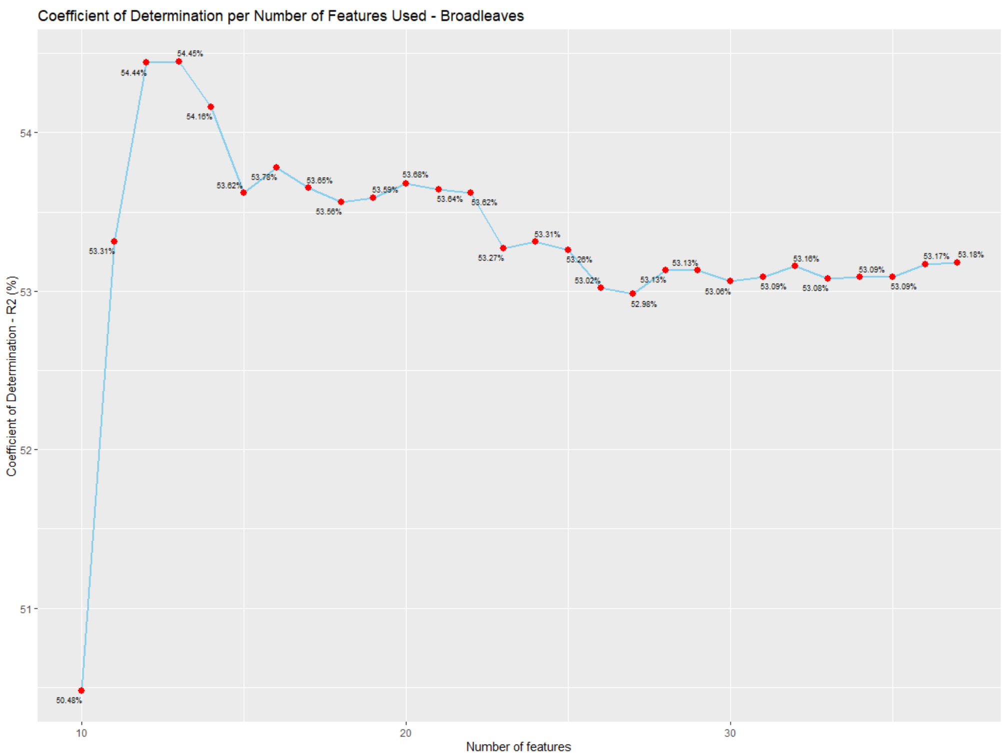

Annex 10. Feature reduction vs performance metrics of Coniferous satellite model

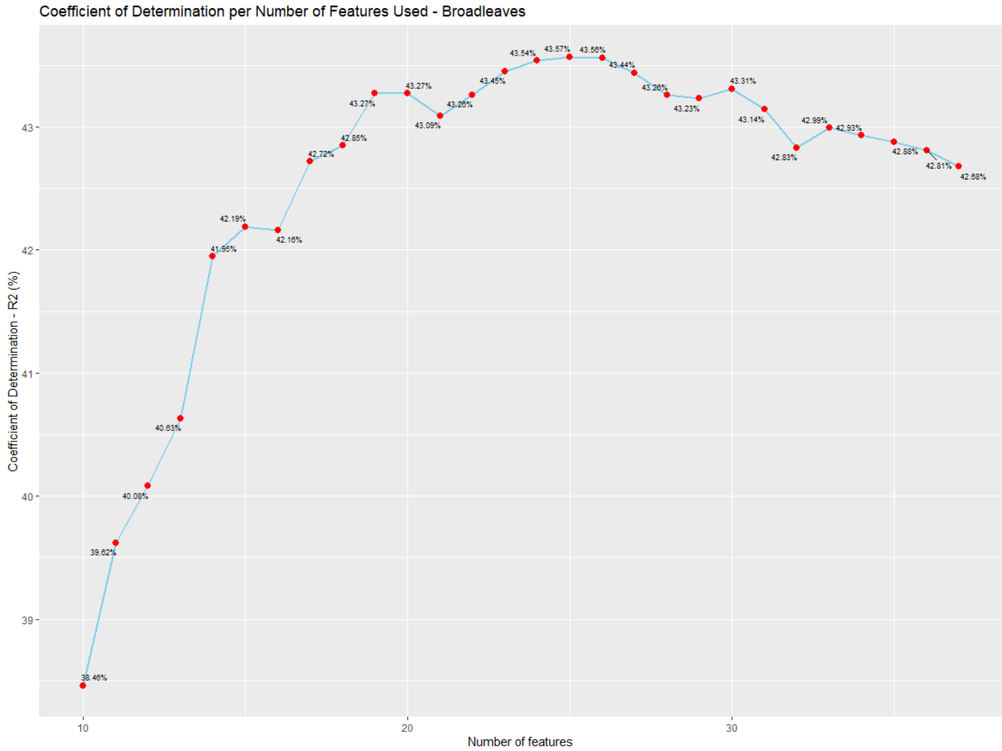

Annex 11. Feature reduction vs performance metrics of Broadleaf satellite model

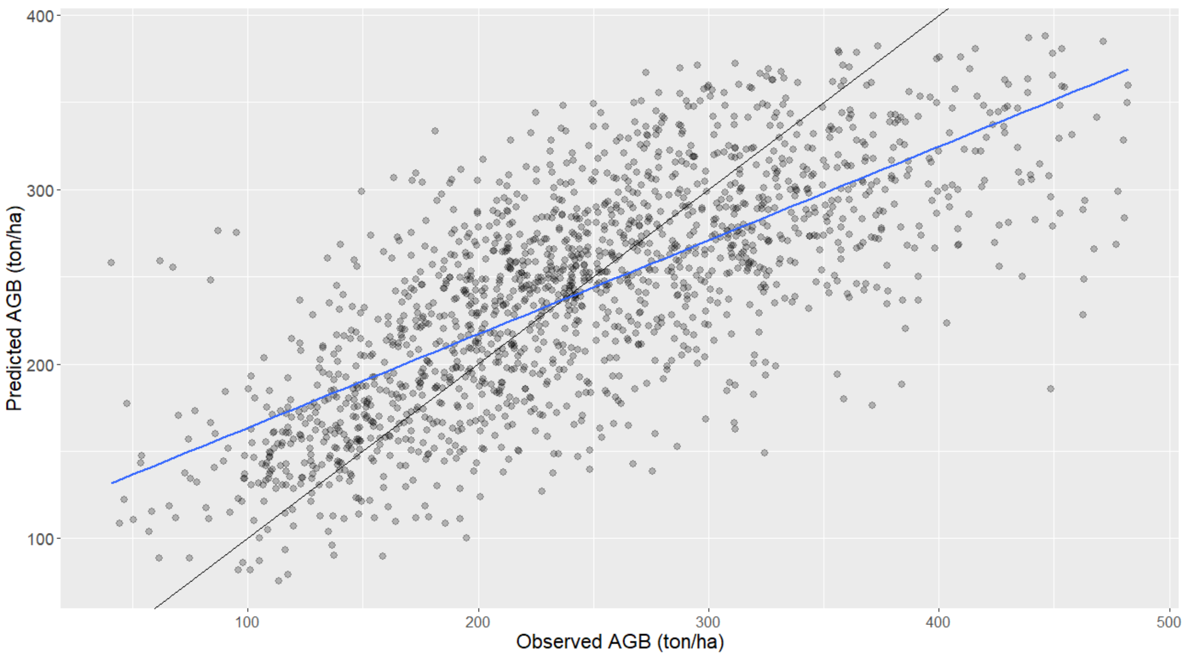

Annex 12. Scatter plot diagram for broadleaf regression model – Satellite

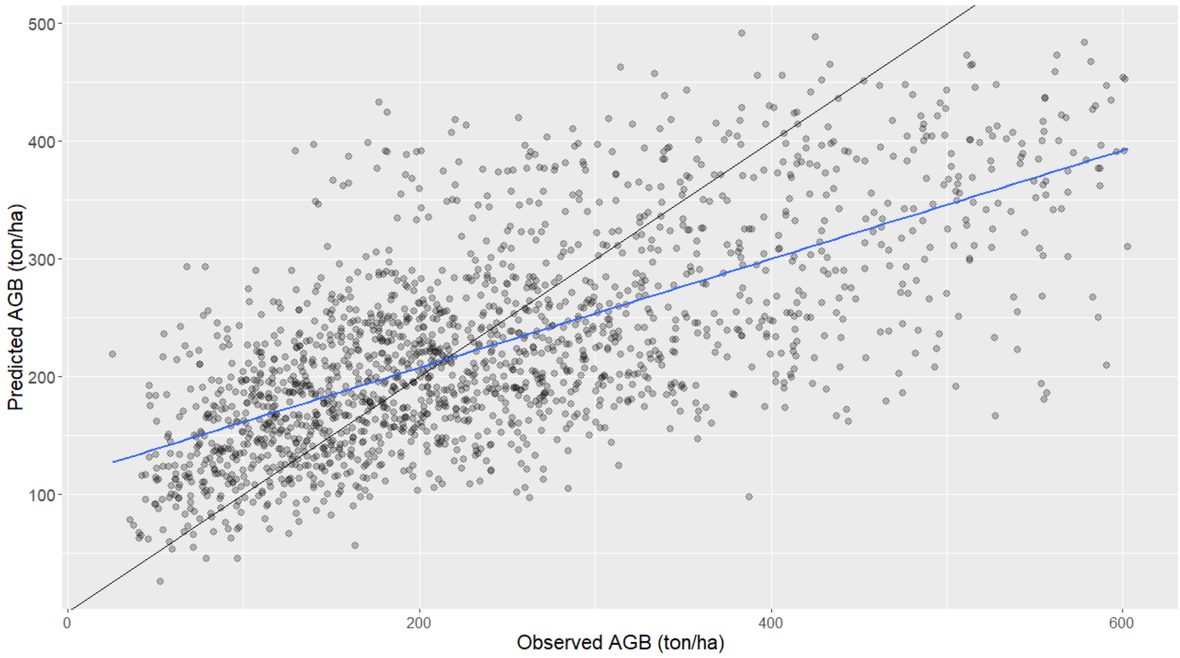

Annex 13. Scatter plot diagram for broadleaf regression model – Satellite

Code segment for SVM model based on UAV explanatory features in RStudio

```
# Don't be afraid of coding. I was, but it is rather easy to catch up. #
set.seed(1337) #For those who know#

## Load Libraries ##
library(randomForest)
library(ggplot2)
library(xlsx)
library(e1071)
library(ggstatsplot)
library(mlbench)
library(caret)
library(dplyr)
library(rminer)

## Set working directory for the file containing the features ##
setwd("C:/Users/luisf/Documents/ITC/Thesis/RF")
full <- read.csv(file.choose(), header = TRUE, sep = ",")
TrainSet <- read.csv(file.choose(), header = TRUE, sep = ",")
TestSet <- read.csv(file.choose(), header = TRUE, sep = ",")
data <- full


## Split into Train and Validation sets ##
data <- subset(full, Species %in% c("Douglas Fir","Norway Spruce","Scots Pine", "Larch"))
data <- subset(full, Species %in% c("Oak", "Birch", "Beech", "Common Ash"))
```

```
data <- drop(full[,8:48])

train <- createDataPartition(data$Species, p = 0.8, list = FALSE)
TrainSet <- data[train,]
TrainSet <- drop(TrainSet[,2:36])
TestSet <- data[-train,]
TestSet <- drop(TestSet[,2:36])

## Run SVM model ##
svm.mdl <- svm(TotalBiomass~., data = TrainSet, kernel = "radial")
svm.mdl
RMSE(svm.mdl$fitted,TrainSet$TotalBiomass)
MAE(svm.mdl$fitted,TrainSet$TotalBiomass)
R2(svm.mdl$fitted,TrainSet$TotalBiomass)*100
plot(svm.mdl$fitted,TrainSet$TotalBiomass)

## Predicting on Test Set ##
test <- predict(svm.mdl, TestSet)
RMSE(test,TestSet$TotalBiomass)
MAE(test,TestSet$TotalBiomass)
R2(test,TestSet$TotalBiomass)*100
plot(test,TestSet$TotalBiomass)

## 10-Fold Cross Validation ##
folds <- createFolds(TrainSet$TotalBiomass, k = 10)
#creating list and arry for storring the resuls for all folds.
cv_svm_result <- list()
cv_svm_cg <- list()
cv_svm_total_result <- array()
for (i in 1:10){
  train <- TrainSet[(-folds[[i]]),]
  valid <- TrainSet[(folds[[i]]),]
  svm.mdl <- svm(TotalBiomass~., data = train, kernel = "radial")
  tunesvm <- tune.svm(TotalBiomass~., data = train,
                      gamma = seq(0.01,0.03,0.01), cost = 2^(seq(2,6,0.5)))
  bestgamma <- tunesvm$best.parameters$gamma
  bestcost <- tunesvm$best.parameters$cost
  cv_svm_cg[[i]] <- cbind(bestgamma, bestcost)
  svm.mdl <- svm(TotalBiomass~., data = train,
                 gamma = bestgamma,
                 cost = bestcost)
  pred <- predict(svm.mdl, valid)
  cv_svm_result[[i]] <- mmetric(valid$TotalBiomass, pred, c("MAE", "RMSE", "R2"))
  print(cv_svm_result[[i]])
  print(cv_svm_cg[[i]])
  cv_svm_total_result <- cbind(cv_svm_total_result, cv_svm_result[[i]])
}
rowMeans(cv_svm_total_result[1:3,-1])
```

```
write.csv(cv_svm_total_result, "10 fold CV Decid.csv", row.names = FALSE)

## Tuning SVR model ##
tunesvm <- tune.svm(TotalBiomass~., data = TrainSet,
                gamma = seq(0.01,0.05,0.005), cost = 2^(seq(2,6,0.5)))
tunesvm
plot(tunesvm)
bestgamma <- tunesvm$best.parameters$gamma
bestcost <- tunesvm$best.parameters$cost

##  SVM with best parameters ##
svm.mdl <- svm(TotalBiomass~., data = TrainSet, gamma = bestgamma, cost = bestcost, cross = 10)
svm.mdl
RMSE(svm.mdl$fitted,TrainSet$TotalBiomass)
MAE(svm.mdl$fitted,TrainSet$TotalBiomass)
R2(svm.mdl$fitted,TrainSet$TotalBiomass)*100
plot(svm.mdl$fitted,TrainSet$TotalBiomass)

test <- predict(svm.mdl, TestSet)
RMSE(test,TestSet$TotalBiomass)
MAE(test,TestSet$TotalBiomass)
R2(test,TestSet$TotalBiomass)*100
plot(test, TestSet$TotalBiomass)
```

Code segment for SVM model based on satellite explanatory features in RStudio

```
set.seed(1337)
library(sp)
library(raster)
library(randomForest)
library(rgdal)
library(ggplot2)
library(e1071)
library(dplyr)
library(tidyr)
library(mlr)
library(ggcorrplot)
library(mlbench)
library(caret)
library(rminer)


## Upload tiff layer ##
setwd("D:/ITC Big Downloads/Thesis/PlanetScope/")
infile <- stack('PlanetScopeErase.tif')
infile <- dropLayer(infile, 18)
names(infile) <- c("Blue", "Green", "Red", "NIR", "NDVI", "GNDVI", "SR", "SAVI",
```

```
              "EVI", "DVI", "GLCM_Mean", "GLCM_Variance", "GLCM_Homogeneity",
              "GLCM_Contrast", "GLCM_Dissimilarity", "GLCM_Entropy",
              "GLCM_2ndMoment", "CHM")
plot(infile)
## Read Pure Pixels ##
AllPts <- read.csv("Pure Pixels/PPAll.csv", header = TRUE, sep = ",")
AllPts <- filter(AllPts, Area >= 8.97*0.60) ## Max area of pixel (not a perfect 3x3 pixel) ##
coordinates(AllPts)<- ~ POINT_X + POINT_Y

## Extract Values from raster ##
rasValue <- raster::extract(infile, AllPts)

## Generate and clean data ##
full <- data.frame(cbind(AllPts,rasValue))
full$BiomPixel <- (full$BiomPixel/9)*10
full <- tidyr::drop_na(full)
full <- full %>% mutate(Type = ifelse(as.character(Type) == "Coniferous", 1, 0)) ## == Coniferous ##
full <- full %>% group_by(FID) %>% summarise(across(everything(), list(mean=mean,sd=sd,
sum=sum),
                                  .names = "{.col}_{.fn}"))
full <- full %>% select(c(2,5,11:63)) %>% select(-contains("sum")) %>% replace(is.na(.), 0)
full <- full %>% filter(Type_mean == 0) %>% select(-c(2))
data <- full
summary(data)
data %>% summarise(across(BiomPixel_mean,sd))

train <- sample(nrow(data),0.7*nrow(data), replace = FALSE)
# train <- createDataPartition(data$Type_mean, p = 0.8, list = FALSE)
TrainSet <- data[train,]
TestSet <- data[-train,]
# summary(TrainSet)
# summary(TestSet)

## Train and Test SVM model ##
svm.mdl <- svm(BiomPixel_mean~., data = TrainSet, kernel = "radial")
svm.mdl
RMSE(svm.mdl$fitted,TrainSet$BiomPixel_mean)
MAE(svm.mdl$fitted,TrainSet$BiomPixel_mean)
R2(svm.mdl$fitted,TrainSet$BiomPixel_mean)*100
plot(svm.mdl$fitted,TrainSet$BiomPixel_mean, abline(a = 0, b = 1)) + grid()

test <- predict(svm.mdl, TestSet)
RMSE(test,TestSet$BiomPixel_mean)
MAE(test,TestSet$BiomPixel_mean)
R2(test,TestSet$BiomPixel_mean)*100
plot(test,TestSet$BiomPixel_mean, abline(a = 0, b = 1)) + grid()

test <- tibble(test)
```

```
results <- cbind(svm.mdl$fitted,TrainSet)
results$diff <- results$BiomPixel_mean - results$test
summary(results)
write.csv(results, "ResultsDecid.csv", row.names = FALSE)

## 10-Fold Cross Validation ##
folds <- createFolds(TrainSet$BiomPixel_mean, k = 10)
#creating list and arry for storring the resuls for all folds.
cv_svm_result <- list()
cv_svm_cg <- list()
cv_svm_total_result <- array()
for (i in 1:10){
  train <- TrainSet[(-folds[[i]]),]
  valid <- TrainSet[(folds[[i]]),]
  svm.mdl <- svm(BiomPixel_mean~., data = train, kernel = "radial")
  pred <- predict(svm.mdl, valid)
  cv_svm_result[[i]] <- mmetric(valid$BiomPixel_mean, pred, c("MAE", "RMSE", "R2"))
  print(cv_svm_result[[i]])
  cv_svm_total_result <- cbind(cv_svm_total_result, cv_svm_result[[i]])
}
rowMeans(cv_svm_total_result[1:3,-1])

write.csv(cv_svm_total_result, "10 fold CV SVM All CHM.csv", row.names = FALSE)
```

7. REFERENCES

Akturk, E., & Altunel, A. O. (2019). Accuracy assesment of a low-cost UAV derived digital elevation model (DEM) in a highly broken and vegetated terrain. *Measurement: Journal of the International Measurement Confederation*, *136*, 382–386. https://doi.org/10.1016/j.measurement.2018.12.101

Ali, I., Greifeneder, F., Stamenkovic, J., Neumann, M., & Notarnicola, C. (2015). Review of machine learning approaches for biomass and soil moisture retrievals from remote sensing data. *Remote Sensing*, *7*(12), 16398–16421. https://doi.org/10.3390/rs71215841

Alonzo, M., Andersen, H. E., Morton, D. C., & Cook, B. D. (2018). Quantifying boreal forest structure and composition using UAV structure from motion. *Forests*, *9*(3), 1–15. https://doi.org/10.3390/f9030119

Anderson, K., & Gaston, K. J. (2013). Lightweight unmanned aerial vehicles will revolutionize spatial ecology. *Frontiers in Ecology and the Environment*, *11*(3), 138–146. https://doi.org/10.1890/120150

Anderson, S., Kupfer, J., Wilson, R., & Cooper, R. (2000). Estimating forest crown area removed by selection cutting: A linked regression-GIS approach based on stump diameters. *Forest Ecology and Management*, *137*(1–3), 171–177. https://doi.org/10.1016/S0378-1127(99)00325-4

Bannari, A., Morin, D., Bonn, F., & Huete, A. R. (1995). A review of vegetation indices. *Remote Sensing Reviews*, *13*(1–2), 95–120. https://doi.org/10.1080/02757259509532298

Bartelink, H. H. (1996). Allometric relationships on biomass and needle area of Douglas-fir. *Forest Ecology and Management*, *86*(1–3), 193–203. https://doi.org/10.1016/S0378-1127(96)03783-8

Basuki, T. M., van Laake, P. E., Skidmore, A. K., & Hussin, Y. A. (2009). Allometric equations for estimating the above-ground biomass in tropical lowland Dipterocarp forests. *Forest Ecology and Management*, *257*(8), 1684–1694. https://doi.org/10.1016/j.foreco.2009.01.027

Beland, M., Parker, G., Sparrow, B., Harding, D., Chasmer, L., Phinn, S., … Strahler, A. (2019). On promoting the use of lidar systems in forest ecosystem research. *Forest Ecology and Management*, *450*(117484). https://doi.org/10.1016/j.foreco.2019.117484

Belgiu, M., & Dra, L. (2016). Random forest in remote sensing : A review of applications and future directions. *Journal of Photogrammetry and Remote Sensing*, *114*, 24–31. https://doi.org/10.1016/j.isprsjprs.2016.01.011

Benz, U. C., Hofmann, P., Willhauck, G., Lingenfelder, I., & Heynen, M. (2004). Multi-resolution, object-oriented fuzzy analysis of remote sensing data for GIS-ready information. *ISPRS Journal of Photogrammetry and Remote Sensing*, *58*(3–4), 239–258. https://doi.org/10.1016/j.isprsjprs.2003.10.002

Breiman, L. (2001). Random Forests. *Machine Learning*, *45*(1), 5–32. https://doi.org/10.1023/A:1010933404324

Brown, S. (1997). *Estimating Biomass and Biomass Change of Tropical Forests: a Primer. (FAO Forestry Paper - 134), Available at http://www.fao.org/docrep/w4095e/w4095e00.htm*. *134*, 1–54.

Brown, S. (2002). Measuring carbon in forests: Current status and future challenges. *Environmental Pollution*, *116*(3), 363–372. https://doi.org/10.1016/S0269-7491(01)00212-3

Bruzzone, L., & Persello, C. (2010). Handbook of Pattern Recognition and Computer Vision. *Handbook of Pattern Recognition and Computer Vision*, 329–352. https://doi.org/10.1142/9789814273398

Buschmann, C., & Nagel, E. (1993). In vivo spectroscopy and internal optics of leaves as basis for remote sensing of vegetation. *International Journal of Remote Sensing*, *14*(4), 711–722. https://doi.org/10.1080/01431169308904370

Chave, J., Réjou-Méchain, M., Búrquez, A., Chidumayo, E., Colgan, M. S., Delitti, W. B. C., … Vieilledent, G. (2014). Improved allometric models to estimate the aboveground biomass of tropical trees. *Global Change Biology*, *20*(10), 3177–3190. https://doi.org/10.1111/gcb.12629

Chih-Wei Hsu, Chang, C.-C., & Lin, C.-J. (2008). A Practical Guide to Support Vector Classification. *BJU International*, *101*(1), 1396–1400. Retrieved from http://www.csie.ntu.edu.tw/%7B~%7Dcjlin/papers/guide/guide.pdf

Clark, D. A., Brown, S., Kicklighter, D. W., Chambers, J. Q., Thomlinson, J. R., Ni, J., & Holland, E. A. (2001). Net primary production in tropical forests: An evaluation and synthesis of existing field data. *Ecological Applications*, *11*(2), 371–384. https://doi.org/10.1890/1051-0761(2001)011[0371:NPPITF]2.0.CO;2

Clarke, T. R., Moran, M. S., Barnes, E. M., Pinter, P. J., & Qi, J. (2001). Planar domain indices: a method for measuring a quality of a single component in two-component pixels. *IGARSS 2001. Scanning the Present and Resolving the Future. Proceedings. IEEE 2001 International Geoscience and Remote Sensing Symposium (Cat. No.01CH37217)*, *3*, vol. 3., 1279–1281, https://doi.org/10.1109/IGARSS.2001.976818

Clinton, N., Holt, A., Scarborough, J., Yan, L. I., & Gong, P. (2010). Accuracy assessment measures for object-based image segmentation goodness. *Photogrammetric Engineering and Remote Sensing*, *76*(3), 289–299. https://doi.org/10.14358/PERS.76.3.289

da Conceição Bispo, P., Rodríguez-Veiga, P., Zimbres, B., do Couto de Miranda, S., Giusti Cezare, C. H., Fleming, S., … Balzter, H. (2020). Woody aboveground biomass mapping of the brazilian savanna with a multi-sensor and machine learning approach. *Remote Sensing*, *12*(17). https://doi.org/10.3390/RS12172685

Dainelli, R., Toscano, P., Di Gennaro, S. F., & Matese, A. (2021). Recent Advances in Unmanned Aerial Vehicle Forest Remote Sensing—A Systematic Review. Part I: A General Framework. *Forests*, *12*(3), 327. https://doi.org/10.3390/f12030327

Damhof, S. (2020). The Hague forest in Twente | Natural monuments. Retrieved August 26, 2020, from https://www.natuurmonumenten.nl/natuurgebieden/snippert/nieuws/het-haagse-bos-twente

Dang, A. T. N., Nandy, S., Srinet, R., Luong, N. V., Ghosh, S., & Senthil Kumar, A. (2019). Forest aboveground biomass estimation using machine learning regression algorithm in Yok Don National Park, Vietnam. *Ecological Informatics*, *50*(3), 24–32. https://doi.org/10.1016/j.ecoinf.2018.12.010

Dempewolf, J., Nagol, J., Hein, S., Thiel, C., & Zimmermann, R. (2017). Measurement of within-season tree height growth in a mixed forest stand using UAV imagery. *Forests*, *8*(7), 1–15. https://doi.org/10.3390/f8070231

Drake, J. B., Knox, R. G., Dubayah, R. O., Clark, D. B., Condit, R., Blair, J. B., & Hofton, M. (2003). Above-ground biomass estimation in closed canopy Neotropical forests using lidar remote sensing: Factors affecting the generality of relationships. *Global Ecology and Biogeography*, *12*(2), 147–159. https://doi.org/10.1046/j.1466-822X.2003.00010.x

Emilien, A.-V., Thomas, C., & Thomas, H. (2021). UAV & satellite synergies for optical remote sensing applications: A literature review. *Science of Remote Sensing*, *3*, 100019. https://doi.org/10.1016/j.srs.2021.100019

Eurostat. (2018). Over 40% of the EU covered with forests - Product - Eurostat. Retrieved August 11, 2020, from https://ec.europa.eu/eurostat/web/products-eurostat-news/-/EDN-20180321-1

Fang, R. (2016). Impacts of tree height-dbh allometry on lidar-based tree aboveground biomass modeling. *International Archives of the Photogrammetry, Remote Sensing and Spatial Information Sciences - ISPRS Archives*, *41*(4), 625–628. https://doi.org/10.5194/isprsarchives-XLI-B8-625-2016

FAO, & UNEP. (2020). *The State of the World's Forests 2020. Forests, biodiversity and people.* https://doi.org/10.4060/ca8642en

Fujimoto, A., Haga, C., Matsui, T., Machimura, T., Hayashi, K., Sugita, S., & Takagi, H. (2019). An end to end process development for UAV-SfM based forest monitoring: Individual tree detection, species classification and carbon dynamics simulation. *Forests*, *10*(8), 1–27. https://doi.org/10.3390/f10080680

Galidaki, G., Zianis, D., Gitas, I., Radoglou, K., Karathanassi, V., Tsakiri–Strati, M., … Mallinis, G. (2017). Vegetation biomass estimation with remote sensing: focus on forest and other wooded land over the Mediterranean ecosystem. *International Journal of Remote Sensing*, *38*(7), 1940–1966. https://doi.org/10.1080/01431161.2016.1266113

Gibbs, H. K., Brown, S., Niles, J. O., & Foley, J. A. (2007). Monitoring and estimating tropical forest carbon stocks: Making REDD a reality. *Environmental Research Letters*, *2*(4). https://doi.org/10.1088/1748-9326/2/4/045023

Gitelson, A. A. (2004). Wide Dynamic Range Vegetation Index for Remote Quantification of Biophysical Characteristics of Vegetation. *Journal of Plant Physiology*, *161*(2), 165–173. https://doi.org/https://doi.org/10.1078/0176-1617-01176

Hickey, S. M., Callow, N. J., Phinn, S., Lovelock, C. E., & Duarte, C. M. (2018). Spatial complexities in aboveground carbon stocks of a semi-arid mangrove community: A remote sensing height-biomass-carbon approach. *Estuarine, Coastal and Shelf Science*, *200*, 194–201. https://doi.org/10.1016/j.ecss.2017.11.004

Hirata, Y., Tsubota, Y., & Sakai, A. (2009). Allometric models of DBH and crown area derived from QuickBird panchromatic data in Cryptomeria japonica and Chamaecyparis obtusa stands. *International Journal of Remote Sensing*, *30*(19), 5071–5088. https://doi.org/10.1080/01431160903022977

Hossain, M. D., & Chen, D. (2019). Segmentation for Object-Based Image Analysis (OBIA): A review of algorithms and challenges from remote sensing perspective. *ISPRS Journal of Photogrammetry and Remote Sensing*, *150*(4), 115–134. https://doi.org/10.1016/j.isprsjprs.2019.02.009

Huete, A., Didan, K., Miura, T., Rodriguez, E. P., Gao, X., & Ferreira, L. G. (2002). Overview of the radiometric and biophysical performance of the MODIS vegetation indices. *Remote Sensing of Environment*, *83*(1), 195–213. https://doi.org/https://doi.org/10.1016/S0034-4257(02)00096-2

Hussin, Y. A., Gilani, H., Van Leeuwen, L., Murthy, M. S. R., Shah, R., Baral, S., … Qamer, F. M. (2014). Evaluation of object-based image analysis techniques on very high-resolution satellite image for biomass estimation in a watershed of hilly forest of Nepal. *Applied Geomatics*, *6*(1), 59–68. https://doi.org/10.1007/s12518-014-0126-z

Iizuka, K., Hayakawa, Y. S., Ogura, T., Nakata, Y., Kosugi, Y., & Yonehara, T. (2020). Integration of multi-sensor data to estimate plot-level stem volume using machine learning algorithms-case study of evergreen conifer planted forests in Japan. *Remote Sensing*, *12*(10).

https://doi.org/10.3390/rs12101649

IPCC. (2014). Climate Change 2014 Mitigation of Climate Change. In *Climate Change 2014 Mitigation of Climate Change*. https://doi.org/10.1017/cbo9781107415416

Jachowski, N. R. A., Quak, M. S. Y., Friess, D. A., Duangnamon, D., Webb, E. L., & Ziegler, A. D. (2013). Mangrove biomass estimation in Southwest Thailand using machine learning. *Applied Geography*, *45*, 311–321. https://doi.org/10.1016/j.apgeog.2013.09.024

James, G., Witten, D., Hastie, T., & Tibshirani, R. (2014). *An Introduction to Statistical Learning: With Applications in R*. Springer Publishing Company, Incorporated.

Jayathunga, S., Owari, T., & Tsuyuki, S. (2018). Evaluating the performance of photogrammetric products using fixed-wing UAV imagery over a mixed conifer-broadleaf forest: Comparison with airborne laser scanning. *Remote Sensing*, *10*(2). https://doi.org/10.3390/rs10020187

Jayathunga, S., Owari, T., & Tsuyuki, S. (2019). Digital Aerial Photogrammetry for Uneven-Aged Forest Management: Assessing the Potential to Reconstruct Canopy Structure and Estimate Living Biomass. *Remote Sensing*, *11*(3). https://doi.org/10.3390/rs11030338

Jin, X., Li, Z., Feng, H., Ren, Z., & Li, S. (2020). Deep neural network algorithm for estimating maize biomass based on simulated Sentinel 2A vegetation indices and leaf area index. *Crop Journal*, *8*(1), 87–97. https://doi.org/10.1016/j.cj.2019.06.005

Joshi, N., Mitchard, E. T. A., Brolly, M., Schumacher, J., Fernández-Landa, A., Johannsen, V. K., … Fensholt, R. (2017). Understanding “saturation” of radar signals over forests. *Scientific Reports*, *7*(1), 1–11. https://doi.org/10.1038/s41598-017-03469-3

Jurjević, L., Liang, X., Gašparović, M., & Balenović, I. (2020). Is field-measured tree height as reliable as believed – Part II, A comparison study of tree height estimates from conventional field measurement and low-cost close-range remote sensing in a deciduous forest. *ISPRS Journal of Photogrammetry and Remote Sensing*, *169*(August), 227–241. https://doi.org/10.1016/j.isprsjprs.2020.09.014

Kachamba, D. J., Ørka, H. O., Gobakken, T., Eid, T., & Mwase, W. (2016). Biomass estimation using 3D data from unmanned aerial vehicle imagery in a tropical woodland. *Remote Sensing*, *8*(11), 1–18. https://doi.org/10.3390/rs8110968

Kattenborn, T., Lopatin, J., Förster, M., Braun, A. C., & Fassnacht, F. E. (2019). UAV data as alternative to field sampling to map woody invasive species based on combined Sentinel-1 and Sentinel-2 data. *Remote Sensing of Environment*, *227*(March), 61–73. https://doi.org/10.1016/j.rse.2019.03.025

KNMI. (2010). *Twente, long-term averages, time period 1981-2010*. Retrieved from https://www.knmi.nl/home

Koh, L. P., & Wich, S. A. (2012). Dawn of drone ecology: Low-cost autonomous aerial vehicles for conservation. *Tropical Conservation Science*, *5*(2), 121–132. https://doi.org/10.1177/194008291200500202

Kopačková-Strnadová, V., Koucká, L., Jelének, J., Lhotáková, Z., & Oulehle, F. (2021). Canopy top, height and photosynthetic pigment estimation using parrot sequoia multispectral imagery and the unmanned aerial vehicle (Uav). *Remote Sensing*, *13*(4), 1–27. https://doi.org/10.3390/rs13040705

Krause, S., Sanders, T. G. M., Mund, J. P., & Greve, K. (2019). UAV-based photogrammetric tree height measurement for intensive forest monitoring. *Remote Sensing*, *11*(7), 1996–2001. https://doi.org/10.3390/rs11070758

Kross, A., McNairn, H., Lapen, D., Sunohara, M., & Champagne, C. (2015). Assessment of RapidEye vegetation indices for estimation of leaf area index and biomass in corn and soybean crops.

International Journal of Applied Earth Observation and Geoinformation, *34*(1), 235–248. https://doi.org/10.1016/j.jag.2014.08.002

Li, Z., Zan, Q., Yang, Q., Zhu, D., Chen, Y., & Yu, S. (2019). Remote estimation of mangrove aboveground carbon stock at the species level using a low-cost unmanned aerial vehicle system. *Remote Sensing*, *11*(9). https://doi.org/10.3390/rs11091018

Lin, J., Wang, M., Ma, M., & Lin, Y. (2018). Aboveground tree biomass estimation of sparse subalpine coniferous forest with UAV oblique photography. *Remote Sensing*, *10*(11). https://doi.org/10.3390/rs10111849

Lin, W., Meng, Y., Qiu, Z., Zhang, S., & Wu, J. (2017). Measurement and calculation of crown projection area and crown volume of individual trees based on 3D laser-scanned point-cloud data. *International Journal of Remote Sensing*, *38*(4), 1083–1100. https://doi.org/10.1080/01431161.2016.1265690

Lu, J., Wang, H., Qin, S., Cao, L., Pu, R., Li, G., & Sun, J. (2020). Estimation of aboveground biomass of Robinia pseudoacacia forest in the Yellow River Delta based on UAV and Backpack LiDAR point clouds. *International Journal of Applied Earth Observation and Geoinformation*, *86*(November 2019), 102014. https://doi.org/10.1016/j.jag.2019.102014

Luo, M., Wang, Y., Xie, Y., Zhou, L., Qiao, J., Qiu, S., & Sun, Y. (2021). Combination of Feature Selection and CatBoost for Prediction: The First Application to the Estimation of Aboveground Biomass. *Forests*, *12*(2), 216. https://doi.org/10.3390/f12020216

Major, D. J., Baret, F., & Guyot, G. (1990). A ratio vegetation index adjusted for soil brightness. *International Journal of Remote Sensing*, *11*(5), 727–740. https://doi.org/10.1080/01431169008955053

Mascaro, J., Asner, G. P., Knapp, D. E., Kennedy-Bowdoin, T., Martin, R. E., Anderson, C., … Chadwick, K. D. (2014). A tale of two "Forests": Random Forest machine learning aids tropical Forest carbon mapping. *PLoS ONE*, *9*(1), 12–16. https://doi.org/10.1371/journal.pone.0085993

McClelland, M. P., van Aardt, J., & Hale, D. (2019). Manned aircraft versus small unmanned aerial system—forestry remote sensing comparison utilizing lidar and structure-from-motion for forest carbon modeling and disturbance detection. *Journal of Applied Remote Sensing*, *14*(02), 1. https://doi.org/10.1117/1.jrs.14.022202

Meyer, H., Reudenbach, C., Wöllauer, S., & Nauss, T. (2019). Importance of spatial predictor variable selection in machine learning applications – Moving from data reproduction to spatial prediction. *Ecological Modelling*, *411*(2), 108815. https://doi.org/10.1016/j.ecolmodel.2019.108815

Miller, G. J., Morris, J. T., & Wang, C. (2019). Estimating aboveground biomass and its spatial distribution in coastal wetlands utilizing planet multispectral imagery. *Remote Sensing*, *11*(17). https://doi.org/10.3390/rs11172020

Modica, G., Messina, G., De Luca, G., Fiozzo, V., & Praticò, S. (2020). Monitoring the vegetation vigor in heterogeneous citrus and olive orchards. A multiscale object-based approach to extract trees' crowns from UAV multispectral imagery. *Computers and Electronics in Agriculture*, *175*(4), 105500. https://doi.org/105500

Mohren, G. M. J., & Vodde, F. (2006). Forests and Forestry in The Netherlands. *Forests and Forestry in European Union Countries*, (In A. Arkuszewska (Ed.)), 334–352.

Mtui, Y. P. (2017). *Tropical rainforest above Ground Biomass and Carbon Stock Estimation for Upper and Lower canopies Using Terrestrial Laser Scanner and Canopy Height Model from Unmanned Aerial Vehicle (UAV) in Ayer-Hitam, Malaysia*. 73. Retrieved from http://www.itc.nl/library/papers_2017/msc/nrm/mtui.pdf

Mugasha, W. A., Bollandsås, O. M., & Eid, T. (2013). Relationships between diameter and height of trees in natural tropical forest in Tanzania. *Southern Forests*, *75*(4), 221–237. https://doi.org/10.2989/20702620.2013.824672

Navarro, A., Young, M., Allan, B., Carnell, P., Macreadie, P., & Ierodiaconou, D. (2020). The application of Unmanned Aerial Vehicles (UAVs) to estimate above-ground biomass of mangrove ecosystems. *Remote Sensing of Environment*, *242*(3), 111747. https://doi.org/10.1016/j.rse.2020.111747

Navarro, J. A., Algeet, N., Fernández-Landa, A., Esteban, J., Rodríguez-Noriega, P., & Guillén-Climent, M. L. (2019). Integration of UAV, Sentinel-1, and Sentinel-2 data for mangrove plantation aboveground biomass monitoring in Senegal. *Remote Sensing*, *11*(1), 1–23. https://doi.org/10.3390/rs11010077

Nguyen, T. H., Jones, S. D., Soto-Berelov, M., Haywood, A., & Hislop, S. (2020). Monitoring aboveground forest biomass dynamics over three decades using Landsat time-series and single-date inventory data. *International Journal of Applied Earth Observation and Geoinformation*, *84*(7), 101952. https://doi.org/10.1016/j.jag.2019.101952

Nordh, N. E., & Verwijst, T. (2004). Above-ground biomass assessments and first cutting cycle production in willow (Salix sp.) coppice - A comparison between destructive and non-destructive methods. *Biomass and Bioenergy*, *27*(1), 1–8. https://doi.org/10.1016/j.biombioe.2003.10.007

Nuthammachot, N., Askar, A., & Stratoulias, D. (2020). Combined use of Sentinel-1 and Sentinel-2 data for improving above-ground biomass estimation. *Geocarto International*, 3(5), 1–11. https://doi.org/10.1080/10106049.2020.1726507

Ota, T., Ogawa, M., Mizoue, N., Fukumoto, K., & Yoshida, S. (2017). Forest Structure Estimation from a UAV-Based Photogrammetric Point Cloud in Managed Temperate Coniferous Forests. *Forests*, *8*(9), 1–11. https://doi.org/10.3390/f8090343

Pandit, S., Tsuyuki, S., & Dube, T. (2018). Estimating above-ground biomass in sub-tropical buffer zone community forests, Nepal, using Sentinel 2 data. *Remote Sensing*, *10*(4). https://doi.org/10.3390/rs10040601

Phua, M. H., Hue, S. W., Ioki, K., Hashim, M., Bidin, K., Musta, B., … Maycock, C. R. (2016). Estimating logged-over lowland rainforest aboveground biomass in sabah, Malaysia using airborne LiDAR data. *Terrestrial, Atmospheric and Oceanic Sciences*, *27*(4), 481–489. https://doi.org/10.3319/TAO.2016.01.06.02(ISRS)

Planet Labs Inc. (2016). *Planet Imagery Product Specification: PlanetScope & RapidEye*. Retrieved from https://www.planet.com/products/satellite-imagery/files/1610.06_Spec Sheet_Combined_Imagery_Product_Letter_ENGv1.pdf

Poley, L. G., & McDermid, G. J. (2020). A systematic review of the factors influencing the estimation of vegetation aboveground biomass using unmanned aerial systems. *Remote Sensing*, *12*(7). https://doi.org/10.3390/rs12071052

Qazi, W. A., Baig, S., Gilani, H., Waqar, M. M., Dhakal, A., & Ammar, A. (2017). Comparison of forest aboveground biomass estimates from passive and active remote sensing sensors over Kayar Khola watershed, Chitwan district, Nepal. *Journal of Applied Remote Sensing*, *11*(2), 026038. https://doi.org/10.1117/1.jrs.11.026038

Reif, D. M., Motsinger, A. A., McKinney, B. A., Crowe, J. E., & Moore, J. H. (2006). Feature selection using a random forests classifier for the integrated analysis of multiple data types. *Proceedings of the 2006 IEEE Symposium on Computational Intelligence in Bioinformatics and Computational Biology, CIBCB'06*, 9(5), 171–178. https://doi.org/10.1109/CIBCB.2006.330987

Riihimäki, H., Luoto, M., & Heiskanen, J. (2019). Estimating fractional cover of tundra vegetation at multiple scales using unmanned aerial systems and optical satellite data. *Remote Sensing of Environment*, *224*(2), 119–132. https://doi.org/10.1016/j.rse.2019.01.030

Roussel, J. R., Auty, D., Coops, N. C., Tompalski, P., Goodbody, T. R. H., Meador, A. S., … Achim, A. (2020). lidR: An R package for analysis of Airborne Laser Scanning (ALS) data. *Remote Sensing of Environment*, *251*(9), 112061. https://doi.org/10.1016/j.rse.2020.112061

Sar, I., & Further, R. (2020). Aboveground biomass. In *Advanced Remote Sensing*. https://doi.org/10.1016/b978-0-12-815826-5.00014-3

SBSTA. (2009). Reducing emissions from deforestation in developing countries : approaches to stimulate action. *United Nations Framework Convention on Climate Change*, (November), 1–11.

Schlesinger, W. H., & Bernhardt, E. S. (2013). Chapter 5 - The Biosphere: The Carbon Cycle of Terrestrial Ecosystems. In W. H. Schlesinger & E. S. Bernhardt (Eds.), *Biogeochemistry (Third Edition)*, pp. 135–172). https://doi.org/https://doi.org/10.1016/B978-0-12-385874-0.00005-4

Sheykhmousa, M., Mahdianpari, M., Ghanbari, H., Mohammadimanesh, F., Ghamisi, P., & Homayouni, S. (2020). Support Vector Machine Versus Random Forest for Remote Sensing Image Classification: A Meta-Analysis and Systematic Review. *IEEE Journal of Selected Topics in Applied Earth Observations and Remote Sensing*, *13*(October), 6308–6325. https://doi.org/10.1109/JSTARS.2020.3026724

Shimano, K. (1997). Analysis of the relationship between DBH and crown projection area using a new model. *Journal of Forest Research*, *2*(4), 237–242. https://doi.org/10.1007/BF02348322

Sinha, S., Jeganathan, C., Sharma, L. K., & Nathawat, M. S. (2015). A review of radar remote sensing for biomass estimation. *International Journal of Environmental Science and Technology*, *12*(5), 1779–1792. https://doi.org/10.1007/s13762-015-0750-0

Su, H., Shen, W., Wang, J., Ali, A., & Li, M. (2020). Machine learning and geostatistical approaches for estimating aboveground biomass in Chinese subtropical forests. *Forest Ecosystems*, *7*(1). https://doi.org/10.1186/s40663-020-00276-7

Suchomel, C. (2012). Biomass equations for sessile oak (Quercus petraea (Matt.) Liebl.) and hornbeam (Carpinus betulus L.) in aged coppiced forests in southwest Germany. *Biomass and Bioenergy*, *46*, 722–730. https://doi.org/10.1016/j.biombioe.2012.06.021

Tiede, D. (2006). Supervised and forest type-specific multi-scale segmentation for a one-level-representation of single trees. *International Archives of Photogrammetry, Remote Sensing and Spatial Information Sciences*, *36*(4), 4.

USAID, & FCMC. (2013). *Redd + Measurement , Reporting and Verification (Mrv) Manual Summary for Policymakers*.

Van Laar, A., & Akça, A. (2005). Forest Mensuration. In *NASPA Journal* (Vol. 13). https://doi.org/10.1017/CBO9781107415324.004

Vashum, K. T., & Jayakumar, S. (2012). Methods to Estimate Above-Ground Biomass and Carbon Stock in Natural Forests - A Review. *Journal of Ecosystem & Ecography*, *02*(04). https://doi.org/10.4172/2157-7625.1000116

Wang, D., Wan, B., Liu, J., Su, Y., Guo, Q., Qiu, P., & Wu, X. (2020). Estimating aboveground biomass of the mangrove forests on northeast Hainan Island in China using an upscaling method from field plots, UAV-LiDAR data and Sentinel-2 imagery. *International Journal of Applied Earth Observation and Geoinformation*, *85*(June 2019), 101986. https://doi.org/10.1016/j.jag.2019.101986

Wang, D., Wan, B., Qiu, P., Zuo, Z., Wang, R., & Wu, X. (2019). Mapping height and aboveground biomass of mangrove forests on Hainan Island using UAV-LiDAR sampling. *Remote Sensing*, *11*(18), 1–25. https://doi.org/10.3390/rs11182156

Wang, Y., Lehtomäki, M., Liang, X., Pyörälä, J., Kukko, A., Jaakkola, A., … Hyyppä, J. (2019). Is field-measured tree height as reliable as believed – A comparison study of tree height estimates from field measurement, airborne laser scanning and terrestrial laser scanning in a boreal forest. *ISPRS Journal of Photogrammetry and Remote Sensing*, *147*(October 2018), 132–145. https://doi.org/10.1016/j.isprsjprs.2018.11.008

Westoby, M. J., Brasington, J., Glasser, N. F., Hambrey, M. J., & Reynolds, J. M. (2012). "Structure-from-Motion" photogrammetry: A low-cost, effective tool for geoscience applications. *Geomorphology*, *179*(4), 300–314. https://doi.org/10.1016/j.geomorph.2012.08.021

Xie, Z., Chen, Y., Lu, D., Li, G., & Chen, E. (2019). Classification of Land Cover, Forest, and Tree Species Classes with ZiYuan-3 Multispectral and Stereo Data. *Remote Sensing*, *11*(2), 164. https://doi.org/10.3390/rs11020164

Xue, J., Ge, Y., & Ren, H. (2017). Spatial upscaling of green aboveground biomass derived from MODIS-based NDVI in arid and semiarid grasslands. *Advances in Space Research*, *60*(9), 2001–2008. https://doi.org/10.1016/j.asr.2017.07.016

Yang, J., He, Y., Caspersen, J. P., & Jones, T. A. (2017). Delineating Individual Tree Crowns in an Uneven-Aged, Mixed Broadleaf Forest Using Multispectral Watershed Segmentation and Multiscale Fitting. *IEEE Journal of Selected Topics in Applied Earth Observations and Remote Sensing*, *10*(4), 1390–1401. https://doi.org/10.1109/JSTARS.2016.2638822

Zhang, Y., Ma, J., Liang, S., Li, X., & Li, M. (2020). An evaluation of eight machine learning regression algorithms for forest aboveground biomass estimation from multiple satellite data products. *Remote Sensing*, *12*(24), 1–26. https://doi.org/10.3390/rs12244015

Zhu, Y., Liu, K., Myint, S. W., Du, Z., Li, Y., Cao, J., … Wu, Z. (2020). Integration of GF2 optical, GF3 SAR, and UAV data for estimating aboveground biomass of China's largest artificially planted mangroves. *Remote Sensing*, *12*(12). https://doi.org/10.3390/RS12122039

Zianis, D., Muukkonen, P., Mäkipää, R., & Mencuccini, M. (2005). Biomass and stem volume equations for tree species in Europe. In *Silva Fennica Monographs* (Vol. 4).

Zou, X., Liang, A., Wu, B., Su, J., Zheng, R., & Li, J. (2019). UAV-based high-throughput approach for fast growing Cunninghamia lanceolata (Lamb.) cultivar screening by machine learning. *Forests*, *10*(9). https://doi.org/10.3390/f10090815